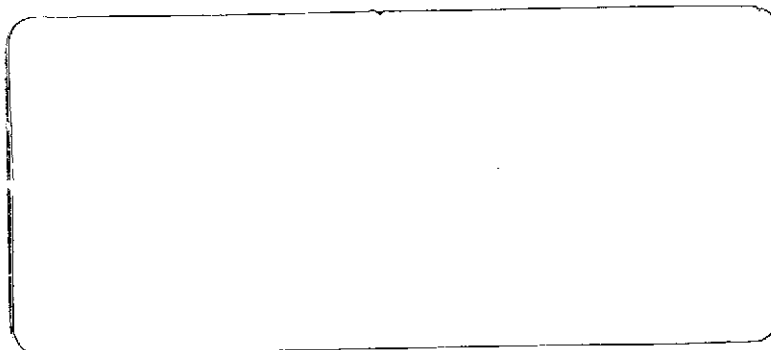


P
2004



(NASA-CR-137345) PLANETARY QUARANTINE: N74-19727
SPACE RESEARCH AND TECHNOLOGY Semiannual
Review, 1 Jul. - 31 Dec. 1973 (Jet
Propulsion Lab.) 132 p HC \$9.75

Unclas
CSCL 06M G3/04 34097

JET PROPULSION LABORATORY
CALIFORNIA INSTITUTE OF TECHNOLOGY
PASADENA, CALIFORNIA

900-655

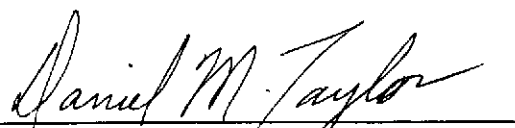
PLANETARY QUARANTINE

Semi-Annual Review
Space Research and Technology

1 July - 31 December 1973

April, 1974

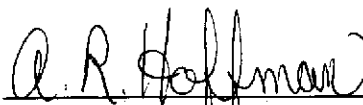
APPROVED BY:



D. M. Taylor, Supervisor
Life Sciences Research



J. R. Puleo, Supervisor
Planetary Quarantine Laboratory



A. R. Hoffman, Supervisor
Planetary Quarantine Analysis



D. Alcorn, Manager
Systems Test and Launch
Operations Section



D. S. Hess, Manager
Environmental Requirements
Section

JET PROPULSION LABORATORY
CALIFORNIA INSTITUTE OF TECHNOLOGY
PASADENA, CALIFORNIA

PREFACE

This document contains a report on Research and Advanced Development at the Jet Propulsion Laboratory during the period 1 July 1973 to 31 December 1973, sponsored by the Planetary Quarantine branch of the NASA Office of Space Science and Applications.

PRECEDING PAGE BLANK NOT FILMED

CONTENTS

| | | |
|-------|--|------|
| I. | PLANETARY QUARANTINE STRATEGIES FOR ADVANCED MISSIONS (NASA No. 193-58-61-01) | |
| 1.1 | STRATEGIES FOR SATELLITE ENCOUNTER | 1-1 |
| 1.1.1 | Subtask A Introduction | 1-1 |
| 1.1.2 | Significant Accomplishments | 1-1 |
| 1.1.3 | Future Activities | 1-6 |
| 1.1.4 | Presentations | 1-6 |
| 1.1.5 | References | 1-6 |
| 1.2 | JUPITER ENTRY ANALYSIS | 1-8 |
| 1.2.1 | Subtask B Introduction | 1-8 |
| 1.2.2 | Significant Accomplishments | 1-8 |
| 1.2.3 | Conclusions | 1-20 |
| 1.2.4 | Future Activities | 1-23 |
| 1.2.5 | Presentations | 1-24 |
| II. | NATURAL SPACE ENVIRONMENT STUDIES (NASA No. 193-58-61-02) | |
| 2.1 | EFFECT OF PLANETARY TRAPPED RADIATION BELT ON MICROORGANISMS | 2-1 |
| 2.1.1 | Subtask A Introduction | 2-1 |
| 2.1.2 | Significant Accomplishments | 2-1 |
| 2.1.3 | Future Activities | 2-11 |
| 2.1.4 | Presentations | 2-12 |
| 2.1.5 | References | 2-12 |
| 2.2 | EFFECT OF SOLAR WIND RADIATION ON MICROORGANISMS | 2-13 |
| 2.2.1 | Subtask B Introduction | 2-13 |
| 2.2.2 | Significant Accomplishments | 2-13 |
| 2.2.3 | Future Activities | 2-14 |
| 2.2.4 | Presentations | 2-14 |
| 2.2.5 | References | 2-14 |
| 2.3 | EFFECT OF SPACE VACUUM ON MICROORGANISMS | 2-15 |
| 2.3.1 | Subtask C Introduction | 2-15 |
| 2.3.2 | Significant Accomplishments | 2-15 |
| 2.3.3 | Future Activities | 2-15 |
| 2.3.4 | References | 2-15 |

CONTENTS (contd)

| | | |
|-------|---|------|
| 2.4 | PROBABILITY OF GROWTH IN PLANETARY ATMOSPHERE AND SATELLITES | 2-16 |
| 2.4.1 | Subtask D Introduction | 2-16 |
| 2.4.2 | Significant Accomplishments | 2-16 |
| 2.4.3 | Future Activities | 2-20 |
| 2.4.4 | Presentations | 2-20 |
| 2.4.5 | Publications | 2-20 |
| 2.5 | EFFECT OF SOLAR ELECTROMAGNETIC RADIATION OF MICROORGANISMS | 2-21 |
| 2.5.1 | Subtask E Introduction | 2-21 |
| 2.5.2 | Significant Accomplishments | 2-21 |
| 2.5.3 | Future Activities | 2-22 |
| III. | POST LAUNCH RECONTAMINATION STUDIES (NASA No. 193-58-62-03) | |
| 3.1 | POST LAUNCH RECONTAMINATION STUDIES | 3-1 |
| 3.1.1 | Subtask A Introduction | 3-1 |
| 3.1.2 | Significant Accomplishments | 3-1 |
| 3.1.3 | Future Activities | 3-22 |
| 3.1.4 | Presentations | 3-24 |
| 3.1.5 | References | 3-24 |
| IV. | SPACECRAFT CLEANING AND DECONTAMINATION TECHNIQUES (NASA No. 193-58-63-02) | |
| 4.1 | PHYSICAL REMOVAL OF SPACECRAFT MICROBIAL BURDEN | 4-1 |
| 4.1.1 | Subtask A Introduction | 4-1 |
| 4.1.2 | Approach | 4-2 |
| 4.1.3 | Significant Accomplishments | 4-3 |
| 4.1.4 | Future Activities | 4-3 |
| 4.2 | EVALUATION OF PLASMA CLEANING AND DECONTAMINATION TECHNIQUES | 4-5 |
| 4.2.1 | Subtask B Introduction | 4-5 |
| 4.2.2 | Approach | 4-5 |
| 4.2.3 | Significant Accomplishments | 4-11 |
| 4.2.4 | Summary and Conclusions | 4-19 |
| 4.2.5 | Future Activities | 4-19 |
| 4.2.6 | Presentations | 4-19 |

CONTENTS (contd)

| | | | |
|------------|--|--|------|
| V. | PLANETARY QUARANTINE KSC OPERATIONS (NASA No. 193-58-63-05) | | |
| 5.1 | TEFLON RIBBON EXPERIMENTS | | 5-1 |
| | 5.1.1 Subtask A Introduction | | 5-1 |
| | 5.1.2 Significant Accomplishments | | 5-1 |
| | 5.1.3 Future Activities | | 5-10 |
| | 5.1.4 Presentations | | 5-11 |
| 5.2 | MICROBIOLOGICAL STUDIES ON UNMANNED SPACECRAFT | | 5-12 |
| | 5.2.1 Subtask B Introduction | | 5-12 |
| | 5.2.2 Significant Accomplishments | | 5-12 |
| | 5.2.3 Future Activities | | 5-12 |
| | 5.2.4 Presentations | | 5-12 |
| Appendix A | CLEANING AND DECONTAMINATION MATERIAL | | A-1 |

FIGURES

| | | |
|---------|---|------|
| 1-B. 1 | Location of plastic materials in ultraviolet spectrometer | 1-9 |
| 1-B. 2 | Thermal decomposition of ultraviolet spectrometer plastics | 1-9 |
| 1-B. 3 | Typical cable cross-section | 1-10 |
| 1-B. 4 | Temperature profiles of a teflon rod for Jupiter entry at 15° entry angle: warm atmosphere, initial altitude = 750 km | 1-11 |
| 1-B. 5 | Temperature profiles in unablated teflon: entry at 15°, warm atmosphere | 1-12 |
| 1-B. 6 | Temperature profiles of a teflon rod for Jupiter entry at 90° entry angle: cool atmosphere, initial altitude = 200 km | 1-12 |
| 1-B. 7 | Temperature profiles in unablated teflon: entry at 90°, cool atmosphere | 1-13 |
| 1-B. 8 | Ablation test of teflon insulated cable | 1-13 |
| 1-B. 9 | Sample of ablated cable | 1-14 |
| 1-B. 10 | Ultraviolet spectrometer disintegration of plastics due to heat of Jupiter entry: warm atmosphere | 1-16 |
| 1-B. 11 | Temperature profile in G10 plastic at the back of ultraviolet spectrometer for Jupiter entry: warm atmosphere | 1-17 |
| 1-B. 12 | Ultraviolet spectrometer disintegration of plastics due to heat of Jupiter entry: cool atmosphere | 1-18 |
| 1-B. 13 | Temperature profile in G10 Plastic at the end of front face recession | 1-19 |
| 1-B. 14 | Typical bus shearplate assembly | 1-19 |
| 1-B. 15 | Bus cabling assembly | 1-20 |
| 1-B. 16 | Illustration of increase in PQ "kill" integral and transfer factor at low speed, in free-molecular flow | 1-21 |
| 1-B. 17 | Variation of V_a^3 with the time from entry; same case as Fig. 1-B.16 | 1-21 |
| 1-B. 18 | Small particle survival corridors: Jupiter nominal atmosphere | 1-22 |
| 1-B. 19 | Small particle survival corridors: Saturn nominal atmosphere | 1-22 |
| 2-A. 1 | Effect of dose and energy on spacecraft spore isolates | 2-8 |
| 2-A. 2 | Effect of dose and energy on spacecraft nonsporeformer isolates | 2-10 |
| 2-D. 1 | Pressure-temperature profiles of engineering models of Titan's atmosphere | 2-18 |

FIGURES (contd)

| | | |
|---------|---|------|
| 2-D. 2 | Pressure-temperature domains for various potential condensates in Titan's atmosphere | 2-19 |
| 2-D. 3 | Candidate surface materials corresponding to pressure-temperature regions at the bottom of Titan's atmosphere | 2-19 |
| 3-A. 1 | Comparison of particle adhesion data with predictions of model, 22 μm glass beads | 3-8 |
| 3-A. 2 | Comparison of particle adhesion data with predictions of model, 48 μm glass beads | 3-8 |
| 3-A. 3 | Comparison of particle adhesion data with predictions of model, 68 μm glass beads | 3-9 |
| 3-A. 4 | Comparison of particle adhesion data with predictions of model, 94 μm glass beads | 3-9 |
| 3-A. 5 | Comparison of particle adhesion data with predictions of model, 110 μm glass beads | 3-10 |
| 3-A. 6 | Surface acceleration for simulation of LRC experiment, Case 1 | 3-15 |
| 3-A. 7 | Surface velocity for simulation of LRC experiment, Case 1 | 3-16 |
| 3-A. 8 | Surface acceleration for simulation of LRC experiment, Case 2 | 3-17 |
| 3-A. 9 | Surface velocity for simulation of LRC experiment, Case 2 | 3-18 |
| 3-A. 10 | Summary of calculated clearing radii | 3-21 |
| 3-A. 11 | Glass bead profile predicted post impact for simulation of LRC experiment, Case 1 | 3-23 |
| 3-A. 12 | Glass bead profile predicted post impact for simulation of LRC experiment, Case 2 | 3-23 |
| 4-B. 1 | Plasma sterilizer research unit | 4-6 |
| 4-B. 2 | Test matrix | 4-7 |
| 4-B. 3 | Sample holders and chamber | 4-9 |
| 5-A. 1 | Viking sterilization cycle | 5-4 |
| 5-A. 2 | Influence of spore N_0 on heat survivors | 5-9 |
| 5-A. 3 | Influence of water concentration on heat survivors | 5-10 |
| I | Bend Recovery Mandrel with Filament | A-5 |
| II | Fatigue Testing | A-5 |
| III | Tufts of Fibres | A-5 |
| IV | Static Electricity and Abrasive Test Apparatus | A-5 |

FIGURES (contd)

| | | |
|-------|---|------|
| V | Tip of Unused Sable Hair (710X) | A-7 |
| VI | Middle of Unused Sable Hair (950X) | A-7 |
| VII | Middle of Used Sable Hair (1200X) | A-7 |
| VIII | Tip of Used Sable Hair (1100X) | A-7 |
| IX | Pony Hair (900X) | A-8 |
| X | Ox Ear Hair (480X) | A-8 |
| XI | Felor, Nylon Filament | A-8 |
| XII | Blunt Cut Tip Nylon 6/6 (200X) | A-8 |
| XIII | Mechanically Treated Felor Filament (200X) | A-10 |
| XIV | Abraded Sable Hair After Fatigue Testing (350X) | A-10 |
| XV | Split Sable Hair After Fatigue Testing (225X) | A-10 |
| XVI | Broken Sable Hair After Fatigue Testing (380X) | A-10 |
| XVII | Cracked Sable Hair (1000X) | A-12 |
| XVIII | Fatigued Felor (1500X) | A-12 |

TABLES

| | | |
|-------|---|------|
| 1-A.1 | Values of $P_{C/I}$ | 1-3 |
| 1-A.2 | Probabilities of Contamination JS-T Mission | 1-4 |
| 2-A.1 | Conversion Data for Electron Tests | 2-3 |
| 2-A.2 | Analysis of Variance of Electron Test Results | 2-4 |
| 2-A.3 | Resistance of Spacecraft Isolates to Electron Isolation. | 2-4 |
| 2-A.4 | Effect of Electron Radiation Environment on Survival of Spacecraft Isolates. | 2-6 |
| 2-A.5 | Percent Survival of Sporeformers Exposed to Electron Irradiation | 2-7 |
| 2-A.6 | Percent Survival of Nonsporeformers Exposed to Electron Irradiation. | 2-9 |
| 2-A.7 | Comparison of Pioneer 10 and JPL Test Matrix for Trapped Belt Electrons | 2-11 |
| 3-A.1 | Experimental Results: Particle Adhesion | 3-3 |
| 3-A.2 | Sample Output of Meteoroid Impact/Particle Release Program: Percent Removal for Glass Beads on 1/8 inch Al plate, 3×10^{-8} kg Cometary Meteoroid | 3-20 |
| 4-B.1 | Test Matrix | 4-8 |
| 4-B.2 | Percent Survival of <u>Bacillus Subtilis</u> Spores Due to Argon Plasma Exposure | 4-12 |
| 4-B.3 | Percent Survival of <u>Bacillus Subtilis</u> Spores due to 15 min Nitrogen Plasma Exposure | 4-13 |
| 4-B.4 | Percent Survival of <u>Bacillus Subtilis</u> Spores due to 15 min Oxygen Plasma Exposure | 4-14 |
| 4-B.5 | Percent Survival of <u>Bacillus Subtilis</u> Spores due to Helium Plasma Exposure | 4-15 |
| 4-B.6 | Temperature of Stainless Steel Planchets Immediately After 15 min Exposure to Helium Plasma, deg. C | 4-16 |
| 4-B.7 | Number of <u>Bacillus Subtilis</u> Spores Surviving 15 min Exposure to Helium Plasma | 4-18 |
| 5-A.1 | Thermal Resistance of Spores Collected on Teflon Ribbons - MSOB, KSC (1.2 mg/L water) | 5-4 |
| 5-A.2 | Thermal Resistance of Spores Collected on Teflon Ribbons - MSOB, KSC (1.2 mg/L water) | 5-5 |
| 5-A.3 | Thermal Resistance of Spores Collected on Teflon Ribbons - MSOB, KSC (0.01 mg/L water) | 5-5 |
| 5-A.4 | Thermal Resistance of Spores Collected on Teflon Ribbons - MSOB, KSC (0.01 mg/L water) | 5-6 |

TABLES (contd)

| | | |
|--------|--|------|
| 5-A. 5 | Thermal Resistance of Spores Collected on Teflon Ribbons — MSOB, KSC (2.4 mg/L water) | 5-6 |
| 5-A. 6 | Thermal Resistance of Spores Collected on Teflon Ribbons — VAB, KSC (2.4 mg/L water) | 5-7 |
| 5-A. 7 | Thermal Resistance of Spores Collected on Teflon Ribbons — VAB, KSC (0.01 mg/L water) | 5-8 |
| I | Brush Fibre Properties | A-11 |

SECTION I

PLANETARY QUARANTINE STRATEGIES
FOR
ADVANCED MISSIONS
(NASA No. 193-58-61-01)

| <u>Contents</u> | <u>Title and Related Personnel</u> |
|------------------------|---|
| Subtask A para. 1.1 | STRATEGIES FOR SATELLITE ENCOUNTER Cognizance: C. Gonzalez Associate Personnel: W. Stavro |
| Subtask B para. 1.2 | JUPITER ENTRY ANALYSIS Cognizance: C. Gonzalez Associate Personnel: W. Jaworski, A. McDonald |

1.1 STRATEGIES FOR SATELLITE ENCOUNTER

1.1.1 Subtask A Introduction

The objectives of this task are to determine the impact of satisfying satellite quarantine constraints on current outer planet mission and spacecraft designs; and to develop tools required to perform trajectory and navigation analyses for determining satellite impact probabilities.

1.1.2 Significant Accomplishments

1.1.2.1 Outer Planet Swing-by Missions. The investigation into the implications of planetary and satellite quarantines on outer planet swing-by and satellite encounter missions has been completed. Numerous JPL internal memoranda, as well as four papers (Ref. 1 to 4) were written during the time of investigation showing the major results of the effort. A summary of the general formulation and methodology of the study as well as the results, conclusions and recommendations is presented below.

The basic procedure that was followed throughout this study was such that it responded to NASA Document NHB-8020.12, "Planetary Quarantine Provisions for Unmanned Planetary Missions." The methodology used was the same as that used on previous Mariner and Pioneer missions.

For missions with multiple encounter (including satellites of planets), the formulation of the large impactable analysis can be generalized as follows:

$$P_{C_j} = (P_{C/I_j}) \sum_i P_{IMP_i} Q_{MM_{i+}} \quad (1)$$

where

P_{C_j} = the probability of contamination of planet (or satellite) j.

P_{C/I_j} = the probability of contamination of planet (or satellite) j, given impact.

P_{IMP_i} = the probability of impacting planet (or satellite) j due to errors in maneuver i .

$Q_{MM_{i+}}$ = the probability that an impact removal maneuver will fail if attempted at some time later than i , say $i+$.

The above calculated P_C for the specific satellite or planet must necessarily be less than or equal to the contamination constraint allocated to large impactables, which is part of the total contamination constraint dictated by the Planetary Quarantine officer.

A few words about the above parameters are appropriate at this point.

The values of P_{IMP_i} can be calculated once a specific nominal trajectory is given together with both the time and errors of a trajectory correction maneuver i to be performed. This mathematical procedure was available for the case of calculating the impact probabilities of planets. In the case of satellites, new procedures had to be developed during the course of this study, and are described in our COSPAR paper (Ref. 4). In essence, therefore, the calculation of this parameter is a trajectory and navigation task.

The determination of $P_{C/I}$ on the other hand involves several disciplines. The value of this parameter is a function of the planet or satellite characteristics (e.g. the atmosphere, to determine the probability of an organism surviving an atmospheric entry and growing on the surface or in the atmosphere) and the space environment (probability of surviving it), as well as the probability that they will be released. Representative values of $P_{C/I}$ for Jupiter and Saturn as well as their satellites are given in Table 1-A.1 for both the propulsion module (PM) and the mission module (MM). Further discussion of this parameter is given in Reference 5.

The parameter $Q_{MM_{i+}}$ has to be considered in the analysis because if a maneuver results in the spacecraft achieving an impact trajectory, this trajectory can still be corrected with a subsequent maneuver. The reliability of the midcourse engine therefore will dictate this value. In general, the

Table 1-A.1. Values of $P_{C/I}$

| | JUPITER | SATURN | SATELLITES |
|-------------------|-----------|-----------|------------|
| PROPULSION MODULE | 10^{-5} | 10^{-4} | 10^{-3} |
| MISSION MODULE | 10^{-3} | 10^{-2} | 10^{-1} |

probability of executing a maneuver shortly after a successful maneuver has been performed is 0.99. This means that, in general, $Q_{MM_{i+}}$ is 10^{-2} . Two points have to be made however regarding this parameter:

- 1) One may not be aware that the S/C is on an impact trajectory (because of ephemeris uncertainty) and might go for a long time before realizing that a corrective maneuver is needed. In this case the reliability deteriorates and $Q_{MM_{i+}}$ should be larger.
- 2) In considering the last planned maneuver in a mission, the assumption should be made a priori that there won't be any fuel left for a corrective maneuver, i. e. $Q_{MM_{i+}} = 1$.

The analysis of the ejecta efflux (small pieces of debris that may be shaken off the spacecraft) problem has also been performed. The methodology, analysis, results, conclusions and recommendations are documented in Ref. 6.

During the course of this study, numerous sample multiple outer planet missions were investigated. The most recent investigations concerned themselves with a Jupiter-Saturn mission with a Titan satellite encounter at Saturn, and a Ganymede satellite encounter at Jupiter. The calculated resulting P_C values for representative errors in the trajectory correction maneuvers are given in Table 1-A.2, together with representative P_C allocations. It is noted that in this case the P_C allocated for Titan is violated. The required biasing to satisfy this constraint will result in a 5 meter/sec penalty in the fuel load requirements (Ref. 7).

Table 1-A.2. Probabilities of Contamination JS- T Mission

| | P_C CALCULATED | P_C ALLOCATED |
|-------------------------|------------------------|-----------------------|
| JUPITER | 2.3×10^{-6} | 3.15×10^{-5} |
| SATURN | 1.0×10^{-5} | 6.35×10^{-5} |
| SATURN, INCLUDING RINGS | 1.9×10^{-5} | 6.35×10^{-5} |
| GANYMEDE | 5.5×10^{-7} | 3.15×10^{-5} |
| TITAN | $2.3 \times 10^{-4}^a$ | 6.35×10^{-5} |

^aViolation will require biasing, with a resulting 5 meter/sec penalty.

The major conclusions arrived at during the course of this study are summarized here:

- 1) Significant differences exist between planetary and satellite quarantine implications for outer planet missions. For example, trajectory correction maneuvers that result in a possible satellite quarantine violation are different from those violating planetary quarantine (Ref. 3).
- 2) Potential satellite quarantine violations are a strong function of the location of the aim-point of the spacecraft with respect to the satellite, especially when maneuver errors are highly elliptic (Ref. 4).
- 3) For ejecta efflux leaving the spacecraft, critical periods can be identified whenever the product of the spacecraft/sun/target angle and the sun/target distance is less than the target's planetary radius (Ref. 6).
4. Including Saturn's rings (to the D'ring) in the analysis of Saturn PQ will nearly double the P_C calculated (see Table 1-A.2), but is still less than the allocated P_C .

1.1.2.2 Outer Planet Orbiters. Recently, an effort was started to investigate the planetary/satellite quarantine constraint implications on outer planet orbiter missions. In particular, the mission selected is a planned 1981 Jupiter multi-satellite swing-by orbiter.

The characteristics of a multi-satellite encounter Jupiter orbiter pose some new and different criteria for PQ and SQ analysis. The typical such mission will last approximately one year, swinging by from satellite to satellite (10 to 15 encounters), performing numerous trajectory correction maneuvers (more than 15). After the mission is completed, the orbiter will presumably be placed in a specified terminal orbit.

It has been shown in a previous study (Ref. 8) that if an uncontrolled orbiter is placed in a typical orbit around Jupiter ($r_p > 3 R_J$, $r_a < 100 R_J$), with a low inclination, the probability that it will impact one of the satellites (or come close enough to one to be perturbed to impact the planet) is very high. Guaranteeing an orbit lifetime of 50 years becomes almost impossible. An orbit with a "critical" inclination is suggested to ease the problem, and if found to be true, will probably be the terminal orbit into which the orbiter will be placed after the mission is complete. Transfer to this high inclination terminal orbit will probably be achieved through the process of "cranking" (see Ref. 9).

From a PQ point of view, a study of the PQ implications of a Jupiter orbiter could be divided into three areas of concentration:

- 1) Study of the PQ allocation methodology for the various satellites to be encountered as well as for the planet itself. Having 3 or 4 encounters of the same satellite with one trajectory is a new mission sequence that hasn't been studied before in terms of PQ allocation methods.
- 2) An analysis of the basic one year mission in terms of probabilities of impacting the encounter satellites due to navigation errors (orbit determination, ephemerides, maneuver and other errors). An important aspect of this phase of the analysis is to study and determine the importance of maneuver reliability. The orbiter

being in a low inclination orbit will be analogous to a spacecraft being on a planet impact trajectory, since if control of the spacecraft maneuver capability is lost, the orbiter will very likely impact one of the satellites within the PQ period. Some analysis of the navigation aspects has already been done (Ref. 10).

- 3) Investigation of the post mission 'terminal' orbit in order to achieve a long lifetime to satisfy PQ and SQ requirements.

A preliminary investigation into the above areas of concern will be performed this year (FY74). It is recommended that for FY75, a more in depth analysis be performed in the second and third areas of concern mentioned above.

1.1.3 Future Activities

The activity for swing-by missions has been completed. The following future activities will be undertaken with reference to outer planet orbiters:

- 1) An analysis of impact probabilities due to navigation uncertainties.
- 2) An analysis of the maneuver reliability problem.
- 3) An investigation of terminal orbit characteristics.

1.1.4 Presentations

Gonzalez, C., and Stavro, W., "The Significance of Outer Planet Satellite Quarantine Constraints on Aim-Point Selection," Paper 73-553, AIAA/AGU Space Science Conference, Denver, Colorado, July 10-12, 1973.

Stavro, W., "Strategies for Satellite Encounter," presented at NASA Spacecraft Sterilization Technology Seminar, San Francisco, California, February, 1974.

1.1.5 References

1. Stavro, W., and Gonzalez, C., "Planetary Quarantine Considerations For Outer Planet Missions," Preprint No. AAS-71-122, AAS 17th Annual Meeting, Seattle, Washington, June 28-30, 1971.
2. Gonzalez, C., and Stavro, W., "Flight Path and Mission Strategies to Satisfy Outer Planet Quarantine Constraints," AAS No. 71-319, AAS/AIAA Astrodynamics Specialists Conference, Ft. Lauderdale, Florida, August 17-19, 1971.

3. Hoffman, A., Stavro, W., and Gonzalez, D., "Quarantine Constraints as Applied to Satellites," Paper L.7.9, 16th Plenary Meeting of COSPAR, Konstanz, W. Germany, May 23-June 6, 1973.
4. Gonzalez, C., and Stavro, W., "The Significance of Outer Planet Satellite Quarantine Constraints on Aim-Point Selection," Paper 73-553, AIAA/AGU Space Science Conference, Denver, Colorado, July 10-12, 1973.
5. Gindorf, T., and Hoffman, A., private communication.
6. Stavro, W., "Planetary Quarantine Ejecta Efflux Analysis for 77 MJS," TM 392-85; June, 1972.
7. Kohlase, C. E., "Preliminary Assessment of Planetary/Satellite Quarantine Constraints Upon MJS77 Trajectory Biasing and ΔV Requirements," EM 392-150; August, 1973.
8. Uphoff, C., "The Long-Term Motion of Artificial Jovian Satellites," Report No. 72-52, Analytical Mechanics Associates Inc., Nov., 1972.
9. Roberts, P., and Uphoff, C., "Jupiter Orbiter Orbit Cranking," EM 393-159, Aug. 23, 1973.
10. Beckman, J., and Smith, D., "The Jupiter Orbiter Satellite Tour Mission," Paper presented at the AAS/AIAA Astrodynamics Conference, Vail, Colorado, July 16-18, 1973.

1.2 JUPITER ENTRY ANALYSIS

1.2.1 Subtask B Introduction

The objective of the Jupiter atmospheric entry analysis subtask is to develop and use the tools to determine the thermal response characteristics of a typical spacecraft and related debris upon entry into the Jupiter atmosphere.

The previous report on the subject has presented the work done on thermal response of small particles, insulating blankets, antenna and supporting struts when the spacecraft passes through the free molecular regime of the atmospheric entry. It was determined that the spacecraft will break up due to heating at the boundary of the continuum flow regime whereupon the antenna, struts and blanket will disintegrate and burn away. The only survivors will probably be the science platform and bus which will enter the continuum flow regime.

In this report the thermal response of the science platform and part of the bus are discussed, and analytical as well as some test results are presented. In addition, the extended analysis on small particles that also covers entries into the atmosphere of Saturn is included.

1.2.2 Significant Accomplishments

The major part of the effort during this reporting period was concerned with determining the thermal response of the science platform. A typical ultraviolet spectrometer (uvs), a very complex instrument of the platform, was selected for a detailed thermal response analysis largely because of the abundance of plastic materials concentrated in the lower part of the instrument. Figure 1-B.1 schematically illustrates the location of these materials.

The plastic materials found within the instrument were: (1) G10 epoxy-fiberglass, (2) Castall, (3) Diallyl phthalate, (4) polycarbonate, and (5) teflon. Figure 1-B.2 provides the decomposition data on these materials needed for the analysis, and the legend explains their application in various parts of the instrument. The data itself was generated at JPL by testing the samples in a precision-type thermogravimometer where each sample was decomposed in a vacuum under constantly increasing heat and the loss of the sample weight was measured as a function of temperature.

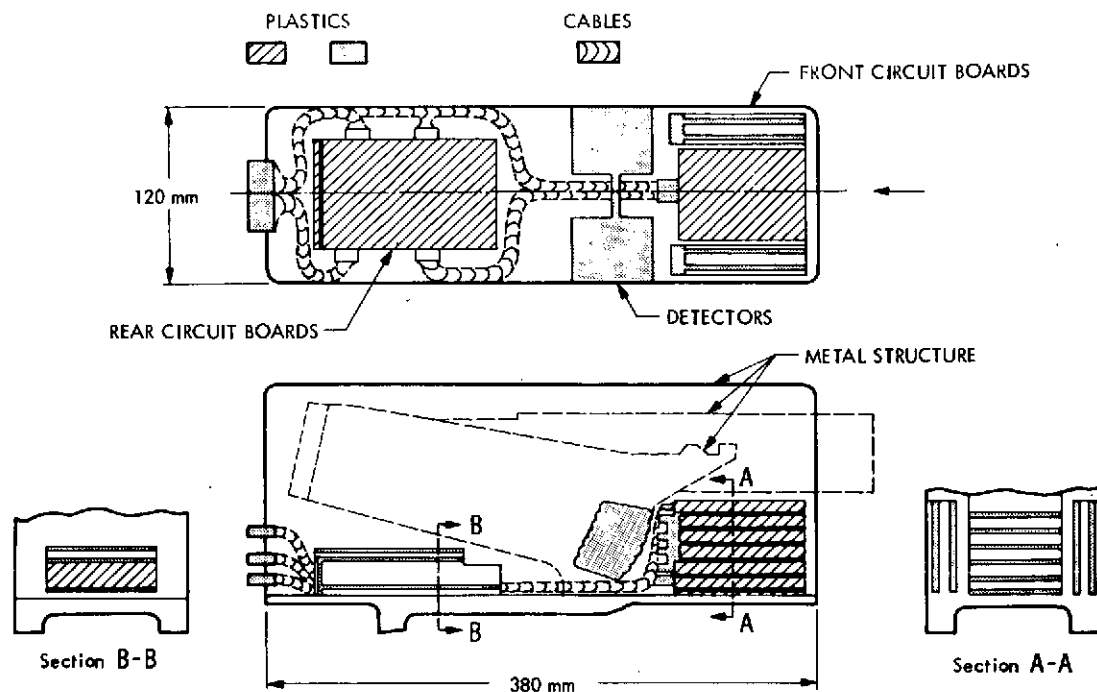


Fig. 1-B.1. Location of plastic materials in ultraviolet spectrometer

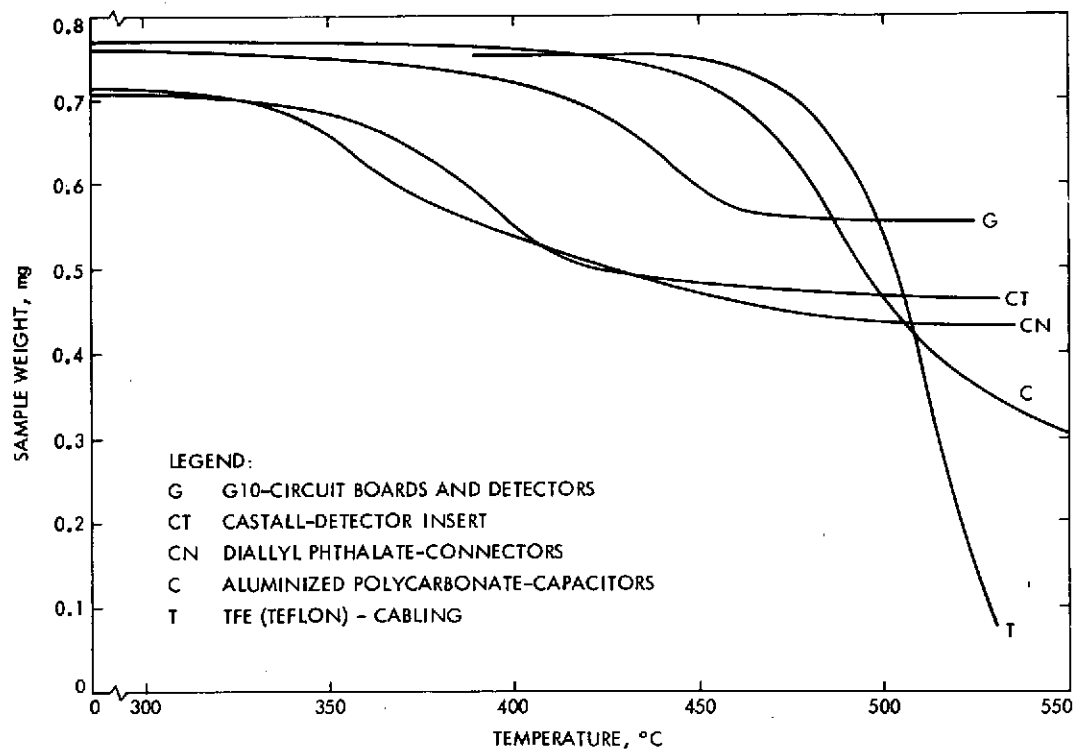


Fig. 1-B.2. Thermal decomposition of ultraviolet spectrometer plastics

In addition to the decomposition data, the thermophysical properties of the above materials as well as their chemical make-up were compiled or otherwise obtained by tests. The materials were also subjected to baking at 650° C in a specially designed vacuum-type oven. The latter was necessary to provide some knowledge on the materials' disintegration status at the melting temperature of aluminum, which constitutes a primary structure of the instrument.

The first item subjected to the analysis was the uvs cable consisting of copper wires insulated with teflon casing. A typical cable cross-section is depicted in Fig. 1-B.3. The cable is approximately 13 mm in diameter. The copper wires, teflon jackets, and voids between the cables are clearly shown. For the analysis it was assumed that the cable length was about 400 mm, and that its configuration was straight for the purposes of the analysis. This approach, although conservative with regard to the uvs instrument, was found to be justified when studying cable configurations in the spacecraft bus. Conservatively, entry along the cable axis was assumed.

The two cases analyzed (considered extremes) were -15° entry into the warm atmosphere and -90° entry into the cool atmosphere. It was assumed initially that teflon casing can be considered separately, and that the influence of the copper wires can be superimposed on the results obtained.

Figures 1-B.4 through 1-B.7 give the analytical results of teflon decomposition for the two entries. It is seen that in both cases only a part of the 400 mm long insulation will be disintegrated, and that the remaining length will not develop a temperature level to sterilize all of the undecomposed portions of the cable. The entry trajectory was followed down to cloud level in each case in order to establish the insulation status at that altitude.

To account for the effects of wire heating and melting on decomposition of the insulation, an ablation test was performed on a 240 mm long sample of the cable. Figure 1-B.8 shows a schematic of the test setup and the results obtained. An oxy-acetylene torch was used to ablate the wire and the insulation. The flame was moved from right to left at a rate corresponding to a complete ablation of the cross-section of the cable (teflon and wires combined). Dual

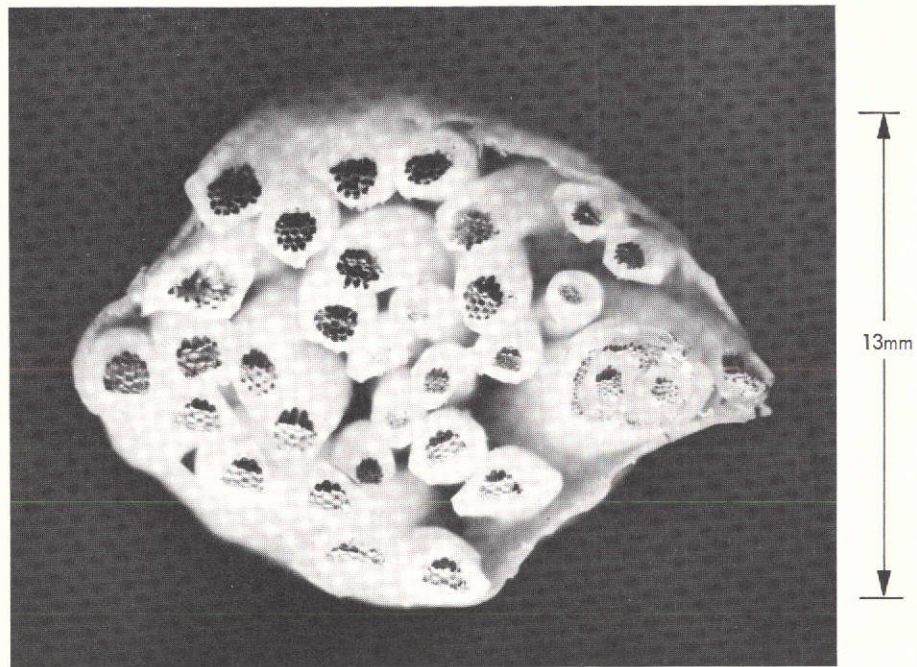


Fig. 1-B.3. Typical cable cross-section

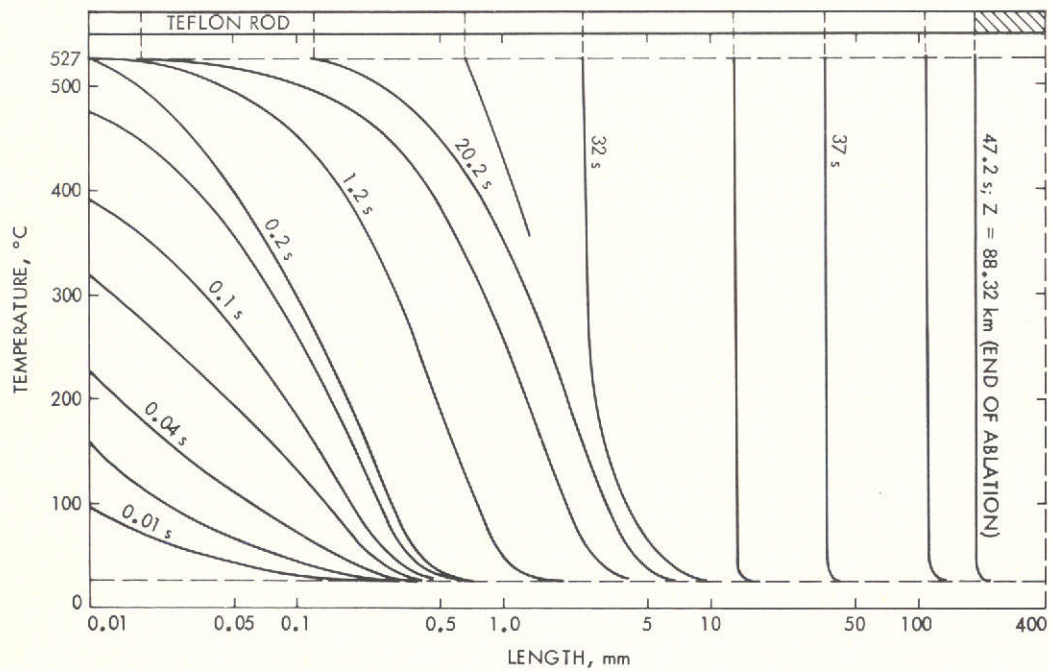


Fig. 1-B.4. Temperature profiles of a teflon rod for Jupiter entry at 15° entry angle: warm atmosphere, initial altitude = 750 km

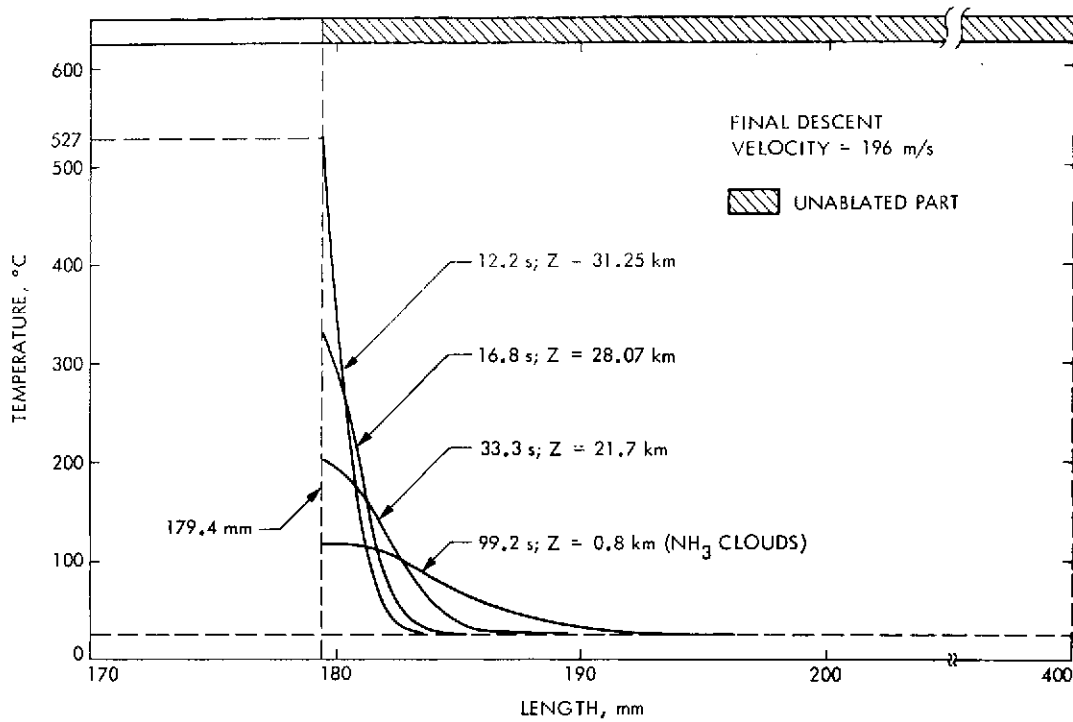


Fig. 1-B.5. Temperature profiles in unablated teflon:
entry at 15°, warm atmosphere

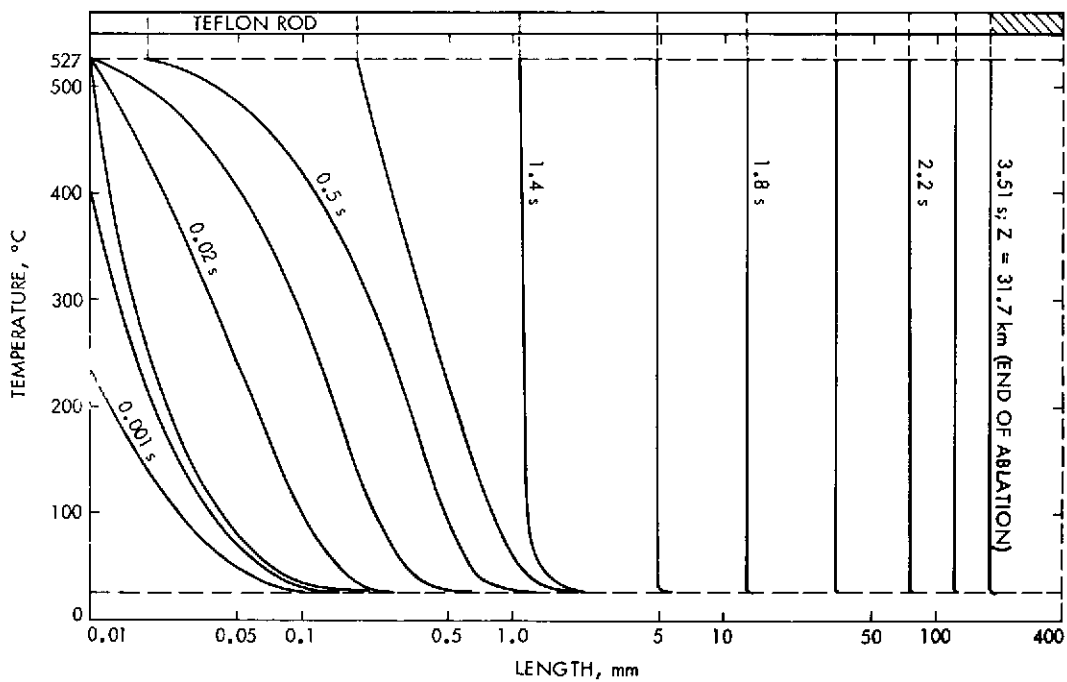


Fig. 1-B.6. Temperature profiles of a teflon rod for
Jupiter entry at 90° entry angle: cool atmosphere,
initial altitude = 200 km

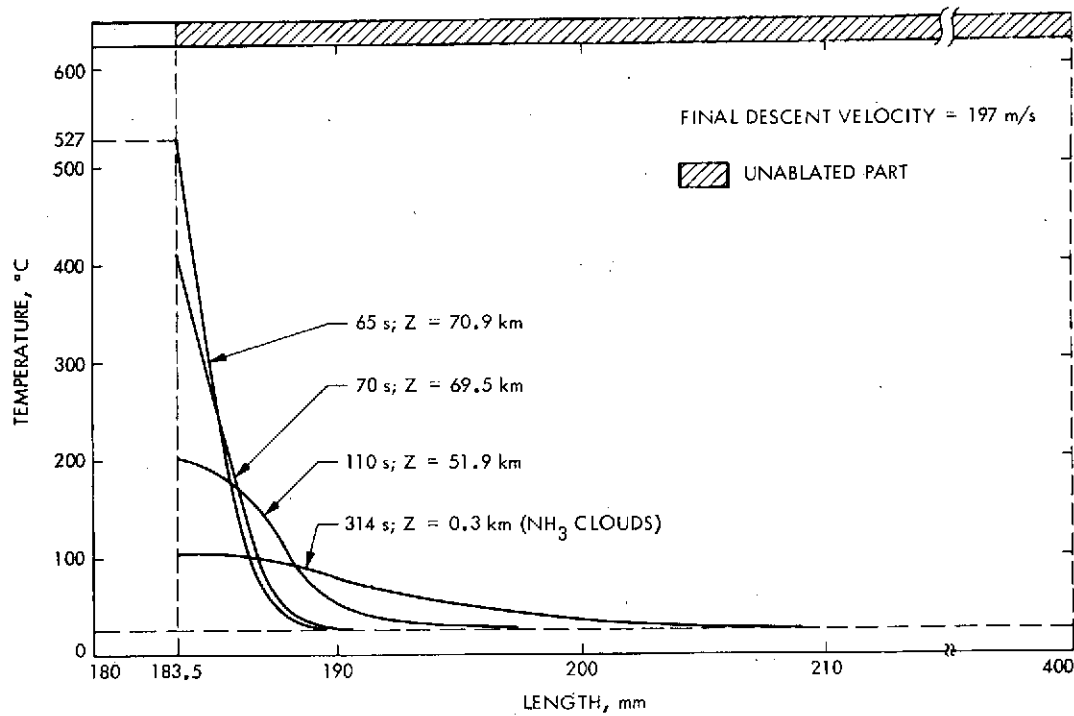


Fig. 1-B.7. Temperature profiles in unablated teflon:
entry at 90°, cool atmosphere

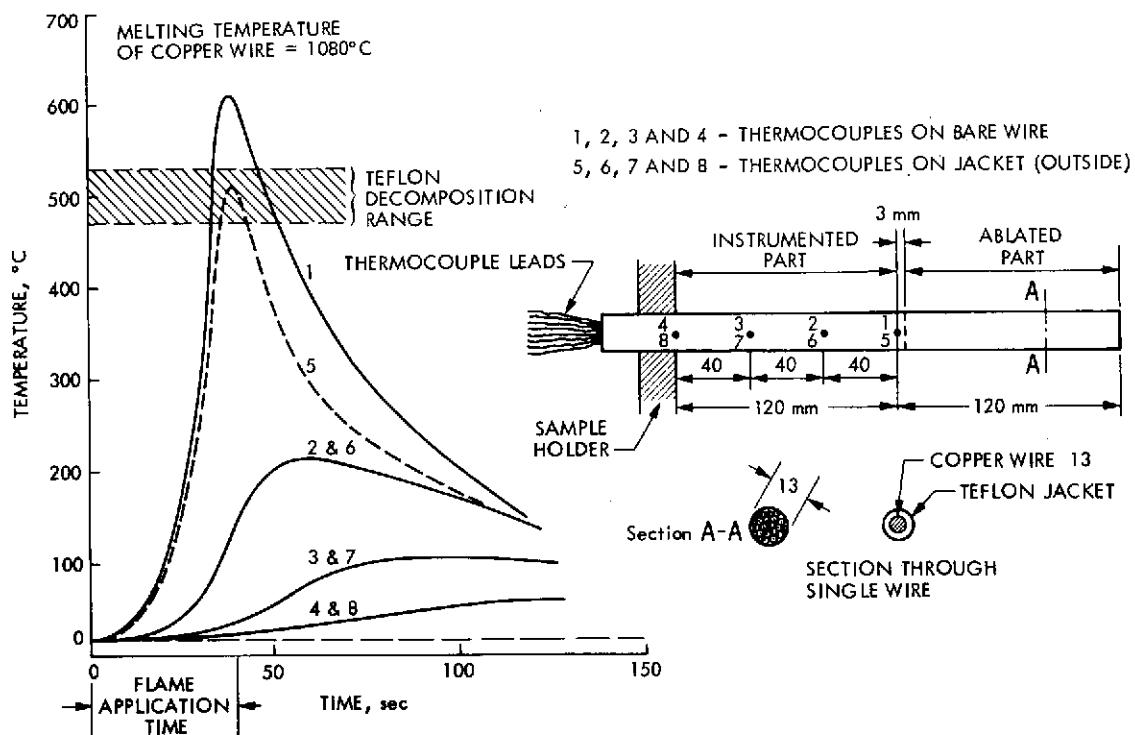


Fig. 1-B.8. Ablation test of teflon insulated cable

thermocouples have been installed at each indicated location on the center wire; one on the bare wire and the other on the outside of its insulation casing. The record of thermocouple temperatures is also shown in Fig. 1-B.8. Figure 1-B.9 shows the sample photographed from two sides. The upper picture shows the side where extra wire braiding is present (see Fig. 1-B.3), and the lower shows the side where singly insulated wires are bunched up. The bubbles on the end of the wires represent solidified melted copper. It is clear from Figure 1-B.8 that approximately 3 mm from the flame front (location of bubbles) the temperatures of the wire and the insulation were between 500 and 600°C, i. e., at the maximum temperature of teflon decomposition, registering only a small difference between them in spite of the closeness of melting of the wires where the temperature was 1080°C. The black residue on the sample is a carbon deposit from the oxy-acetylene flame.

It should be concluded that the presence of wires did not significantly affect the process of insulation decomposition, giving the analytical results described previously an adequate degree of validity. A test in a plasma arc jet, however, is needed to ascertain the influence of the side aerodynamic heating to arrive at a final conclusion of the cable survivability. An inspection of the

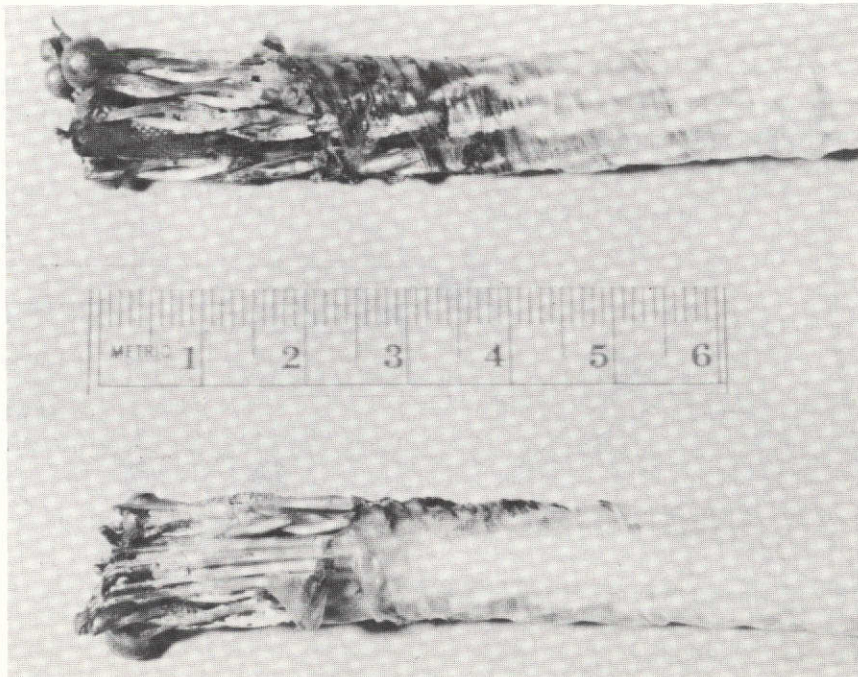


Fig. 1-B.9. Sample of ablated cable

spacecraft bus reveals that cable harnesses can be thicker and longer than the sample analyzed.

The next items collectively analyzed were circuit boards (cards) and detectors both made of G10 epoxy-fiberglass. Referring to Fig. 1-B.1, and assuming entry into the atmosphere to the right of the instrument schematic, a set of front circuit boards are followed by a bank of detectors and finally a set of the rear circuit boards. Each set will, in turn, be exposed to the heat pulse upon disintegration of the predecessor. It was assumed that the thin aluminum cover will instantly melt away, and that the rest of the aluminum structure, placed some distance away from the concentration of plastics, will also be melting and blown away ahead of the plastic disintegration. The melting of the aluminum very close to or adjacent to the plastic materials will be delayed due to heat blockage provided by the great amount of gas resulting from plastic decomposition. In short, the adjacent metal will be melting approximately with the speed of plastic decomposition, insuring some structural integrity during the process.

Figures 1-B.10 through 1-B.13 give the results of the analysis. In the case of -15° entry into the warm atmosphere, the data shows that all three plastic groups will be disintegrated, whereas in the case of -90° entry into the cool atmosphere the third group (rear circuit boards) will partially be decomposed. In the first case the fourth group was added to find out how far into the atmosphere disintegration could proceed. The data indicates (Fig. 1-B.10) that only some 12 mm of this group would disintegrate, and that in-depth temperature profiles in unablated material (Fig. 1-B.11) would not sterilize more than an additional 6 mm.

To evaluate in-depth temperature profiles for -90° cool atmosphere entry, two profiles at the end of recession are compared in Fig. 1-B.13. One profile is from Fig. 1-B.11 at 31.3 s and the other from the -90° cool atmosphere entry data. It can be concluded from this comparison that in the -90° cool atmosphere entry the temperature penetration will be shallower, leaving the unablated portion of rear circuit boards unsterilized.

The analysis of the parts of the Mariner Jupiter Saturn (MJS) spacecraft bus is currently underway. Figure 1-B.14 shows a typical bay unit assembly. Each bay has a different complement of electronics and their

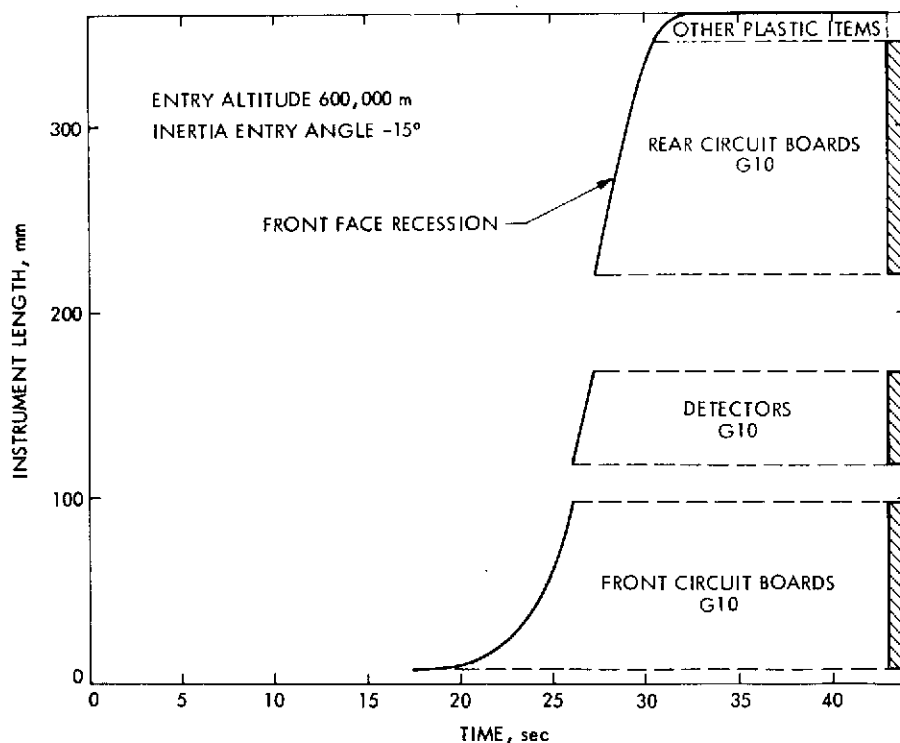


Fig. 1-B.10. Ultraviolet spectrometer disintegration of plastics due to heat of Jupiter entry: warm atmosphere

abbreviated names are indicated for reference purposes. It should be noted that a 500 mm straight cable harness is a part of the bay unit shown in Fig. 1-B.14.

Figure 1-B.15 shows a Mariner '71 cable harness in the spacecraft bus. The total length of the main cable is about 1.8 m (6 feet), and the cable thickness varies from about 10 to 25 mm. In addition, the cable harness has numerous branches at whose ends are heavily potted connector plugs. The situation here is far more complex than in the ultraviolet spectrometer. The branches of the bus harness may easily become steering fins which might tend to straighten or stabilize the entire harness during entry.

During this period, small particle heating calculations were done for two areas:

- 1) The effect of the increased heat transfer rate at low speed in free-molecular entry.

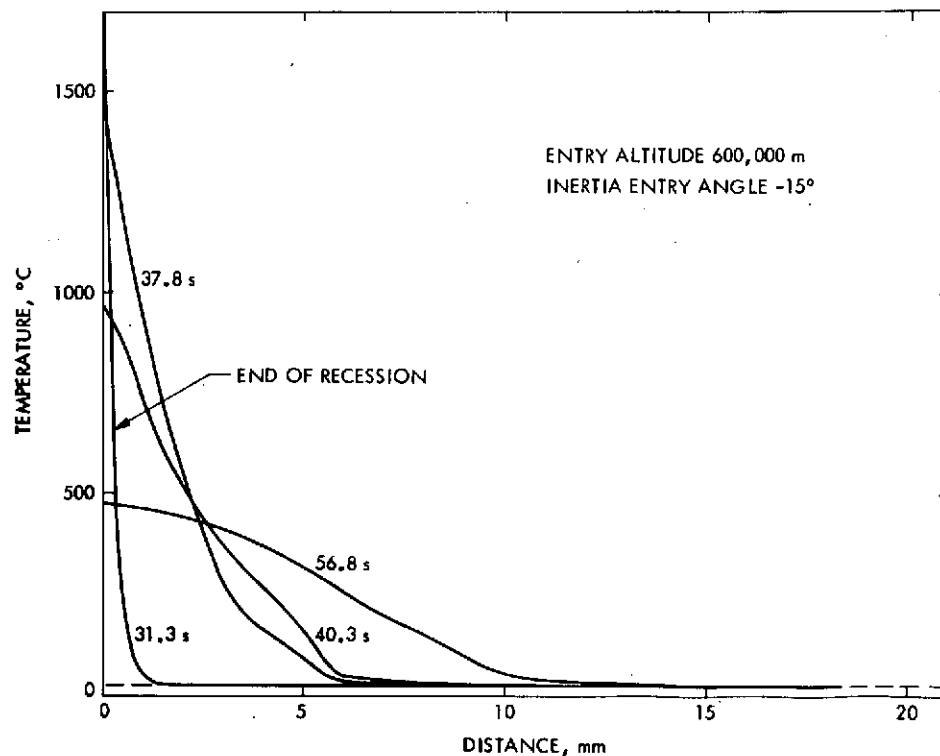


Fig. 1-B.11. Temperature profile in G10 plastic at the back of ultraviolet spectrometer for Jupiter entry: warm atmosphere

- 2) The contraction of the small size, small entry angle, non-sterilized corridor for particles liberated at successively greater levels of ambient atmospheric density.

Figure 1-B.16 shows features of a typical small particle entry into the Jupiter warm atmosphere, where this low-speed heating effect should be greatest. It can be seen that, although the heat transfer factor increases appreciably toward the end of the entry, the contribution to the PQ "kill" integral is very small. The increased heating factor is greatly overshadowed by the much reduced value of the available heating power, i. e., ρV_a^3 (Fig. 1-B.17).

Figure 1-B.18 shows the contraction of the survival entry corridor for Jupiter, which moves progressively toward smaller entry angle and smaller particle size with an increase of the atmospheric density at which the particle leaves the spacecraft. Similar calculations were performed for the other

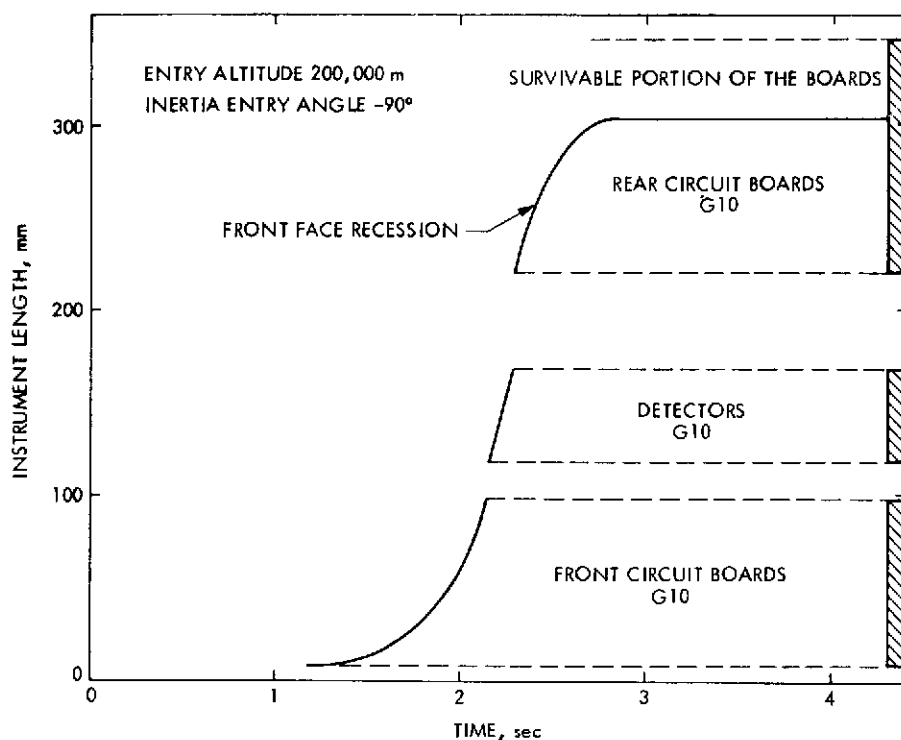


Fig. 1-B.12. Ultraviolet spectrometer disintegration of plastics due to heat of Jupiter entry: cool atmosphere

Jupiter atmospheres and for the three Saturn model atmospheres. Figure 1-B.19 shows this result for one of the Saturn calculations.

In addition, a first cut has been taken at determining the entry body and trajectory conditions likely to give least total heating for the major components of a spacecraft entering Saturn. Total convective plus radiative heating in the stagnation region, per unit mass, was calculated for bodies of different size and weight, in entry at 90° , 15° , and 3° into the three Saturn model atmospheres.

The main differences from the Jupiter case are:

- 1) The heating is always considerably less than the corresponding Jupiter case.
- 2) The radiative heating, which comes into play at large nose radius for heavy bodies, is a smaller fraction of the convective heating.

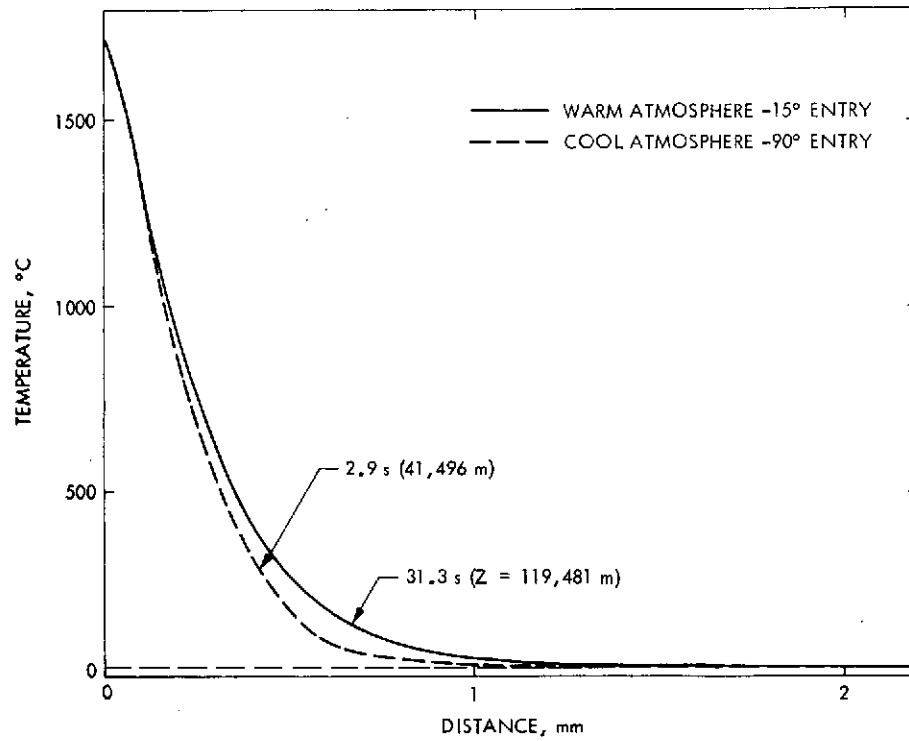


Fig. 1-B.13. Temperature profile in G10 plastic at the end of front face recession

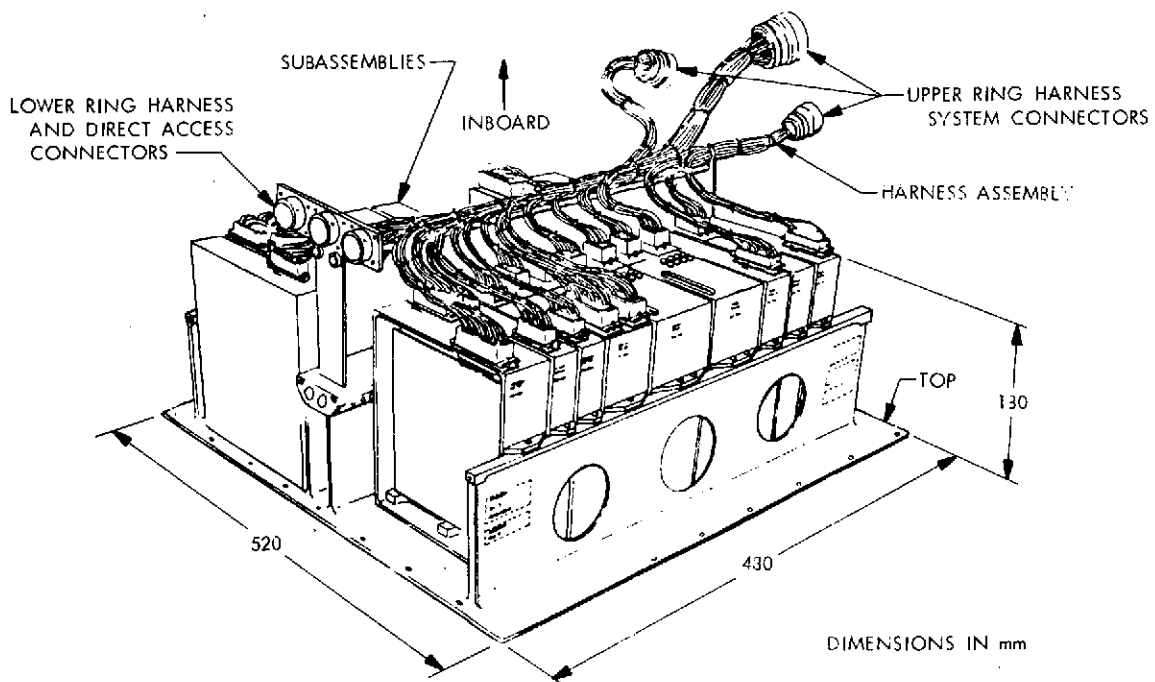


Fig. 1-B.14. Typical bus shearplate assembly

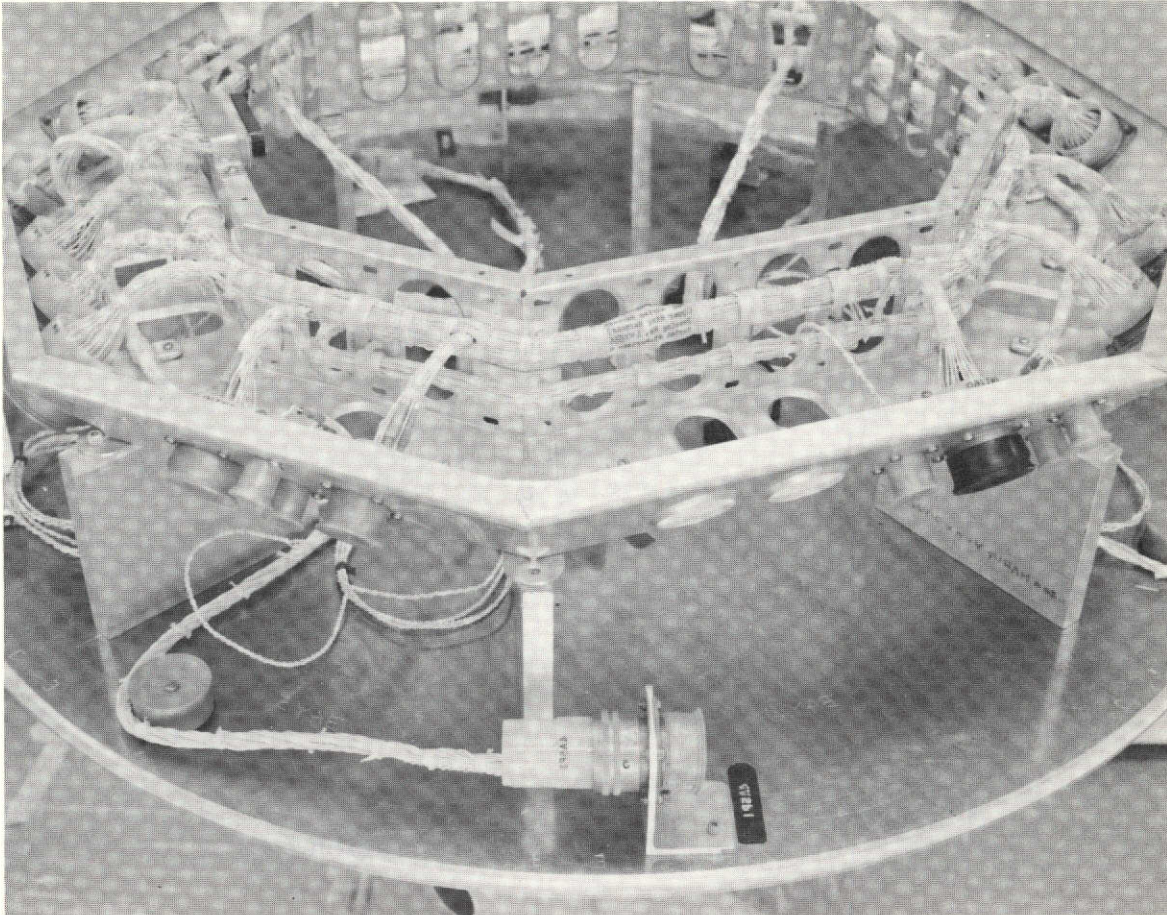


Fig. 1-B.15. Bus cabling assembly

- 3) The total heating at 15° entry is considerably less than at 90° and 3° , in contrast to the Jupiter case, where the result of a high heating rate for a short entry time at 90° entry is comparable to that of a low heating rate for a long entry time at 3° entry and is also comparable to the 15° entry case.

1.2.3 Conclusions

1.2.3.1 Jupiter — Large Impactables. In contrast to previous expectations, a possibility of survival of organisms which reside within the large impactables has been uncovered in the present analysis. The surviving remnants of plastic materials may descend down to the cloud level where conditions of growth are regarded as favorable.

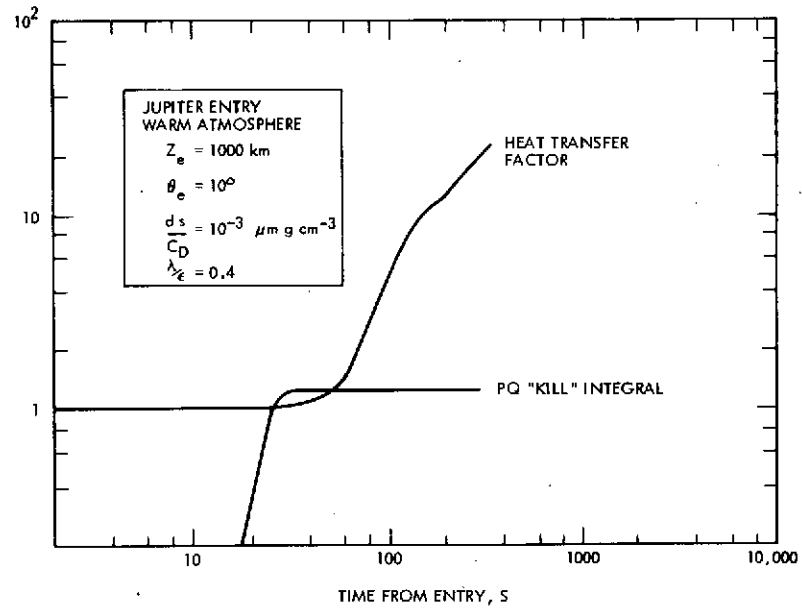


Fig. 1-B.16. Illustration of increase in PQ "kill" integral and transfer factor at low speed, in free-molecular flow

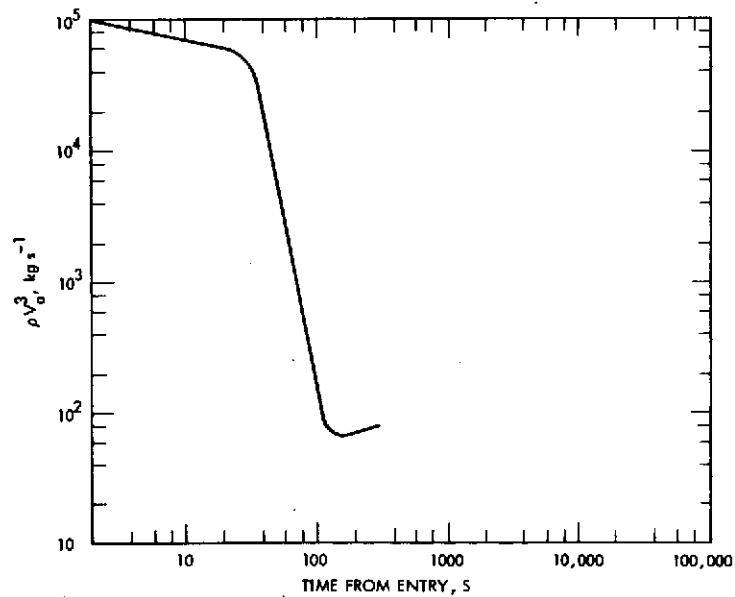


Fig. 1-B.17. Variation of ρV_a^3 with the time from entry; same case as Fig. 1-B.16

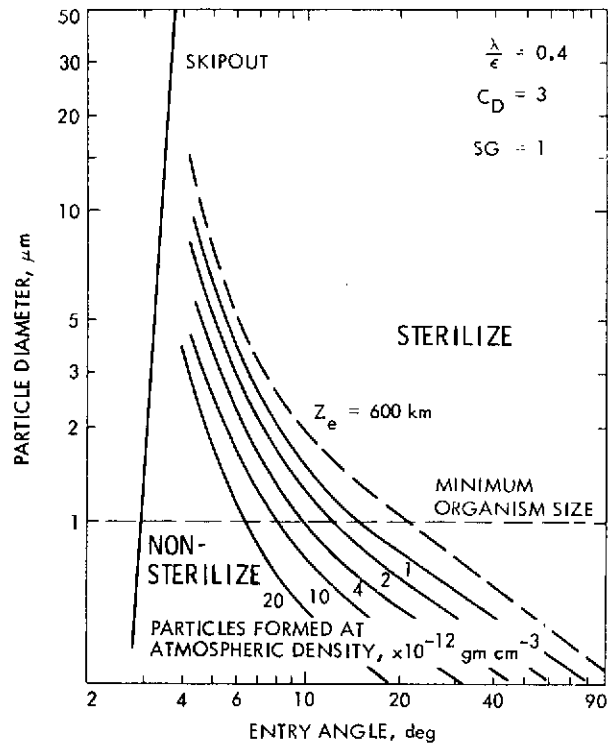


Fig. 1-B.18. Small particle survival corridors:
Jupiter nominal atmosphere

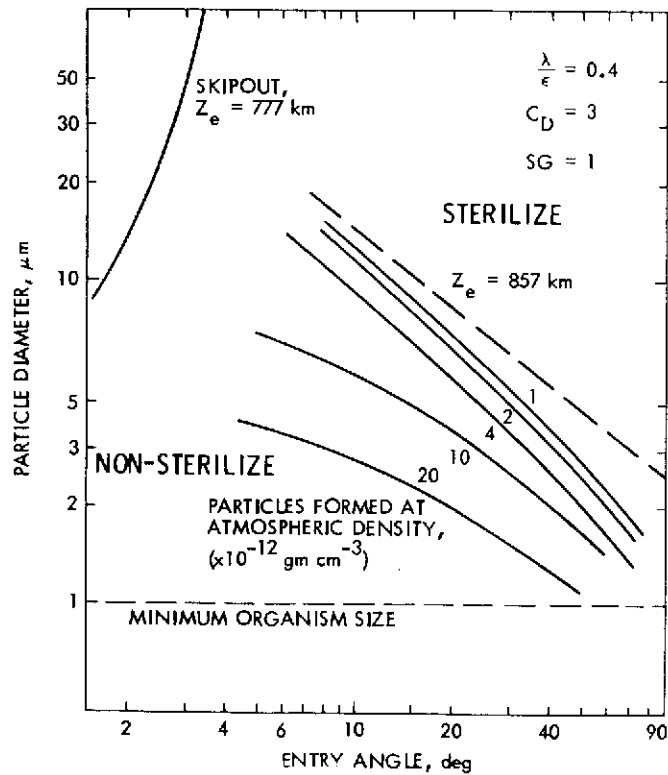


Fig. 1-B.19. Small particle survival corridors:
Saturn nominal atmosphere

One of the most critical components, due to their abundance on a typical spacecraft, are the cable harnesses which have a finite chance of surviving Jupiter entries without being sterilized. This is also true of circuit boards where microbial survival depends on their grouping, size and orientation; those placed in a series stand a better chance to survive. It has been shown that the last group of boards in the ultraviolet spectrometer may survive, in part, a -90° entry into the cool atmosphere. The results presented are also applicable to the elements of the spacecraft bus which have a similar design configuration to that of the UVS.

1.2.3.2 Jupiter - Small Particles. Small particles, which include spheres, flakes and needles with characteristic dimension in the range 1 to at least several hundred μm , have no chance of unsterilized entry into Jupiter. The exception is small particles entrained with a spacecraft at first entry, for which a narrow non-sterilizing entry corridor exists for a shallow entry. The entry corridor, spanning a size range of from 1 to about 30 μm at most, rapidly contracts if the particle liberation is delayed until ambient atmospheric density levels in the range 1 to $20 \times 10^{-12} \text{ gm cm}^{-3}$, vanishing for liberation at ambient atmospheric density levels above about $30 \times 10^{-12} \text{ gm cm}^{-3}$. Particles generated later from spacecraft break-up (mainly around a density level of about $10^{-9} \text{ gm cm}^{-3}$) have no chance of unsterilized entry.

1.2.3.3 Saturn - Large Impactables. Based on a cursory study of large impactable entry into the atmosphere of Saturn it is concluded that the components with the best chance of survival in Saturn entry are the heavy components with large nose radius entering at about 15° angle.

1.2.3.4 Saturn - Small Particles. The same general conclusions are obtained concerning survival of small particles during Saturn entry as for Jupiter except for displacement of entry corridors. The corridor for a particle vanishes when liberation occurs at ambient atmospheric densities of $50 \times 10^{-12} \text{ gm cm}^{-3}$.

1.2.4 Future Activities

The following future activities will be completed, based on a re-allocation of resources for the task:

- 1) Spacecraft bus analysis.
- 2) Application of the Jupiter study results to Saturn entries.

- 3) Generation of shock layer thermochemistry and radiative flux data for the case of entry into Titan.
- 4) Thermal response of spacecraft materials in Titan entries.

1.2.5 Presentations

Jaworski, W., "Jupiter Entry Analysis," presented at NASA Spacecraft Sterilization Technology Seminar, San Francisco, California, February, 1974.

SECTION II

NATURAL SPACE ENVIRONMENT STUDIES
(NASA No. 193-58-61-02)

| <u>Contents</u> | <u>Title and Related Personnel</u> |
|------------------------|--|
| Subtask A para. 2.1 | <p>EFFECT OF PLANETARY TRAPPED RADIATION BELT ON MICROORGANISMS</p> <p>Cognizance: D. Taylor C. Hagen (Bionetics)</p> <p>Associate Personnel: B. Anspaugh J. Barengoltz G. Simko (Bionetics) C. Smith (Bionetics) J. Yelinek (Bionetics)</p> |
| Subtask B para. 2.2 | <p>EFFECT OF SOLAR WIND ON MICROORGANISMS</p> <p>Cognizance: J. Barengoltz D. Taylor</p> <p>Associate Personnel: C. Hagen (Bionetics)</p> |
| Subtask C para. 2.3 | <p>EFFECT OF SPACE VACUUM ON MICROORGANISMS</p> <p>Cognizance: C. Hagen (Bionetics) D. Taylor</p> <p>Associate Personnel: R. Gildersleeve (Bionetics) G. Simko (Bionetics) C. Smith (Bionetics) J. Yelinek (Bionetics)</p> |
| Subtask D para. 2.4 | <p>PROBABILITY OF GROWTH IN PLANETARY ATMOSPHERE AND SATELLITES</p> <p>Cognizance: N. Divine D. Taylor</p> <p>Associate Personnel: R. Berkman</p> |
| Subtask E para. 2.5 | <p>EFFECT OF SOLAR ELECTROMAGNETIC RADIATION ON MICROORGANISMS</p> <p>Cognizance: M. Wardle D. Taylor</p> <p>Associate Personnel: C. Hagen (Bionetics) D. Ross J. Smith</p> |

2.1 EFFECT OF PLANETARY TRAPPED RADIATION BELT ON MICROORGANISMS

2.1.1 Subtask A Introduction

The objective of this subtask is to determine the effect of planetary trapped radiation belts on the survival of microorganisms associated with an unsterile spacecraft.

With flyby missions now planned for Jupiter and Saturn and possible Jupiter orbiters and probes, the trapped radiation belts may represent an environment lethal to microorganisms and thereby reduce the requirement for decontamination of spacecraft before launch.

The major components of planetary trapped radiation belts are electrons and protons. The approach of the present task is to evaluate possible biological effects of these belts by subjecting spacecraft microbial isolates to different energies, exposures, and dose rates of those particles.

2.1.2 Significant Accomplishments

2.1.2.1 Description of Study. During this report period the test matrix for 0.6 MeV electrons was completed. The completion of the 0.6 MeV electrons concludes that portion of the Natural Space Environment Studies dealing with planetary trapped radiation belt electrons. This report will discuss the effects of 0.6, 2, 12, and 25 MeV electrons on spacecraft isolates.

As with all the radiation studies, a spacecraft bacterial subpopulation (nine sporeforming and three nonsporeforming isolates) plus two comparative organisms, Staphylococcus epidermidis and spores of Bacillus subtilis var. niger, were exposed to electron radiation at different exposures, exposure rates, and electron energies with simultaneous exposure to a vacuum of 10^{-6} torr at -20 and 20°C.

2.1.2.2 Experimental Conditions.

1. Microbiology. The derivation, culture, and assay procedures for the test organisms were previously described in para. 3.2.1.2 of JPL Doc. No. 900-597, February, 1973.

2. Vacuum Equipment. Photographs, together with a description of the test facilities, were presented in para. 3.2.3.4 of JPL Doc. No. 900-484, 1 July-31 December 1970.

3. Radiation Equipment. The 0.6 and 2 MeV electrons were produced by a dynamitron, a direct current accelerator. The flux profile was established and the exposure was monitored with the use of Faraday cups. The 12 and 25 MeV electrons were produced by a LINAC operated at 15 pulses sec^{-1} and a pulse width of 2 to 3 μsec . The absolute fluence per pulse was established prior to each run with LiF thermoluminescent detectors (TLD). The magnitude and number of pulses in these maps and during the test runs was standardized by a center mounted PIN diode.

The bacterial isolates were exposed to 0.6, 2, 12, and 25 MeV electrons at 150, 300, and 450 krad (tissue) with dose rates of 30, 300, and 3,000 rad sec^{-1} .

Since the current model of the trapped radiation belt of Jupiter is given in terms of flux and energy, Table 2-A.1 presents conversion data for dose (krad) to fluence (particles cm^{-2}) and dose rate (rad sec^{-1}) to flux (particles $\text{cm}^{-2} \text{sec}^{-1}$) for electrons. As shown in Table 2-A.1 the highest dose rate with both 12 and 25 MeV electrons was slightly lower than the highest dose rate with the 0.6 and 2 MeV electron energies. This was the result of limitations in source capability.

2.1.2.3 Results. All reported data, expressed as geometric mean percent survivals, are based on data obtained from replication of each test condition four times. In addition, the data for each single replication is the geometric mean of three plate counts.

An analysis of variance performed on electron test results is shown in Table 2-A.2. All of the main effects (organism, temperature, dose, dose rate, and energy) were significant at the $P < 0.05$ level or greater.

The resistance of the spacecraft isolates together with the comparative organisms is shown in Table 2-A.3. Based on the Duncan Multiple Range test the relative resistance of the sporeforming spacecraft isolates was distributed into four groups. Isolates 16, 18, and 11 were the most resistant to

Table 2-A.1. Conversion Data for Electron Tests

| Energy, MeV | | Flux, $\text{cm}^{-2} \text{sec}^{-1}$ | Dose Rate, rad sec^{-1} | Fluence, cm^{-2} | Dose, krad (tissue) | |
|-------------|--------|---|-------------------------------------|------------------------------|------------------------|--------|
| Nominal | Actual | | | | Nominal | Actual |
| 0.7 | 0.6 | 9.1×10^8 | 30 | 4.5×10^{12} | 150 | 145 |
| | | 9.1×10^9 | 300 | 9.1×10^{12} | 300 | 290 |
| | | 9.1×10^{10} | 3000 | 1.4×10^{13} | 450 | 440 |
| 2 | 1.93 | 1×10^9 | 30 | 4.85×10^{12} | 150 | 145 |
| | | 1×10^{10} | 300 | 9.70×10^{12} | 300 | 290 |
| | | 1×10^{11} | 3000 | 1.45×10^{13} | 450 | 440 |
| 12 | 10.65 | 8.4×10^8 | 30 | 4.10×10^{12} | 150 | 145 |
| | | 8.4×10^9 | 300 | 8.20×10^{12} | 300 | 290 |
| | | 6.5×10^{10} | 2200 | 1.24×10^{13} | 450 | 440 |
| 25 | 23.40 | 7.0×10^8 | 30 | 3.50×10^{12} | 150 | 145 |
| | | 7.1×10^9 | 300 | 7.00×10^{12} | 300 | 290 |
| | | 5.4×10^{10} | 2200 | 1.07×10^{13} | 450 | 440 |

Table 2-A. 2. Analysis of Variance of Electron Test Results

| SOURCE OF VARIANCE | SPORES | | NONSPOREFORMERS | |
|--------------------|--------------------|---------|--------------------|---------|
| | DEGREES OF FREEDOM | F RATIO | DEGREES OF FREEDOM | F RATIO |
| ORGANISM (A) | 9 | * | 3 | * |
| TEMPERATURE (B) | 1 | * | 1 | * |
| DOSE (C) | 2 | * | 2 | * |
| DOSE RATE (D) | 2 | * | 2 | * |
| ENERGY (E) | 3 | * | 3 | * |
| AB | 9 | * | 3 | - |
| AC | 18 | * | 6 | * |
| AD | 18 | * | 6 | * |
| AE | 27 | * | 9 | * |
| BC | 2 | * | 2 | - |
| BD | 2 | * | 2 | * |
| BE | 3 | * | 3 | - |
| CD | 4 | - | 4 | * |
| CE | 6 | * | 6 | * |
| DE | 6 | * | 6 | * |
| ABC | 18 | - | 6 | * |
| ABD | 18 | - | 6 | - |
| ABE | 27 | - | 9 | - |
| ACD | 36 | * | 12 | - |
| ACE | 54 | * | 18 | * |
| ADE | 54 | * | 18 | - |
| BCD | 4 | - | 4 | - |
| BCE | 6 | * | 6 | - |
| BDE | 6 | * | 6 | - |
| CDE | 12 | * | 12 | * |
| ABCD | 36 | - | 12 | - |
| ABCE | 54 | - | 18 | - |
| ABDE | 54 | - | 18 | - |
| ACDE | 108 | * | 36 | - |
| BCDE | 12 | * | 12 | - |

*P < 0.05

Table 2-A. 3. Resistance of Spacecraft Isolates to Electron Irradiation

| ORGANISM | MEAN PERCENT SURVIVAL ¹ |
|-----------------|------------------------------------|
| SPORES | |
| 16 | 6.80 a |
| 18 | 6.61 a |
| 11 | 6.15 ab |
| 12 | 5.77 b |
| 13 | 5.60 b |
| 9 | 2.99 c |
| 8 | 2.93 c |
| 2 | 2.77 c |
| 1 | 2.49 d |
| BSN | 1.85 e |
| NONSPOREFORMERS | |
| 5 | 0.903 a |
| 4 | 0.039 b |
| 19 | 0.008 c |
| SE | 0.002 d |

¹ Mean followed by same letter not significantly different at P < 0.05

the test environments with mean percent survivals of 6.80, 6.61, and 6.15, respectively. Isolate 1 was the least resistant with a 2.49 percent survival which was, however, significantly higher than the 1.85 percent survival of the comparative organism, B. subtilis.

The relative resistance of the nonsporeforming spacecraft isolates is also presented in Table 2-A.3. Each percent survival was statistically different. Isolate 5 was the most resistant with a 0.903 percent survival and S. epidermidis, the comparative organism, the least resistant with a 0.002 percent survival.

Since in studies of this type a consideration of the resistance of the spacecraft total microbial population (and not the resistance of an individual isolate) is more helpful to the area of Planetary Quarantine, the resistance of spacecraft isolates, both sporeforming and nonsporeforming, were considered as groups. This consideration was based on several factors: 1) the frequency of occurrence of the individual sporeforming isolates and the individual nonsporeforming isolates were similar within the two groups; and 2) although there was a statistical difference existing between the mean percent survivals of the spacecraft isolates, the percent survivals, especially of the sporeforming isolates, approached a normal distribution.

The effects of the other environmental parameters (electron energy, dose, dose rate, and temperature) on the spacecraft isolates are shown in Table 2-A.4. The most effective electron energy was 2 MeV with sporeformers and 12 MeV with nonsporeformers. As would be expected, an increase in the dose resulted in a decrease in mean percent survival with both sporeformers and nonsporeformers. Changes in dose rate, while not as profound an effect as dose, were statistically different. The 300 rad sec^{-1} dose rate was the most effective with the sporeformers while $3,000 \text{ rad sec}^{-1}$ dose rate was the most effective with the nonsporeformers. Temperature affected both the sporeformers and nonsporeformers in a similar manner. Exposure to the radiation environments at 20°C resulted in a greater decrease in initial populations than exposure to the same environments at -20°C .

The mean percent survival of sporeformers exposed to electron irradiation is shown in Table 2-A.5. The test results were meaned across temperature with the resultant mean percent survival presented for dose versus

Table 2-A.4. Effect of Electron Radiation Environment on Survival of Spacecraft Isolates*

| | | Sporeformers | Nonsporeformers |
|---|--------|--------------|-----------------|
| Energy, MeV | 0.6 | 2.59 c | 0.0294 b |
| | 2.0 | 0.16 d | 0.0160 bc |
| | 12.0 | 6.90 b | 0.0107 c |
| | 25.0 | 9.68 a | 0.0980 a |
| Dose, krad | 150 | 20.96 a | 3.0660 a |
| | 300 | 3.91 b | 0.0284 b |
| | 450 | 0.77 c | 0.0002 c |
| Dose Rate, rad sec ⁻¹ | 30 | 4.46 a | 0.0411 a |
| | 300 | 3.65 c | 0.0402 a |
| | 3000** | 3.88 b | 0.0113 b |
| Temperature, °C | -20 | 4.94 a | 0.0719 a |
| | 20 | 3.21 b | 0.0098 b |
| *Survival fractions expressed as mean percent survivals. For each parameter reported the mean percent survival followed by the same letter not significantly different at $P < 0.05$. Sporeformers and nonsporeformers analyzed independently. **Dose rate for 12 and 25 MeV electron energies was 2200 rad sec ⁻¹ . | | | |

dose rate for each electron energy studied. Without exception the survival of the comparative organism, *B. subtilis*, was less than the mean survival of the spacecraft isolates. The 2 MeV electron energy with a single exception, the 150 krad exposure at 30 rad sec⁻¹, was the most effective energy studied. Initial populations were reduced approximately 1 log at 300 krad and 2 logs at 450 krad doses with 0.6, 2, and 12 MeV electrons. An approximate 1 log reduction of initial populations occurred at 450 krad dose with 25 MeV electrons.

Figure 2-A.1 shows the effect of dose and energy on the survival of spacecraft spore isolates. Electron energy became increasingly effective as the dose increased from 150 through 300 to 450 krad. The upturn of the

Table 2-A. 5. Percent Survival of Sporeformers Exposed to Electron Irradiation

| DOSE, krad | ENERGY, MeV | | | | | | | | | | | |
|---------------|---|-----------------|-----------------|----------------------------------|-----------------|------------------|----------------------------------|------------------|------------------|----------------------------------|------------------|------------------|
| | 0.6 | | | 2 | | | 12 | | | 25 | | |
| | DOSE RATE, rad sec ⁻¹ | | | DOSE RATE, rad sec ⁻¹ | | | DOSE RATE, rad sec ⁻¹ | | | DOSE RATE, rad sec ⁻¹ | | |
| | 30 | 300 | 3000 | 30 | 300 | 3000 | 30 | 300 | 2200 | 30 | 300 | 2200 |
| 150 | 19.21 ^a (7.61) ^b | 16.13 (7.98) | 17.60 (7.96) | 21.4 (11.73) | 11.40 (7.62) | 16.17 (10.81) | 34.46 (25.83) | 28.42 (23.60) | 33.50 (16.91) | 27.64 (30.02) | 29.12 (23.71) | 22.37 (14.92) |
| 300 | 2.47 (0.77) | 2.72 (0.54) | 2.97 (0.63) | 1.32 (0.53) | 0.77 (0.37) | 1.00 (0.40) | 8.92 (6.27) | 6.10 (3.92) | 8.78 (6.23) | 16.84 (12.41) | 15.26 (5.96) | 12.87 (8.19) |
| 450 | 0.53 (0.14) | 0.50 (0.05) | 0.61 (0.11) | 0.50 (0.12) | 0.07 (0.03) | 0.42 (0.06) | 1.26 (0.54) | 2.77 (1.12) | 1.08 (0.27) | 2.40 (0.91) | 5.16 (3.44) | 1.83 (0.45) |

^a Mean of spacecraft isolates^b *B. subtilis*

survival plane from 2 to 0.6 MeV electron energies was significant and implies that for the range of electron energies studied the most effective energy lies somewhere between 12 and 0.6 MeV.

Table 2-A.6 shows the percent survival of nonsporeformers after exposure to the electron irradiation environments. Initial populations were reduced at least 1 log during exposure to all the radiation environments studied. At the 150 krad dose at 30, 300, and 3000 rad sec⁻¹ the 2 MeV electron energy was the most effective of the energies tested; but with an increase in dose to the 300 and 450 krad the most effective electron energy was 12 MeV. The comparative organism, *S. epidermidis*, was more sensitive to the radiation environments than the mean of the nonsporeforming spacecraft isolates. The nonsporeforming spacecraft isolates were found to be considerably less resistant to the radiation environments than the sporeforming isolates.

Figure 2-A.2 shows the effect of dose and energy on spacecraft nonsporeforming isolates. As previously stated the electron energies were less effective at the lowest dose tested, 150 krad, than their effectiveness

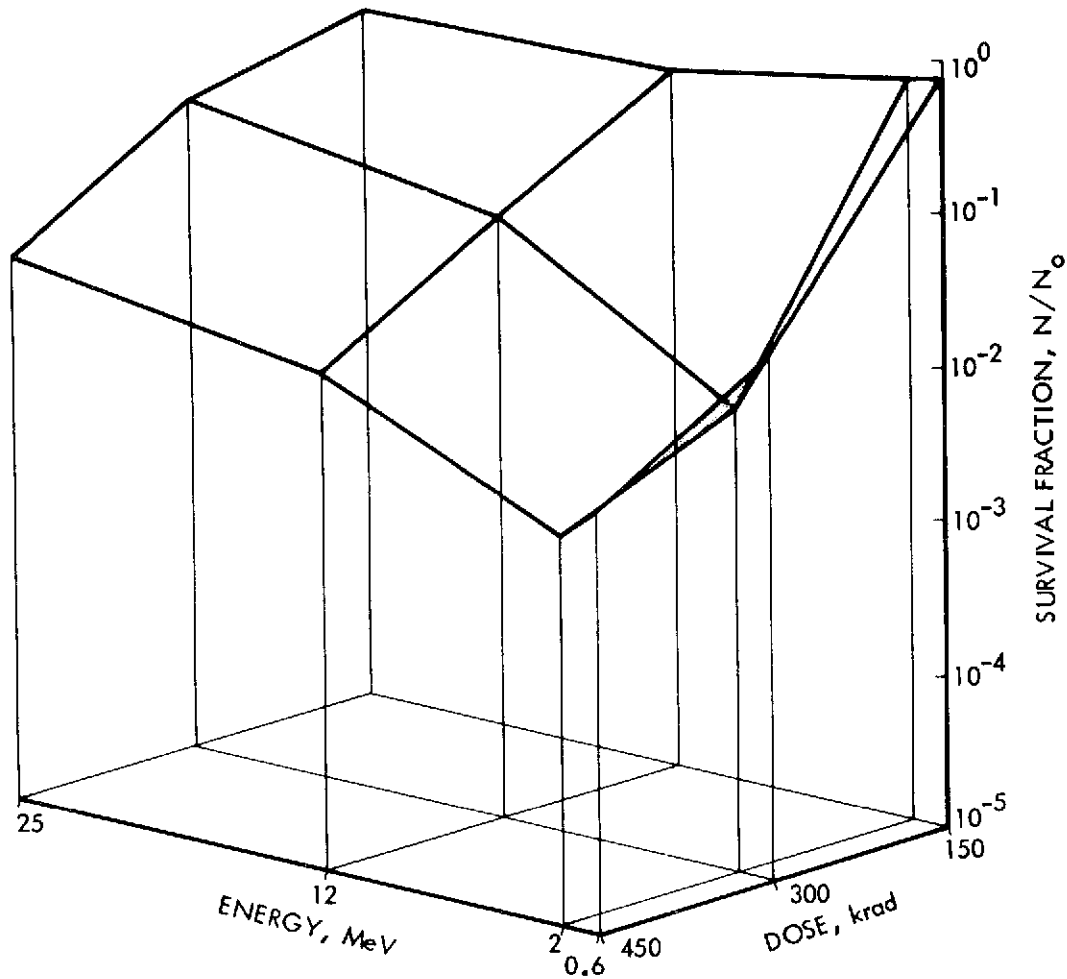


Fig. 2-A. 1. Effect of dose and energy on spacecraft spore isolates

at 300 and 450 krad doses. At the latter two doses tested the 12 MeV electron energy was the most effective energy tested. The upturn of the survival plane at a dose of 450 krad with 0.6 and 25 MeV energies is significant, which implies that for the electron energy range studied the most effective energy with nonsporeforming isolates lies between 0.6 and 25 MeV.

In summary a comparison of Pioneer 10 and JPL test matrix for trapped belt electrons is presented in Table 2-A. 7. Based on Pioneer 10 preliminary test results for electron energies equal to, or greater than, 3 MeV the peak flux observed during the mission was $5 \times 10^8 \text{ e cm}^{-2} \text{ sec}^{-1}$ (Ref. 1).

Table 2-A.6. Percent Survival of Nonsporeformers Exposed to Electron Irradiation

| EXPOSURE, krad | ENERGY, MeV | | | | | | | | | | | |
|-------------------|--|--------------------|-------------------|----------------------------------|--------------------|---------------------|----------------------------------|--------------------|---------------------|----------------------------------|----------------|---------------------|
| | 0.6 | | | 2 | | | 12 | | | 25 | | |
| | DOSE RATE, rad sec ⁻¹ | | | DOSE RATE, rad sec ⁻¹ | | | DOSE RATE, rad sec ⁻¹ | | | DOSE RATE, rad sec ⁻¹ | | |
| | 30 | 300 | 3000 | 30 | 300 | 3000 | 30 | 300 | 2200 | 30 | 300 | 2200 |
| 150 | 4.70 ^a (0.52) ^b | 7.16 (0.52) | 7.77 (2.43) | 2.21 (0.77) | 9.31 (1.03) | 2.14 (0.006) | 8.37 (0.56) | 7.45 (1.22) | 4.92 (2.97) | 9.37 (1.18) | 9.24 (4.04) | 0.79 (0.18) |
| 300 | 0.06 (0.0008) | 0.29 (0.00008) | 0.59 (0.002) | 0.31 (0.003) | 0.34 (0.0003) | 0.20 (0.00002) | 0.41 (0.42) | 0.04 (0.0004) | 0.008 (0.00003) | 2.60 (0.07) | 0.48 (0.07) | 0.05 (0.003) |
| 450 | 0.0006 (0.00003) | 0.003 (0.00001) | 0.01 (0.00003) | 0.001 (0.00002) | 0.006 (0.00004) | 0.0004 (0.00001) | 0.0002 (0.00002) | 0.001 (0.00001) | 0.0002 (0.00001) | 0.01 (0.0004) | 0.15 (0.02) | 0.0002 (0.00001) |

^a Mean of spacecraft isolates

^b S. epidermidis

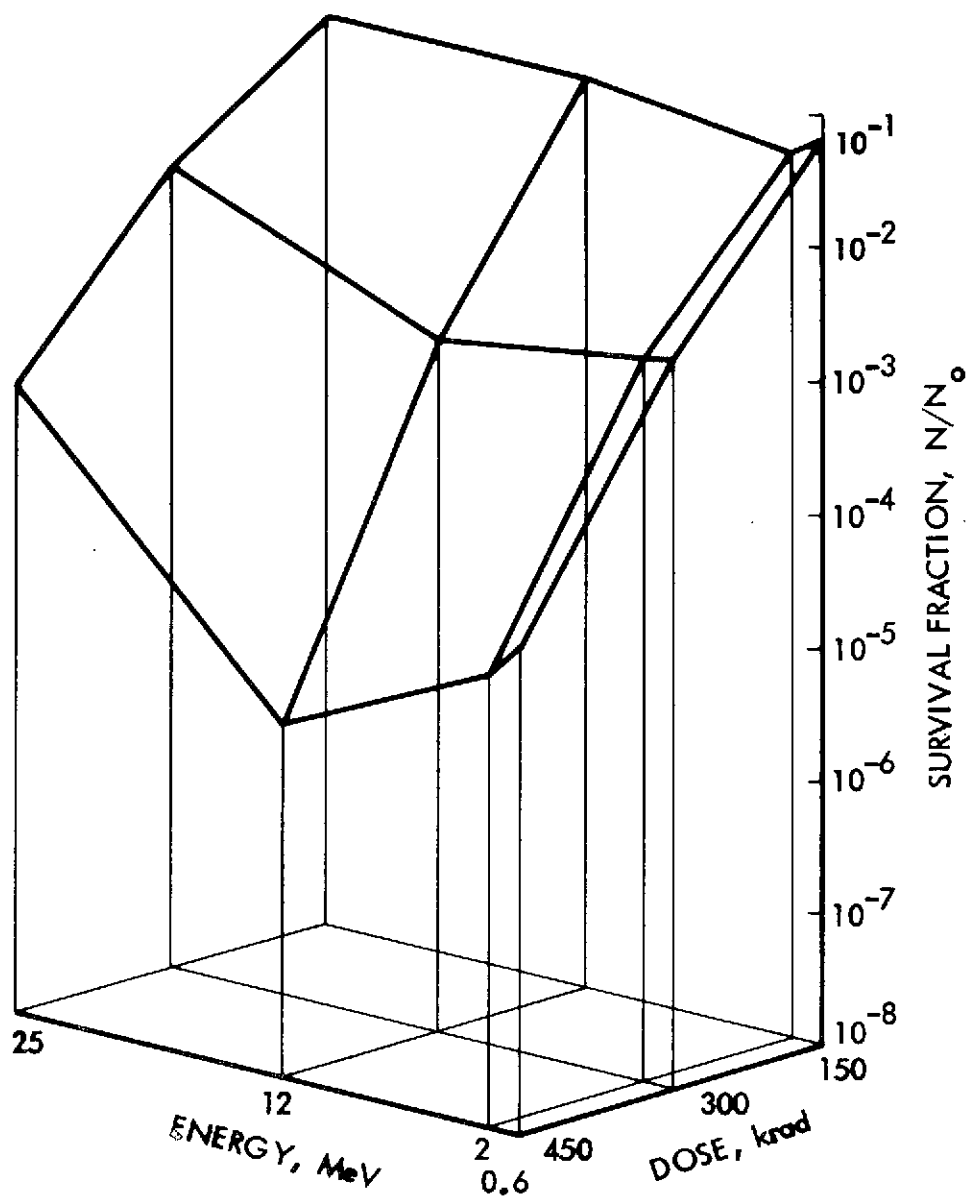


Fig. 2-A. 2. Effect of dose and energy on spacecraft nonsporeformer isolates

The total fluence observed during the mission was $1.5 \times 10^{13} \text{ e cm}^{-2}$ (Ref. 2). Selecting a particular electron energy studied in the JPL test matrix, 2 MeV for example, the fluxes used were 10^9 , 10^{10} , and $10^{11} \text{ e cm}^{-2} \text{ sec}^{-1}$ with fluences of 5×10^{12} , 1×10^{13} , and $1.5 \times 10^{13} \text{ e cm}^{-2}$ for each flux tested.

Because of the similarity and overlapping of the Pioneer 10 data with that of the JPL test matrix, the implication of the JPL test results is that, for

Table 2-A. 7. Comparison of Pioneer 10 and JPL Test Matrix for Trapped Belt Electrons

| | |
|--|--|
| ● PIONEER 10 PRELIMINARY RESULTS: | $E \geq 3 \text{ MeV}$ |
| ● PEAK FLUX OBSERVED: ^a | $5 \times 10^8 \text{ e cm}^{-2} \text{ s}^{-1}$ |
| ● TOTAL FLUENCE OBSERVED: ^b | $1.5 \times 10^{13} \text{ e cm}^{-2}$ |
| ● JPL TEST MATRIX: | $E = 2 \text{ MeV}$ |
| ● FLUX: | $10^9, 10^{10}, 10^{11} \text{ e cm}^{-2} \text{ s}^{-1}$ |
| ● FLUENCE: | $5 \times 10^{12}, 1 \times 10^{13}, 1.5 \times 10^{13} \text{ e cm}^{-2}$ |

^a Simpson, J. A., et al., Science 183, pp. 306-309, 1974

^b Divita, E. L., private communication

missions similar to Pioneer 10, a 1 log reduction of the spacecraft surface microbial burden could occur. With the generation of spacecraft debris that would be exposed to the radiation environment for longer periods of time, the reduction in surface microbial burden could be several orders of magnitude higher.

2.1.3 Future Activities

The future activities of this task area will be to investigate the effects of high energy protons, similar to those present in planetary trapped radiation belts, on the survival of microorganisms. Other activities will be involved with the analyses of data and subsequent modeling of the radiation sensitivity of microbial populations that would allow evaluation of radiation environments, encountered by future spacecraft missions, on the survival of spacecraft surface

microbial populations. Additional activities will be to evaluate the effect of secondary radiation on the survival of microorganisms. This activity could become an important factor for future orbiter-type missions because, if it is found that forms of secondary radiation effectively reduce the internal microbial burden of spacecraft, then the orbiter lifetime could be proportionately reduced to avoid violating planetary quarantine constraints for a particular mission.

2.1.4 Presentations

Hagen, C., "Effect of Planetary Trapped Radiation Belt on Microorganisms (Electrons)," presented at NASA Spacecraft Sterilization Technology Seminar, San Francisco, California, February, 1974.

2.1.5 References

1. Simpson, J. A., et al., Science 183, pp. 306-309, 1974.
2. Divita, E. L., private communication.

2.2 EFFECT OF SOLAR WIND RADIATION ON MICROORGANISMS

2.2.1 Subtask B Introduction

The objective of this subtask is to determine the effect of solar wind radiation on microorganisms associated with nonsterile spacecraft.

This study is directed towards determining the reduction in spacecraft associated microbial burden attributable to solar wind radiation.

The approach does not attempt a simulation of the total radiation environment, but rather an examination of the effect of low energy electrons and protons as a function of fluence and energy. The data acquired would apply to all missions.

2.2.2 Significant Accomplishments

Preliminary tests to determine the effect of 100 eV electrons on bacterial spores have been conducted. No effect was observed at fluences as high as $3 \times 10^{15} \text{ cm}^{-2}$, corresponding to an average exposure at 1 AU of 0.1 year (all energies included).

A literature search has shown that the fluence expected to produce a measurable biological effect at energies below 300 eV may be as large as 10^{17} cm^{-2} . However, at higher energies the electrons become increasingly lethal; e.g., for 1.5 keV electrons incident on B. subtilis (Marburg strain), D_{37} is $2 \times 10^{14} \text{ cm}^{-2}$ (Ref. 1).

Accordingly, an inquiry into the abundance of high energy electrons ($E > 1 \text{ keV}$) in the solar wind has been in progress. A large degree of uncertainty exists. However, one model and one set of data have been used, together with experimental data on the energy and fluence dependence of the radio-sensitivity of B. subtilis, to estimate the survival fraction. The result for a 1 year exposure at 1 AU is in the range 0.1 to 2×10^{-7} for the survival fraction, depending on the environment assumed.

2.2.3 Future Activities

Design and procurement of an electron source capable of 1 to 5 keV electrons. Conduct a study with spacecraft isolates in a matrix of energy, exposure, and rate. Conduct an analogous study with naturally occurring organisms.

Plan and conduct a proton test program.

2.2.4 Presentations

Barengoltz, J. B., "Effect of Solar Wind Radiation on Microorganisms," presented at NASA Spacecraft Sterilization Technology Seminar, San Francisco, California, February, 1974.

2.2.5 References

Davis, M., Arch. Biochem. and Biophys. 48, pp. 469-481, 1954.

2.3 EFFECT OF SPACE VACUUM ON MICROORGANISMS

2.3.1 Subtask C Introduction

This study was designed to examine the combined effects of space vacuum and spacecraft temperatures on the survival of microorganisms. The scope of study has changed slightly and incorporates into the test matrix the higher temperatures that will be experienced by the Viking solar panels (Ref. 1). In addition, the number of MM'71 spacecraft isolates normally used were reduced to five sporeformers and one nonsporeformer. The sporeformer, Bacillus subtilis var. niger, and the nonsporeformer, Staphylococcus epidermidis ATCC 17917, were included in the tests for comparative purposes.

2.3.2 Significant Accomplishments

The microbial subpopulation from MM'71 spacecraft was exposed to simulated space vacuum of 10^{-7} torr at temperatures of 55, 65, and 75°C for periods of 7, 14, and 28 days.

A partial examination of data indicates a dependency upon duration of exposure, isolate, and temperature. As an example, the 28-day vacuum survival at 55°C ranged from approximately 1 to 30 percent whereas comparable survival at 75°C ranged from approximately 0.002 to 5 percent. The comparative organisms, B. subtilis and S. epidermidis, were found to be among the more sensitive of the organisms tested.

2.3.3 Future Activities

Future activities of the vacuum temperature task will be to complete the present studies, including data analysis, on cultured spacecraft isolates. Additional activities will be to initiate studies to investigate the thermal vacuum resistance of naturally occurring (uncultured) microbial populations present in spacecraft assembly areas.

2.3.4 References

Wang, J., private communication.

2.4 PROBABILITY OF GROWTH IN PLANETARY ATMOSPHERE AND SATELLITES

2.4.1 Subtask D Introduction

The objectives of this subtask are to relate environmental parameters affecting microbial growth to conditions present in the atmospheres of Jupiter and Saturn, and to identify and study satellites of Jupiter and Saturn having possible biological interest.

2.4.2 Significant Accomplishments

2.4.2.1 Titan Atmosphere Update. This material builds on earlier work on the first of these two objectives, namely model atmospheres and probability of growth considerations for Jupiter and Saturn. It addresses the second of these objectives, namely to identify and study satellites of Jupiter and Saturn having possible biological interest. Among the satellites, Titan, Saturn's largest satellite, has been known for a long time to possess a substantial atmosphere and is thus a prime candidate for biological interest. Basic to this work are the composition and structure of Titan's atmosphere.

A workshop on the atmosphere of Titan was held at Ames Research Center in July, 1973, with about a dozen scientists participating, all having made some contribution to a subject previously receiving only occasional attention in the astronomical literature. Consensus was obtained on several physical parameters, namely a radius and mass considerably larger than the moon's, a gravity comparable to the moon's, and a very cold effective temperature (at 10 AU from the Sun). Intensive consideration was devoted to analysis of the spectroscopic and infrared observations, and to theoretical derivations concerning the atmosphere. The only gas molecule identifiable in the spectra is methane, but there may be other major constituents, namely hydrogen, nitrogen or argon. Water and ammonia may occur in the warmer regions of the atmosphere inaccessible to direct observations with present techniques. The data also place various constraints on atmospheric variables, for example that surface pressures and temperatures exceed 20 millibars and

80 degrees Kelvin respectively. Several related topics were also discussed at the workshop, notably recommendations for additional observations of Titan from the Earth.

Although the workshop did not derive model atmospheres for Titan, it did choose several likely compositions and pairs of pressure-temperature points as well as consider various theoretical aspects of model atmospheres. The profiles of temperature (abscissa) and pressure (ordinate, corresponding to height above Titan's surface) shown in Fig. 2-D. 1 include the points and theory from the workshop. The solid line represents the nominal atmospheric model and corresponds to a pure methane atmosphere (mean molecular weight $\mu = 16$ gram/mole). The dashed lines represent extreme atmosphere profiles ("Heavy" composition, with $\mu = 26$, and "Light" composition, $\mu = 6$). Two regions are of interest here. In the upper atmosphere, at pressures near 1 mb, peak deceleration and heating will occur for spacecraft or debris entering the atmosphere; in this region the atmospheric structure has an important effect on the survivability of organisms through the heating profile. In particular, the density scale height in the region is large, of the order of 60 ± 20 km.

In the lower atmosphere (for pressures exceeding 1 atmosphere) a shaded region is shown. This region represents the intersection of the Titan atmospheric profiles with approximate limits on pressure and temperature for survival and growth of terrestrial organisms. This region, a few hundred kilometers thick, is the one within which a high probability of growth occurs, relative to other outer solar system environments.

Note that no surface (that is, an upper bound on the pressure) is shown for this set of Titan atmosphere profiles. This occurs because present data do not establish surface pressure, but are consistent with either a thin atmosphere or a thick atmosphere; that is, surface pressures equal to or greater than 20 mb. The profiles shown here could thus be terminated by a surface anywhere below the level at 2×10^3 N/m² pressure. The growth region lies completely within those portions of the atmospheric profiles inaccessible to observation with present astronomical techniques. In this region several concerns affect growth. One of these is atmospheric dynamics

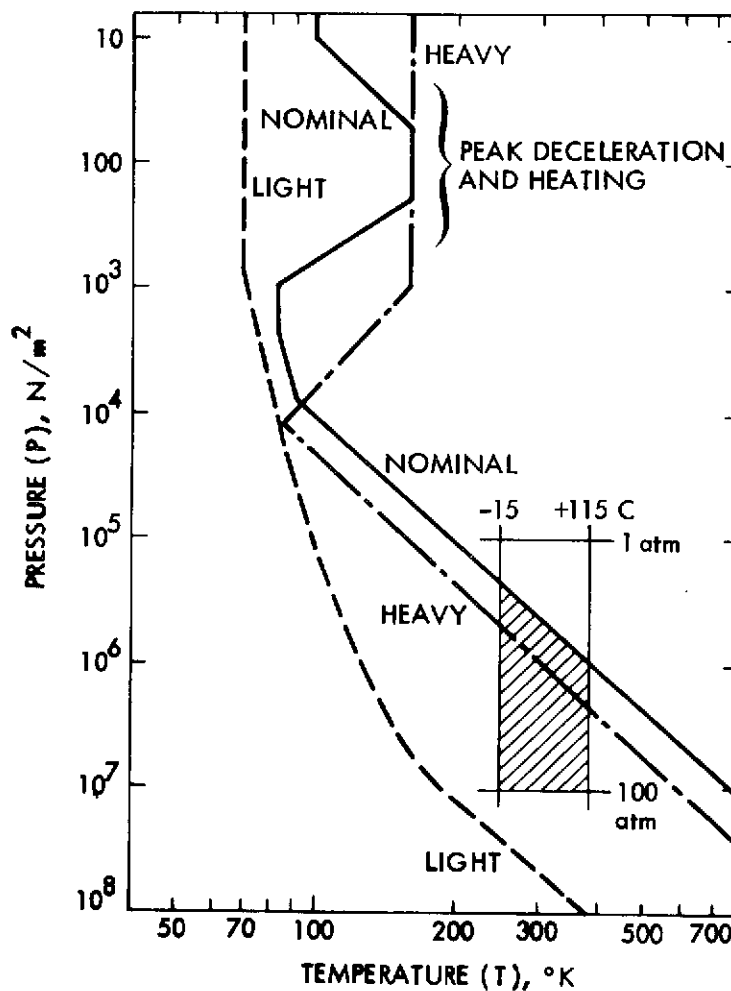


Fig. 2-D.1. Pressure-temperature profiles of engineering models of Titan's atmosphere

(winds, weather, and other temporal and local variations), expected to be subdued on Titan because of its slow rotation (period 16 days). Another is the likelihood of condensates.

The profiles are partially reproduced in Fig. 2-D.2, on the same scales. Regions where various condensates involving methane, ammonia and water are likely are shown shaded. The calculations are based on expected abundance ratios (among carbon, nitrogen, hydrogen and oxygen) and on saturation vapor-pressure curves for the several materials shown. If the atmosphere is very deep, water probably condenses at temperatures too high for growth. The growth region shown earlier includes only liquid ammonia as a

candidate for cloud formation. However if a surface is present, condensation of vaporized surface material, whatever it is, is likely just above the surface.

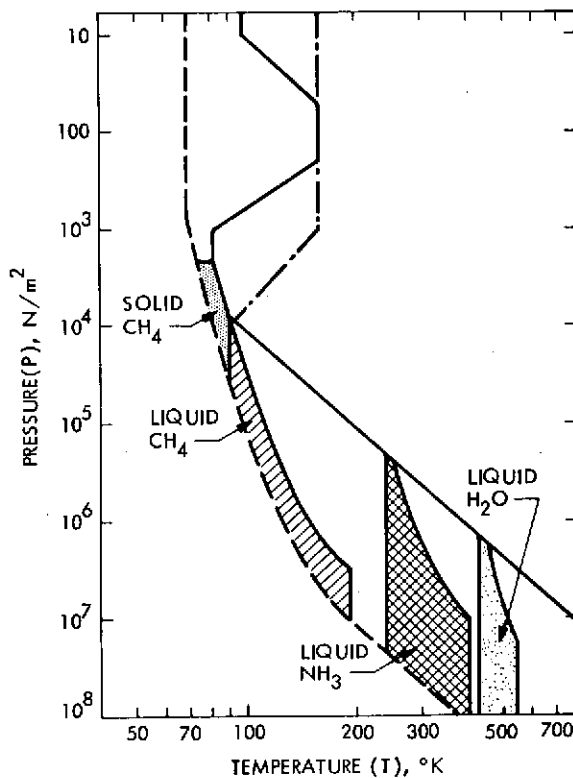


Fig. 2-D.2. Pressure-temperature domains for various potential condensates in Titan's atmosphere

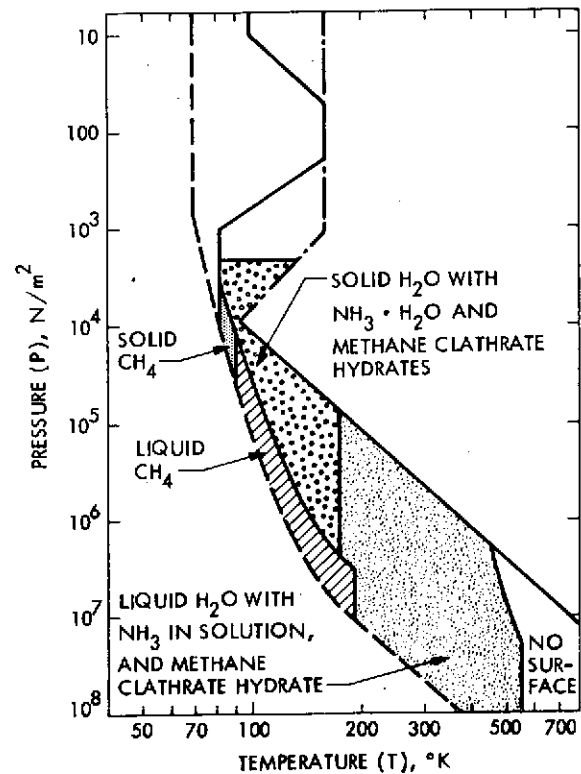


Fig. 2-D.3. Candidate surface materials corresponding to pressure-temperature regions at the bottom of Titan's atmosphere

The profiles are shown again in Fig. 2-D.3, where the shaded regions specify candidate surface materials. If the atmosphere profile is terminated by a surface at, for example, a pressure of 1 atm and a temperature of 150 K the surface is expected to be solid water ice with one or two major hydrates. This is the most probable surface material, and is compatible with current understanding of the structure of Titan's interior. If the surface is a solid ice crust, thermal and tidal stresses within the underlying liquid water mantle may produce the analogs of geological activity, such as volcanism, seepages, and icequakes involving water, steam, ammonia, etc.

In the case of a thicker atmosphere, liquid water is the likely surface material in the growth region. This water would have ammonia in solution, at concentrations which lead to pH values between about 11 and 12.5. Such a surface ocean might serve as a growth medium for some organisms, particularly considering the availability of carbon from atmospheric methane, and water with other needed materials in solution.

This work has led to a better specification of the structure of Titan's atmosphere, using detailed numerical models, than has previously been available. The large uncertainties are apparent in these atmospheric profiles and in the surface pressure. Survival and growth of some terrestrial organisms is possible if the surface pressure falls in the range 2 to 100 atmospheres; in this case the probability of growth on Titan exceeds that for every other outer planet satellite, according to present considerations.

2.4.3 Future Activities

As future effort, it is hoped that additional astronomical observations, recommended by the workshop, will narrow the range of surface pressures compatible with the data. The pH estimates will be more carefully carried out, considering solutes in addition to ammonia. The analysis will be extended to five other outer planet satellites, whose size and structure resemble Titan's, particularly to Io, shown to have at least some atmosphere by the recent Pioneer 10 fly-by of Jupiter. For these objects and the outer planets themselves, the relative probability of growth will be redetermined.

2.4.4 Presentations

Divine, Neil, "Titan Atmosphere Update", presented by J. B. Barengoltz at NASA Spacecraft Sterilization Technology Seminar, San Francisco, California, 20-21 February 1974.

2.4.5 Publications

Divine, Neil, "Titan Atmosphere Models (1973)", JPL Technical Memorandum 33-672, 1 February 1974.

2.5 EFFECT OF SOLAR ELECTROMAGNETIC RADIATION OF MICROORGANISMS

2.5.1 Subtask E Introduction

The objective of this task is to determine the effect of solar electromagnetic radiation on the survival of microbial populations in a simulated environment. The task will provide vital information on the survival of microorganisms on outbound craft when exposed to the solar electromagnetic radiation of space. Such information will enable updating of probability constants in the assessment of applicable planetary quarantine constraints. Significant effects of certain spectra of solar electromagnetic radiation on microorganisms have been previously noted in the literature. The present approach is to study this radiation in a fashion that permits direct transference of the data to considerations of planetary quarantine.

2.5.2 Significant Accomplishments

The effort on this task has been directed towards equipment procurement and fabrication and test design. The three main elements of the test system are the following:

- 1) a vacuum chamber capable of 1×10^{-7} torr and accommodation of the requisite test fixtures and solar light source;
- 2) test fixtures for the study of pure culture and naturally occurring microbial populations; and
- 3) a solar light source capable of providing a beam of one sun intensity to the plane of the test fixture under vacuum.

All three elements of the system have been prepared and are ready for initial testing.

Under the test plan defined during this reporting period, the effect of solar electromagnetic radiation as a function of intensity, temperature, and microbial population will be studied. Sun intensities will be varied from 0.1 to 1 sun for time durations necessary to achieve 1, 2, and 3 log reductions of the test microbial population. Temperatures to be studied will range from -125°C to $+70^{\circ}\text{C}$ with concentration on those expected to nominally occur on

the surface of the sun side of the Viking solar panels (-15°C to +70°C). Pure culture microbial populations will be formed from Mariner '71 isolates (5 sporeformers and 1 nonsporeformer). In addition reference populations will be studied, i. e., Bacillus subtilis var. niger and Staphylococcus epidermidis. The effect of solar electromagnetic radiation on naturally-occurring microbial populations will also be investigated. To accomplish this, 12 x 12 inch sections of Viking-type solar panels will be exposed to natural fallout in a spacecraft assembly area for a one week period. The panel sections will then be subjected to the simulated space environment at different temperatures and sun intensities and assayed for survivors.

2.5.3 Future Activities

Future work on this task will involve enactment of the previously described test plan.

SECTION III

POST LAUNCH RECONTAMINATION STUDIES
(NASA No. 193-58-62-03)

Contents

Subtask A
para. 3.1

Title and Related Personnel

POST LAUNCH RECONTAMINATION STUDIES

Cognizance: J. Barengoltz

Associate

Personnel: C. Bauerle (Bionetics)
R. Gildersleeve (Bionetics)
E. Robinson

3.1 POST LAUNCH RECONTAMINATION STUDIES

3.1.1 Subtask A Introduction

The objective of the task is the development of an analytical technique for the evaluation of the probability of the relocation of particles from non-sterile to sterile areas on a spacecraft. The recontamination process is important for all multiple missions with separate microbiological burden allocations for various major spacecraft systems, and critical for life detection experiments that risk contamination from nonsterile components.

The approach has been to study the effects of typical mission environments on the distribution of particles on spacecraft surfaces both analytically and experimentally.

The analysis consists of three logical components, which have been reflected in the effort: (1) particle adhesion, (2) dynamic release mechanisms, and (3) particle transport. The effort in particle adhesion has been principally a particle release experiment, together with analytical work and attempts to correlate other data found in the literature and elsewhere. Under dynamic release mechanisms, the modeling of meteoroid impacts has continued. The other important release mechanism during the spaceflight phase, pyro firings, has been treated and reported earlier. The particle transport study is an analytical effort which includes the development of codes for spacecraft geometry and orientation, forces acting on released particles, and trajectory.

3.1.2 Significant Accomplishments

3.1.2.1 Particle Adhesion Force Study. The effort in the particle adhesion force study during this reporting period has been the analysis of the particle release data for glass beads and the development of the acoustic emission detection system.

In order to analyze the particle release data obtained (Table 3-A.1) and to extend any conclusions to other cases, a literature search was initiated. Some general observations may be made. The four adhesion forces which may play an important role are: Van der Waals, contact potential, Coulomb, and

capillary. The Van der Waals or molecular force is proportional to the particle dimension, depends critically on surface roughness, and is fairly unaffected by material conditions. Although the other forces may be much larger under certain circumstances, it is the only source of adhesion for inert contaminants seeded in air onto a surface and then evacuated. Contact potential differences due to the surface effects of dissimilar materials cause an electrostatic binding proportional to the particle dimension to the $2/3$ power. Coulomb forces arise from actual charges on the particles due to external ambient electric fields. Since these forces are inversely proportional to the particle dimension, they are quite important for small particles. However, the electric charges involved in both contact potential and Coulomb forces will neutralize in the presence of ambient water. More importantly, for particles seeded in air (or even dry nitrogen) onto a surface which is then evacuated, the Paschen limit places an upper limit on the residual charge. During evacuation, a region of corona breakdown, where the field in the small gap between particles and the surface causes the air to ionize, is passed. Finally, the capillary or water surface tension force is potentially largest. It is, however, negligible in a reasonable vacuum. At ambient air pressures, the capillary force exhibits a definite hysteresis effect with respect to relative humidity. That is, the force depends on the history as well as the relative humidity at a given time.

Some conclusions relevant to the recontamination task may be drawn from the preceding discussion. The Van der Waals force, proportional to particle size, is the best model for the vacuum problem in space. During ascent, the adhesion force changes in a very complicated fashion, but approaches the Van der Waals as a lower limit. Conversely, the present particle adhesion experiment should reliably measure the Van der Waals force. One may compare vacuum results with results obtained under ambient pressures only with caution.

The data to be modelled (Table 3-A.1) was obtained by an impulse method for glass beads on stainless steel. The details of the apparatus and the test procedures have been previously reported (Ref. 1). It should be noted that these tests had the glass beads seeded in air and then the removal occurred in vacuum.

Table 3-A.1. Experimental Results: Particle Adhesion

| Particle Dia. (μm) | Acceleration A (kG) | % Removed |
|------------------------------------|------------------------|-----------|
| 22.00 | 2.20 | 11.00 |
| 22.00 | 3.00 | 5.00 |
| 22.00 | 5.00 | 11.00 |
| 22.00 | 1.20 | 3.00 |
| 22.00 | 18.00 | 17.00 |
| 22.00 | 13.00 | 74.00 |
| 22.00 | 12.00 | 82.00 |
| 22.00 | 22.50 | 90.00 |
| 22.00 | 18.00 | 91.00 |
| 22.00 | 2.30 | 37.00 |
| 22.00 | 1.00 | 10.00 |
| 22.00 | 4.00 | 3.00 |
| 48.00 | 3.30 | 39.00 |
| 48.00 | 0.60 | 3.00 |
| 48.00 | 2.50 | 10.00 |
| 48.00 | 15.00 | 57.00 |
| 48.00 | 5.50 | 9.00 |
| 48.00 | 37.50 | 76.00 |
| 48.00 | 32.00 | 93.00 |
| 68.00 | 0.80 | 57.00 |
| 68.00 | 2.50 | 92.00 |
| 68.00 | 3.00 | 57.00 |
| 68.00 | 4.20 | 80.00 |
| 68.00 | 4.50 | 87.00 |
| 68.00 | 12.00 | 98.00 |
| 68.00 | 10.50 | 97.00 |
| 94.00 | 0.60 | 84.00 |
| 94.00 | 1.10 | 82.00 |
| 94.00 | 1.20 | 97.00 |
| 94.00 | 4.00 | 85.00 |
| 94.00 | 5.00 | 53.00 |
| 94.00 | 7.50 | 90.00 |
| 110.00 | 4.00 | 33.00 |
| 110.00 | 1.00 | 10.00 |
| 110.00 | 10.00 | 95.00 |
| 110.00 | 11.00 | 81.00 |
| 110.00 | 30.00 | 95.00 |
| 110.00 | 20.00 | 91.00 |
| 110.00 | 1.80 | 37.00 |
| 110.00 | 2.10 | 25.00 |

Previous models used in this task have related the applied force (given by the product of the applied acceleration and the particle mass) to the removal fraction. In each case a characteristic acceleration (or force) corresponding to a fixed removal fraction was defined. In Ref. 2, the characteristic acceleration a_o for a removal fraction of 0.63 was given as:

$$a_o = \frac{2 \times 10^{-4} (0.4 + 0.006 \text{ RH})}{\pi d^2 \rho G} \quad (1)$$

where a_o is in units of kilo-gee (kG), ρ is the particle density ($\text{g } \mu\text{m}^{-3}$), d is the particle diameter (μm), and G is the acceleration due to gravity (980 cm s^{-2}), and RH is the relative humidity (percent) during release. The numerical constants in Eq. 1 were determined empirically from data in the literature. On the other hand, the threshold acceleration for particle removal was found in our experiments to vary as the inverse of the particle diameter.

This apparent inconsistency in the particle size dependence, reported in Ref. 3, is not real. The threshold acceleration, or the force required for small removal fractions may tend to a constant independent of the particle size. The concept of threshold for this problem is not useful. That is, a removal fraction to characterize the adhesion should be in the vicinity of 0.5 (Ref. 4). Note that Eq. 1 satisfies this criterion.

As discussed above, for this experiment and for the recontamination analysis, one expects a characteristic force, F_o , corresponding to a removal fraction of 0.5 given by:

$$F_o = kd \quad (2)$$

or the characteristic acceleration a_o given by:

$$a_o = \frac{6k}{\pi d^2 \rho} \quad (3)$$

where d is the diameter and ρ is the density of the particle. Note that Eq. 1 and 3 are of the same form for zero relative humidity.

The next component of the model must relate the applied force or acceleration and the characteristic force or acceleration to predict the removal fraction. Since a distribution of adhesion forces is expected even for a collection of identical particles because of the variation in microscopic surface conditions, a probabilistic model is indicated. In the new model, the constant k of Eq. 2 is assumed to be log-normally distributed with a mean value of $\log k$ equal to m and a standard deviation σ_r . Then the removal fraction for a specific d is given by the probability that the applied force F^* exceeds the characteristic force F_o . This probability may be written:

$$P(F^* > F_o) = \frac{1}{\sqrt{2\pi}} \int_{-\infty}^{(\log k^* - m)/\sigma_r} dt \exp(-t^2/2) \quad (4)$$

where

$$k^* = F^*/d = \frac{\pi d^2 \rho a^*}{6} \quad (5)$$

and a^* is the applied acceleration.

By inverting Eq. 4, for a given data point and an assumed value of σ_r , one can calculate an estimate for m . Such a collection of estimates for m may be averaged to provide a best estimate m_o for the selected σ_r . There is also a standard deviation of this collection, σ_m , which should be minimized. The program for search over σ_r , treating the data, and minimizing σ_m has been incorporated into a computer code. The best fit to the data was obtained for $\sigma_r = 0.4$, $m_o = -0.882$, and $\sigma_m = 0.52$. These values are consistent with MKS metric units; e.g., k^* and 10^{m_o} have units of newton meter⁻¹.

Up to this point the theoretical development is due to B. Nelson (Ref. 5). Nelson, however, uses Eq. 4 with σ_m substituted for σ_r and

$m = m_0$ for the most probable removal fraction. I claim the correct procedure is to use σ_r and m_0 for the most probable calculation. Further, the meaning of σ_m is such that if one calculates the removal fraction with $m = m_0 - \sigma_m$ substituted into Eq. 4 and with $m = m_0 + \sigma_m$, there is the usual 68% probability that a test result will fall between the two answers. If one is concerned only with an upper limit on the removal fraction, there is an 84 percent (50 + 34) probability that the prediction with $m = m_0 - \sigma_m$ will not be exceeded. These comments may be extended in the usual way.

The results of this analysis are shown in Figs. 3-A. 1, 3-A. 2, 3-A. 3, 3-A. 4, and 3-A. 5. Each figure corresponds to a particular size of glass bead. The data and the predictions of Eq. 4 are given as removal fractions in percent vs. surface acceleration in kG. The most probable and the "conservative" ($m = m_0 - \sigma_m$) predictions are shown and, in the case of 110 μm beads, the "non-conservative" ($m = m_0 + \sigma_m$) prediction is also given.

It is interesting to compare our new results for the adhesion force with the previous model and with results published in the literature. The present prediction of the mean adhesion force (N) is given by Eq. 2 with the diameter d expressed in meters and a value of $k = 0.13 \text{ N/m}$. Corn (Ref. 6) used the same formula and obtained the following values (converted to MKS units): 0.17 N/m for the adhesion of Pyrex particles to optical glass, 0.12 N/m for the adhesion of quartz particles to optical glass, and 0.075 N/m for the adhesion of quartz particles to Pyrex glass. Since these data were obtained at 95% relative humidity, the agreement with the JPL results must be considered somewhat fortuitous.

A comparison with the characteristic acceleration of the previous model, Eq. 1, requires some algebra. One may express the prediction of that model in terms of the force required to cause a 63% removal in air (RH = 0%):

$$F(0.63) = 0.13d \quad (6)$$

where F is expressed in newtons and the particle diameter d is expressed in meters. The predictions of the present model has a coefficient of 0.18 for this removal fraction (compare to 0.13). This fair agreement may also be

coincidental. The previous model was based on data for many materials in air with a relative humidity of 50 - 60%.

From a comparison of the data in the literature and a consideration of the Van der Waals and capillary adhesion forces only, one may predict the trend of total adhesion between ambient pressure with 100% relative humidity and vacuum. As the relative humidity is decreased the capillary force decreases in a linear fashion (Ref. 6). As long as water is present, the Van der Waals force is reduced to a negligible factor by the molecular interaction with the interface water (Ref. 4). For small relative humidity ($< 50\%$), there is a minimum adhesion. Finally, as the test system is evacuated, the capillary force becomes negligible and the Van der Waals force attains its maximum value. On the basis of the data, the adhesion force in vacuum is commensurate with that in air at 100% relative humidity and certainly exceeds values for low (but non-zero) relative humidity.

As reported in an earlier report (Ref. 3), a feasibility study on the applicability of acoustic emission detection technology to particle adhesion tests was conducted. During this reporting period, release velocity distribution measurements have been attempted. This activity has been much delayed by a low level of support and resources. On the technical level, the acoustic isolation of the particle detector from the launch system for timing purposes has proven difficult (Ref. 7). However, the isolation problem has been improved at this writing. A preliminary release velocity distribution of $1 - 10 \text{ ms}^{-1}$ for $100 \text{ }\mu\text{m}$ glass beads released by a peak acceleration of approximately 25 kG has been obtained. The schedule calls for extensive tests for the various acceleration levels and particle sizes to be completed by the end of February. Due to the resource and schedule limitations, the meteoroid impact simulation will not be attempted.

3.1.2.2 Meteoroid Impact Study. The meteoroid impact study consists of a series of analyses for different conditions and geometry to provide the acceleration of struck surfaces and an experimental verification task. The major efforts during this reporting period have been the improvement of the loading function model and the refinement of the computer codes for surface response.

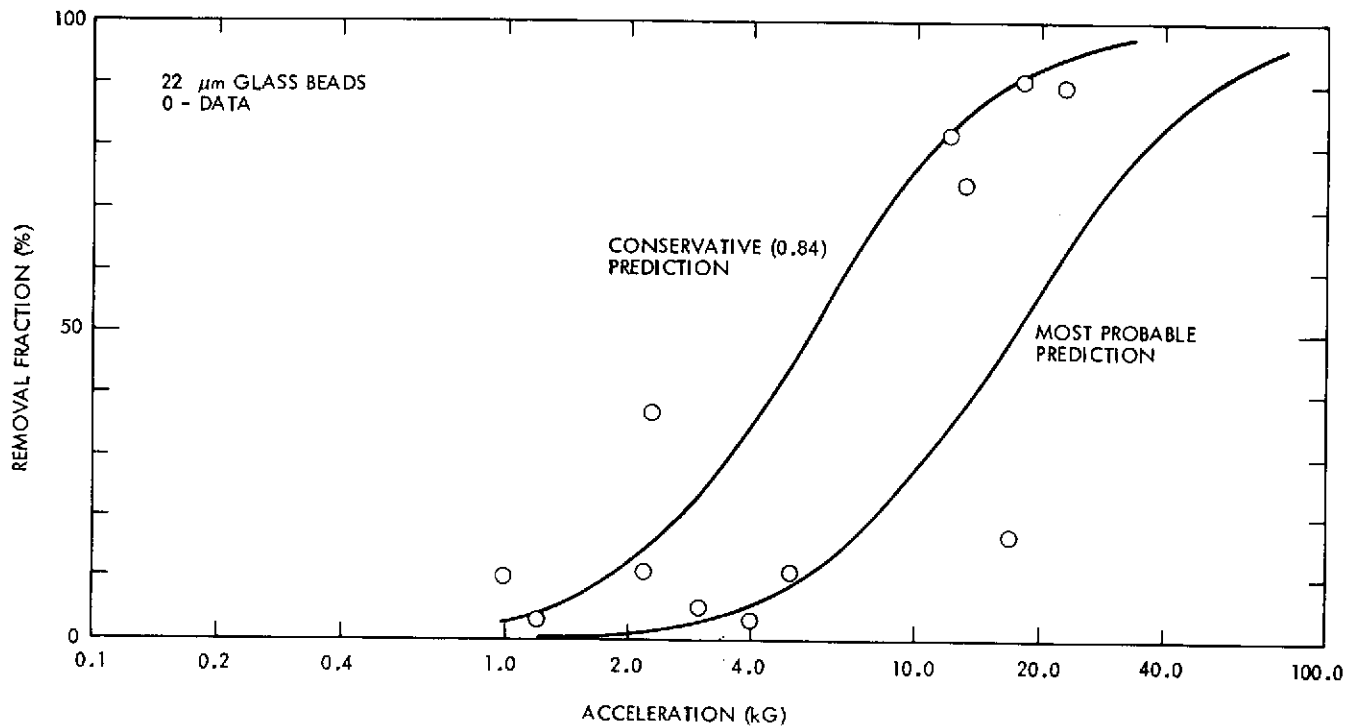


Fig. 3-A.1. Comparison of particle adhesion data with predictions of model, 22 μm glass beads

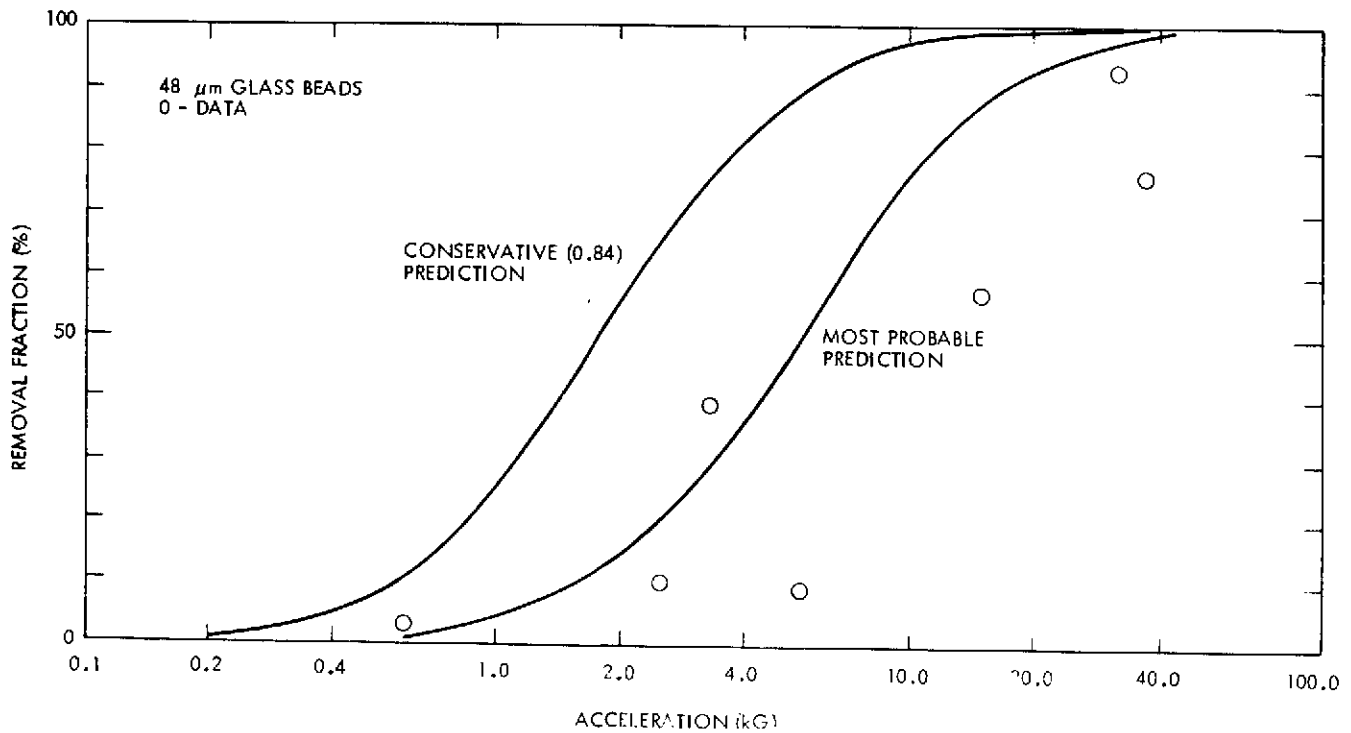


Fig. 3-A.2. Comparison of particle adhesion data with predictions of model, 48 μm glass beads

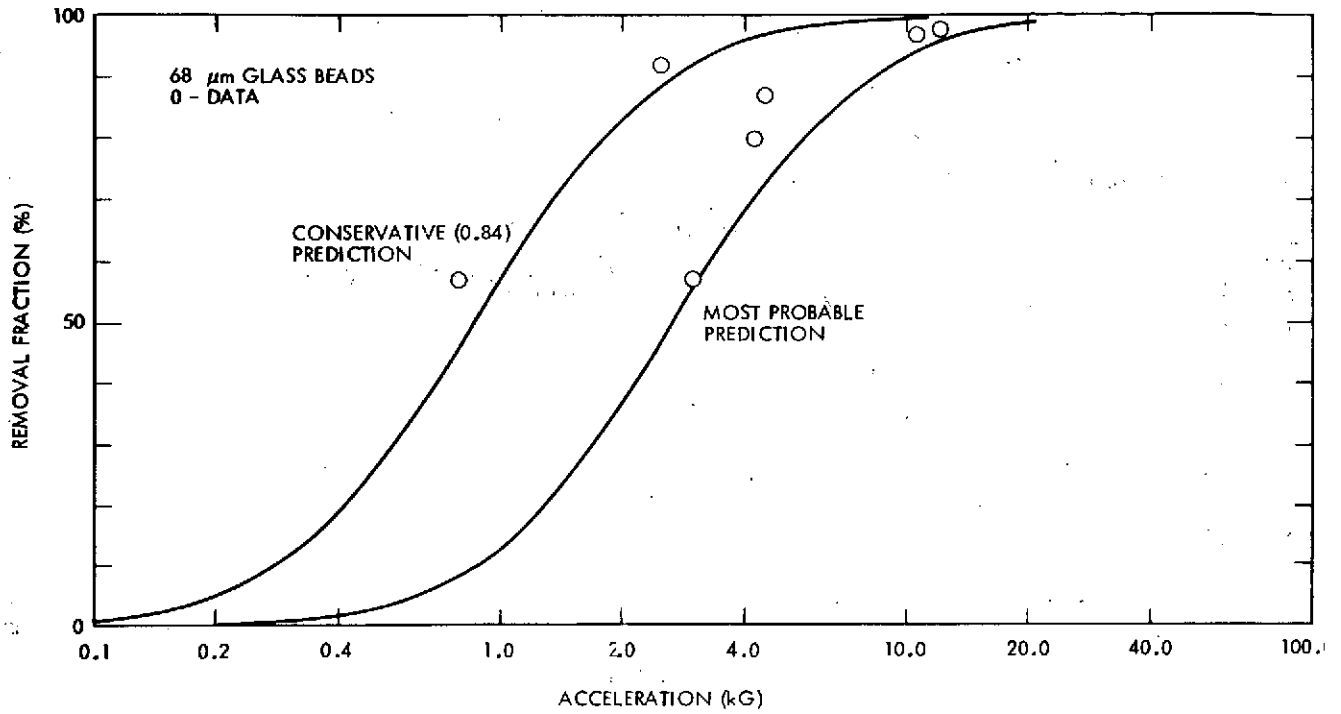


Fig. 3-A.3: Comparison of particle adhesion data with predictions of model, 68 μm glass beads

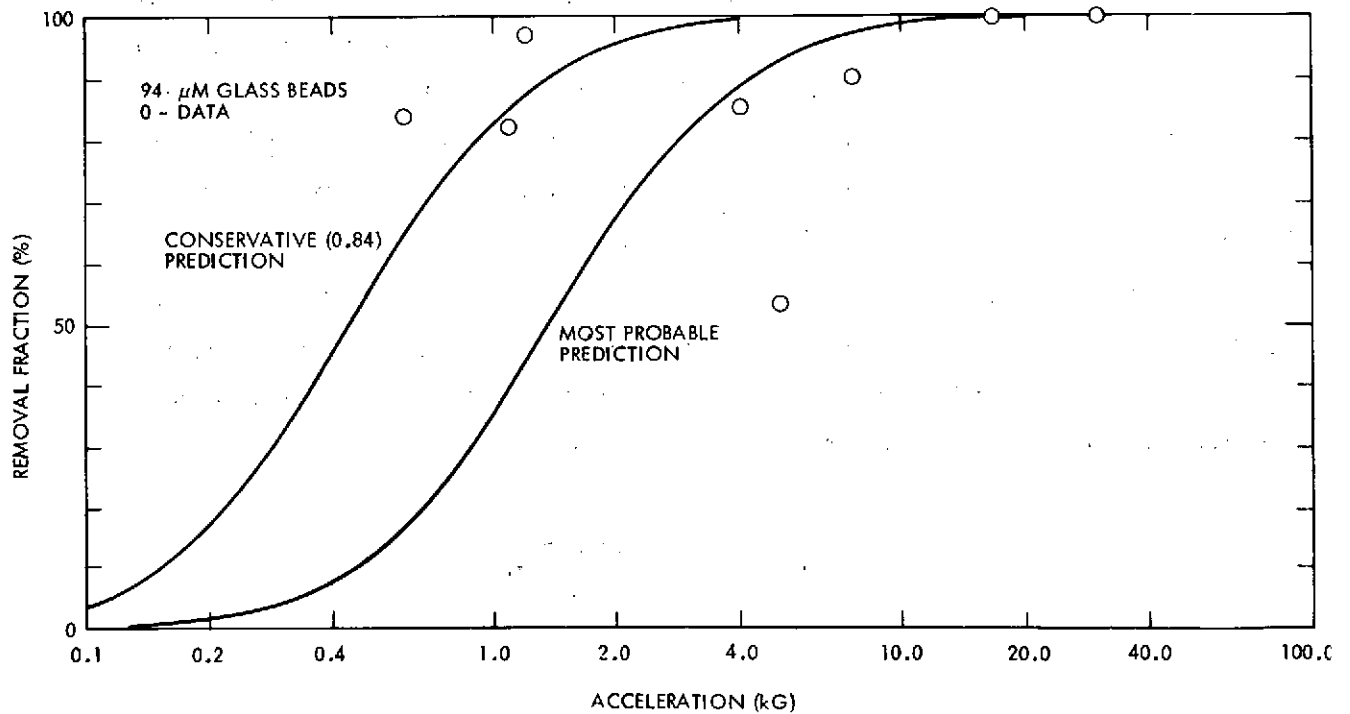


Fig. 3-A.4: Comparison of particle adhesion data with predictions of model, 94 μm glass beads

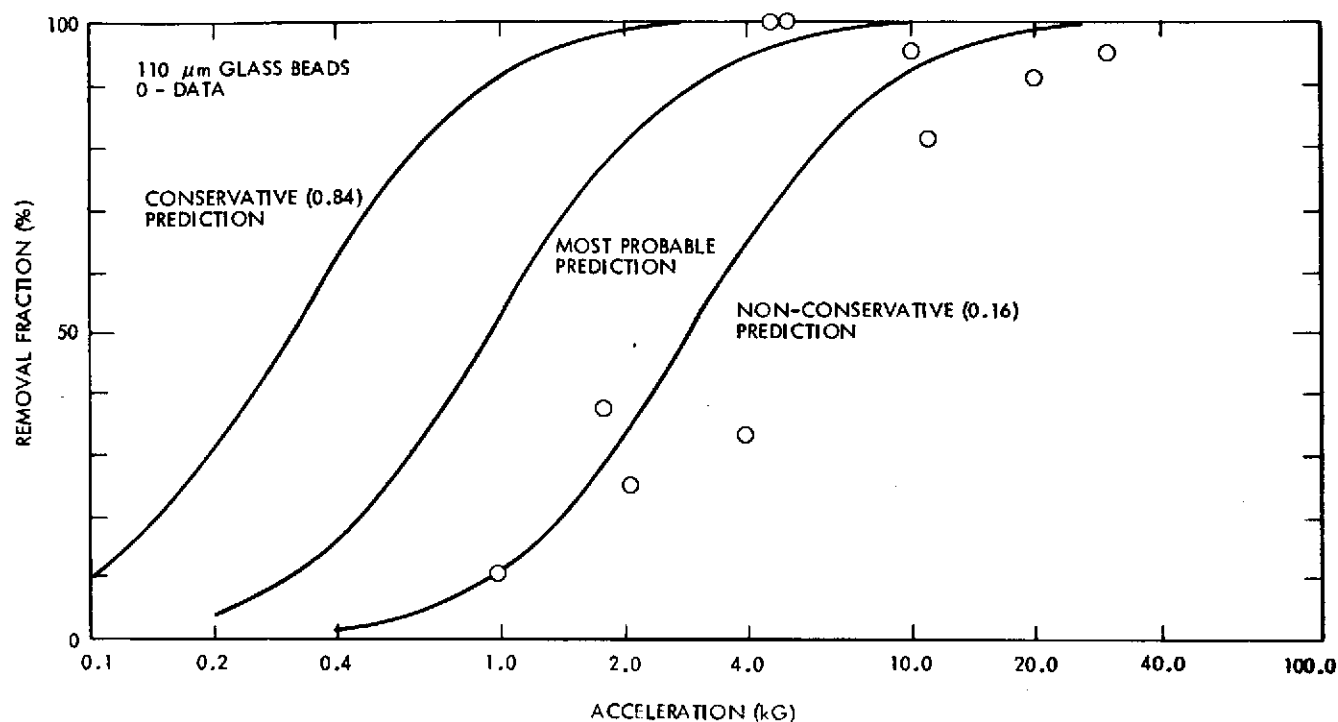


Fig. 3-A.5. Comparison of particle adhesion data with predictions of model, 110 μm glass beads

The computer code development of the new surface response analyses due to Yang (Ref. 1) has also continued. The results of the meteoroid impact codes have been combined with the results of the particle adhesion study to provide predictions on particle removal due to meteoroid impact. The predictions compare favorably with the experimental results of the group at Langley Research Center (LRC) (Ref. 8).

The loading function model predicts a pressure P , in general a function of time t , and r , position on the surface relative to the center of impact, for a given meteoroid event. For simplicity, the positional dependence has been assumed to be Gaussian and factorable:

$$P(r, t) = P_0 e^{-r^2/s^2} f(t) \quad (7)$$

This choice was motivated by the existence of a closed-form solution velocity response for a thin plate subjected to a loading of this form with the impulse time function. In the preliminary considerations reported previously (Ref. 3), it was found that for reasonable forms of the time dependence $f(t)$, only a characteristic time T_0 of the impact was important for the peak acceleration, our primary interest. The detailed behavior of $f(t)$ certainly determines the detailed time history of the surface acceleration.

The function $f(t)$ has been chosen:

$$f(t) = \left(1 + \frac{t}{T_0}\right)^{-2} \quad (8)$$

This form has been derived along the lines of an analysis due to Ludloff (Ref. 9). This treatment takes into account the transport of molten target material in the crater region. The result depends on Ludloff's form for the crater radius; the crater is assumed to be hemispherical. The expression for the crater radius R in terms of the target material strength S , the projectile diameter d , density ρ_P and velocity v_o is:

$$\frac{R}{d} = \frac{1}{2} \left(\frac{\rho_P v_o^2}{S} \right)^{1/3} \quad (9)$$

This formula agrees reasonably well with the data in the literature.

In this analysis, the time history of Eq. 8 is valid only for the boundary of the crater being formed. This restriction appears to pose no problem in calculating the post-impact elastic wave far from the crater. The solution of the equation of motion leads to Eq. 8. The characteristic time T_0 may be immediately identified as:

$$T_0 = \frac{4}{3} \frac{d S^{1/6}}{v_o^{4/3} \rho_P^{1/6}} \left(1 + \frac{4 \rho_P v_o^2}{S} \right) \quad (10)$$

One may also identify $P_0 = 2S$. In the formula for T_0 , ρ_T is the target density and all other symbols have been previously defined. Ludloff, in keeping with his treatment of the molten target material, takes as the target material strength S :

$$S = \lambda_F \rho_T \quad (11)$$

In this formula λ_F is the latent heat of fusion. For aluminum, for example, $S = 8.7 \times 10^8$ nt/m².

Finally, we have chosen for the parameter in the loading function (Eq. 7), a value of $(1/3)R$, where R is the crater radius given in Eq. 9. At this point the loading function is completely expressed in terms of known parameters of a meteoroid impact.

Classical plate theory provides the velocity response WDOT, of a thin plate to an impulsive loading with a Gaussian shape factor (Ref. 10). The existing computer code yielded the surface velocity \dot{w} and surface acceleration \ddot{w} by a convolution with $f(t)$:

$$\dot{w}(r, t) = \int_0^t d\tau \text{WDOT}(r, \tau) f(t-\tau) \quad (12)$$

$$\ddot{w}(r, t) = \int_0^t d\tau \text{WDOT}(r, \tau) \dot{f}(t-\tau) \quad (13)$$

In the process of inserting the new $f(t)$ into the thin plate code and testing it, several errors in the existing code were discovered. The correction of these errors has eliminated the unreasonable oscillations of the peak acceleration versus the lateral distance noted in the previous report (Ref. 3). The purpose of a close inspection of the code was to find a way of shortening it. By an analysis of the convolution integral and the shapes of WDOT and $f(t)$, we have succeeded in predicting the time t for a given lateral distance r at which peak acceleration occurs. Since the calculation of the surface velocity and

acceleration for a given position requires two integrations for each value of time, a great savings is realized by limiting the values of time to near the time of peak acceleration. In addition, the convolution integration can be optimized for these values. As a result, the present code yields peak acceleration and the simultaneous velocity as a function of position by a limited search over t . An entire curve of peak acceleration versus position is computed in about the time the previous code required for the time history of the acceleration at one position.

The analysis of the impact of a small meteoroid and/or the analysis for positions close to, but not in the impact area, entails a consideration of the semi-infinite half-space problem. This analysis which treats the plate as though it were infinitely thick, has been published in the literature (Ref. 11). The computer code based on this analysis yields peak accelerations inversely proportional to the position r beyond the impact locus. Because our problem is limited to finite plate thicknesses, the absolute values of the peak accelerations predicted are suspect.

In the past we have taken the transition between the "thick" and "thin" regions to be the value of r equal to three plate thicknesses and have matched the peak acceleration at that point. In fact, however, this transition region beyond which shear waves dominate the compressional waves depends on the other plate properties and the impacting projectile properties. Fortunately, the prediction of the classical thin plate program levels off and then actually decreases with decreasing values of r . One may interpret this odd behavior of the peak acceleration as due to destructive interference between the various contributions to it from the different parts of the finite region of disturbance. Since the thin plate analysis treats shear waves only, the leveling off of its prediction identifies the transition region uniquely.

The meteoroid impact program developed for this task uses this identification by searching for the maximum peak acceleration predicted by the classical thin plate program for decreasing values of r . For all smaller values of r than the specified value found, the peak acceleration is taken as inversely proportional to r . The infinitely thick plate analysis code, a cumbersome long-running code, is not used at all for production runs. For very large values of

r, the prediction of the program drops off, finally below a cut-off in acceleration, and calculations cease. As stated above, a significant reduction in computer costs together with an improvement in accuracy has been realized.

During this reporting period, the meteoroid impact program was exercised for a parametric range of cometary meteoroid masses to yield peak acceleration and the simultaneous surface velocity as a function of position relative to the impact. The spacecraft wall parameters were chosen to correspond to 3.175×10^{-3} m (1/8 in.) of aluminum. The meteoroid parameters were a density of 600 kg m^{-3} , a velocity of $1.567 \times 10^4 \text{ ms}^{-1}$ and masses in the range 3×10^{-13} kg to 1×10^{-6} kg. In addition to print-out and plots of the results, the program generates punched cards which are used in the prediction of the release of particulate contamination (see para. 3.1.2.4). As an example of the form of the results, Figs. 3-A.6, 3-A.7, 3-A.8, and 3-A.9 provide the peak acceleration and simultaneous surface velocity for two specific sets of parameters. These values are intended to simulate two experiments conducted by a research group at Langley Research Center (Ref. 8). These results will be discussed in the section on Program Integration (para. 3.1.2.4).

A manual analytical study has been started to develop empirical formulas for the predicted peak accelerations and velocities to replace the computer code. Preliminary results indicate that the extrapolation of certain of the parameters, e.g. plate thickness, is feasible.

The last activity under meteoroid impact analysis is the continuing effort in the code development for the new analyses due to Yang (Ref. 1). The approach developed by JPL programming consultants and reported previously (Ref. 3) has proved to be inadequate for the range of parameters required. An accurate computation of Yang's solutions necessitates the development of codes to calculate rather exotic mathematical functions. This effort is now almost complete.

3.1.2.3 Particle Transport Analysis. The particle transport analysis addresses the problem of following the motion of the released particles. Formally stated, given the particle parameters, the initial conditions, and the

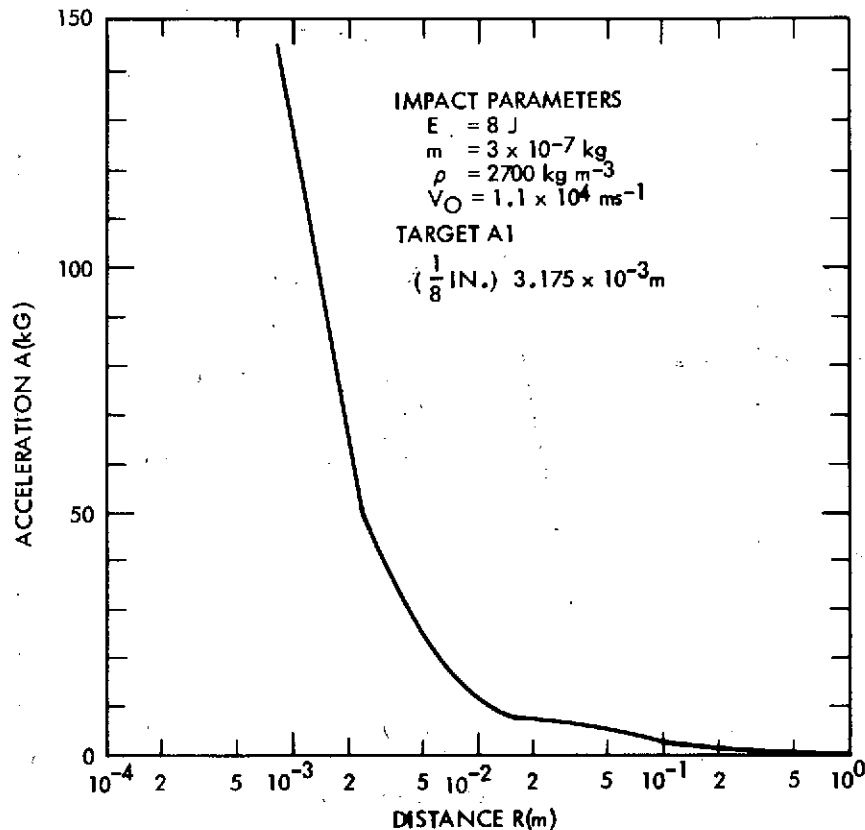


Fig. 3-A.6. Surface acceleration for simulation of LRC experiment, Case 1

forces acting on the particle, the analysis is to solve for the equation of motion. Of the important forces, the electrostatic force on the particle due to the electric field of the spacecraft is most difficult to predict. The major effort during this reporting period has been in the electrostatic area. The basic approach has been to analyze particle charging so that the particle charge as a function of time is known and to analyze the potential solution for the spacecraft-solar plasma system (Ref. 3).

The particle charging model deals with spherical particles for simplicity and consists of three special cases: illuminated particle, shaded (by the spacecraft) particle in the wake, and shaded particle outside the wake. The wake region of the spacecraft is a complicated analysis that is discussed under the electric field heading. Given the geometry of the particle and the potential-dependent currents flowing into it, one may express the charging rate in an implicit form.

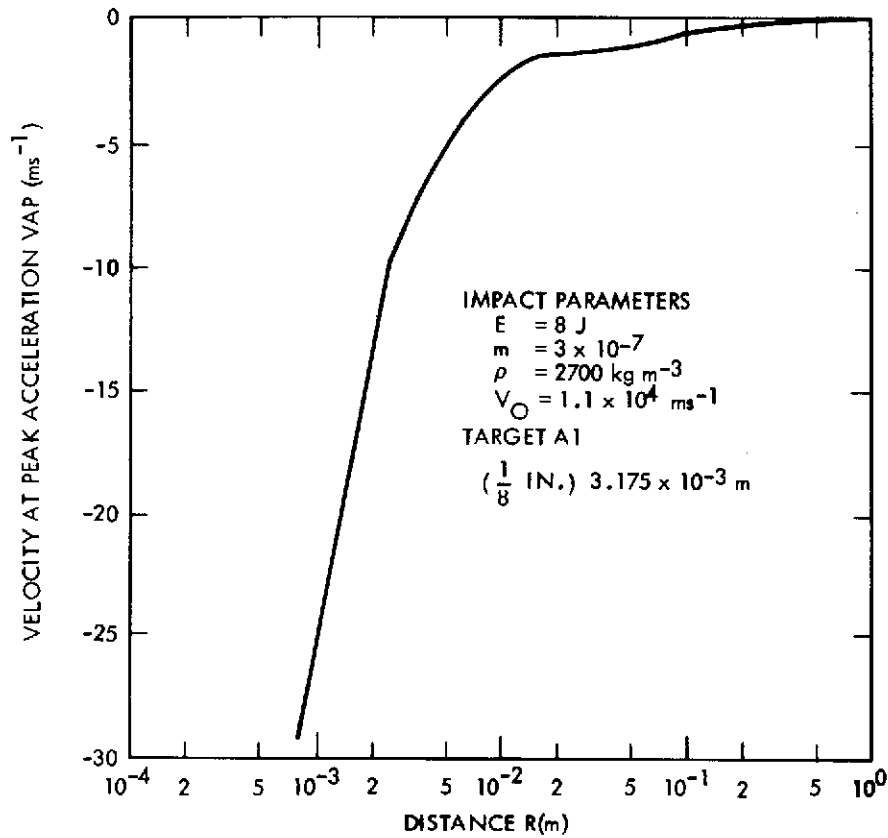


Fig. 3-A.7. Surface velocity for simulation of LRC experiment, Case 1

For the illuminated particle, the charging rate $d\phi/dt$ is given by:

$$\frac{d\phi}{dt} = \frac{2.9 \times 10^{-9}}{R^2} \pi d \left[A_p + (1 - \alpha) A_e + A_v \right] \quad (14)$$

$$A_p = \frac{n_p v_o}{4} \quad \text{for } |\phi| \ll \frac{M v_o^2}{2e}$$

$$A_e = -\frac{n_e \bar{v}_e}{4} \begin{cases} \exp(e\phi/kT_e) & \text{for } \phi \leq 0 \\ \left[1 + 2e\phi/kT_e\right]^{1/2} & \text{for } \phi > 0 \end{cases}$$

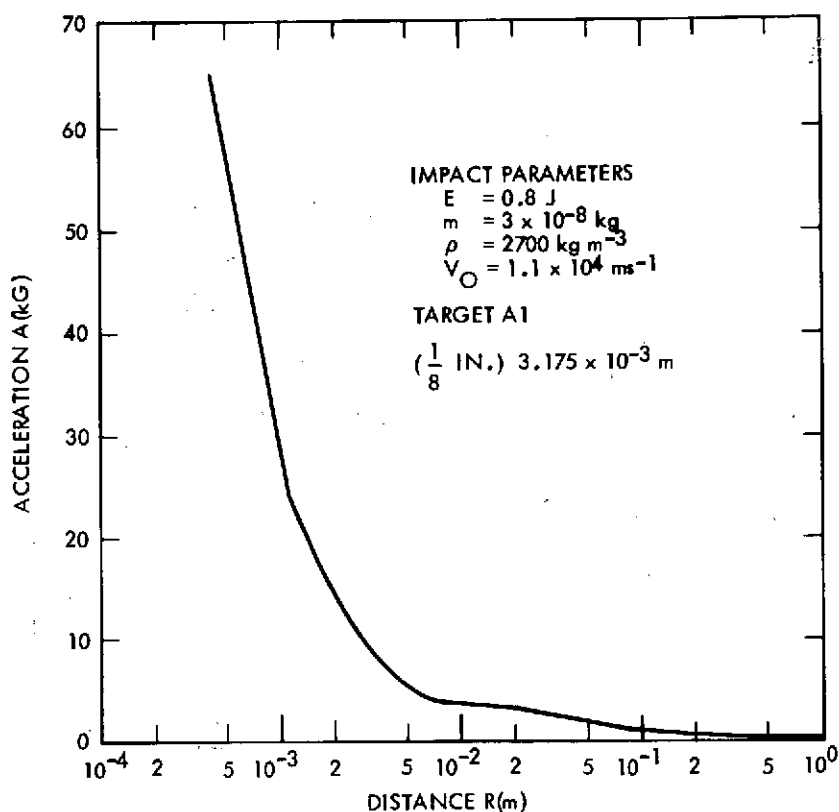


Fig. 3-A. 8. Surface acceleration for simulation of LRC experiment, Case 2

A_v = photoelectron flux, dependent on ϕ

α = secondary emission yield, dependent on ϕ

In this equation, the proton flux A_p depends on the number density $n_p (\text{m}^{-3})$ and the directed velocity $v_o (\text{ms}^{-1})$ and the electron flux A_e depends on the number density $n_e (\text{m}^{-3})$, the mean thermal speed $\bar{v}_e (\text{ms}^{-1})$ and the temperature $kT_e (\text{eV})$. The photoelectron flux is calculated from photoelectric yield data for the solar spectrum, material of the particle, and surface potential $\phi (\text{V})$. Since the previous report (Ref. 3), a model for the secondary emission yield α (unitless) (Ref. 12) has been incorporated. For the illuminated particle, secondary emission affects $d\phi/dt$ only when $\phi < 0$, so that the equilibrium potential (Ref. 3) is unchanged. With A_p , A_e , and A_v in units of $\text{m}^{-2} \text{s}^{-1}$, the

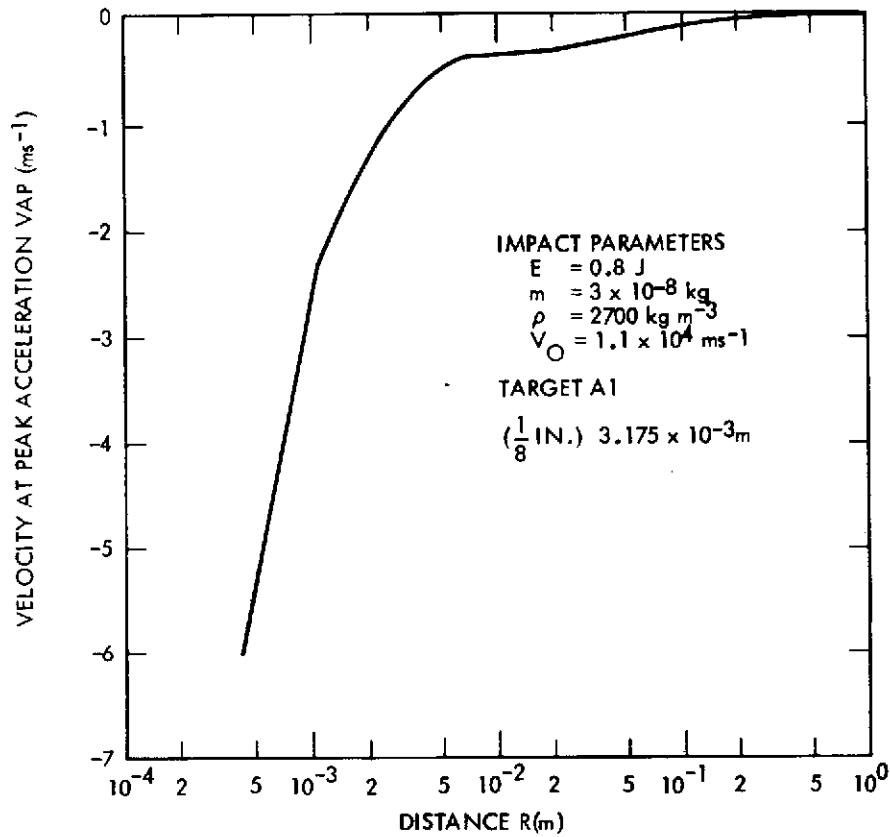


Fig. 3-A. 9. Surface velocity for simulation of LRC experiment, Case 2

particle diameter d in m and the heliocentric distance R in AU, one obtains $d\phi/dt$ in Vs^{-1} . These values have changed slightly from previous reports (Ref. 3) due to the use of better solar wind parameters (Ref. 13).

For the shaded particle, the photoelectron flux A_v is zero. The electron flux A_e and the secondary emission yield α are essentially unchanged. The crux of the problem is the proton flux A_p . The proton accretion may be expected to depend only on the thermal motion of the protons, since there is no line of sight in the shade. It follows then that for this case:

$$A_p = \frac{\bar{n}_p \bar{v}_p}{4} \begin{cases} \exp(-e\phi/kT_p) & \text{for } \phi \geq 0 \\ \left[1 - 2e\phi/kT_p\right]^{1/2} & \text{for } \phi < 0 \end{cases} \quad (15)$$

where \bar{v}_p is the proton mean thermal speed and kT_p is the proton temperature. This equation, an analog to the electron flux equation, is only approximate. The quality of the approximation depends largely on the value taken for \bar{n}_p , an effective proton number density in the shade.

The effective proton density \bar{n}_p in the shade depends on the complete solution to the potential problem of the spacecraft itself. Poisson's equation relates the potential everywhere to the charge distribution everywhere. The boundary condition (surface potential of the spacecraft), the potential, and the charge distribution form a self-consistent set. At this writing, a very approximate partial model is available. For a spherical spacecraft, a conical wake region is assumed where $\bar{n}_p = 0$. The base of this cone contains the center of the sphere and is a cross-section of the sphere. The altitude of the cone lies in the anti-sun direction. The half-angle of the cone is given by (Ref. 14):

$$\tan \theta = \frac{2}{\sqrt{\pi}} \frac{\bar{v}_p}{v_o} \quad (16)$$

Outside this cone one may use Eq. 15 with $\bar{n}_p = n_p$ for particle charging. Efforts to develop an approximate solution which will specify the spacecraft surface potential and the electric field in its vicinity are continuing.

3.1.2.4 Program Integration. Program integration consists of the fusion of the results and computer codes obtained from the various activities of this task into programs capable of spanning the input/output gaps. During this reporting period, for example, the particle adhesion code and the meteoroid impact code have been combined into one program. The meteoroid impact program calculates a matrix of peak accelerations and velocities of the surface for given impact and target parameters and provides this intermediate output in punched card form. The particle release program accepts this data as input, uses the particle adhesion code, and predicts particle removal. For each case, this program calculates the removal fraction for contaminants of various sizes in the range 10 - 100 μm , as a function of the distance from the center of impact. A sample output is shown in Table 3-A.2.

Table 3-A.2. Sample Output of Meteoroid Impact/Particle
Release Program: Percent Removal for Glass Beads on
1/8 inch Al plate, 3×10^{-8} kg Cometary Meteoroid

| Radius (m.) | Percent Removal | | | | | | | | | |
|-------------|--------------------------------|------|------|------|-------|-------|-------|-------|-------|-------|
| | Contaminant Diameter (Microns) | | | | | | | | | |
| | 10 | 20 | 30 | 40 | 50 | 60 | 70 | 80 | 90 | 100 |
| 8.58-04 | 52.0 | 94.0 | 99.3 | 99.9 | 100.0 | 100.0 | 100.0 | 100.0 | 100.0 | 100.0 |
| 2.49-03 | 13.4 | 65.5 | 89.9 | 97.1 | 99.2 | 99.7 | 99.9 | 100.0 | 100.0 | 100.0 |
| 4.13-03 | 4.9 | 44.1 | 76.8 | 91.2 | 96.7 | 98.7 | 99.5 | 99.8 | 99.9 | 100.0 |
| 5.76-03 | 2.2 | 30.4 | 64.4 | 84.0 | 93.0 | 97.0 | 98.6 | 99.4 | 99.7 | 99.9 |
| 7.40-03 | 1.1 | 21.7 | 53.9 | 76.5 | 88.6 | 94.5 | 97.4 | 98.7 | 99.3 | 99.7 |
| 9.04-03 | 0.6 | 15.9 | 45.2 | 69.3 | 83.9 | 91.7 | 95.7 | 97.8 | 98.8 | 99.4 |
| 1.07-02 | 0.4 | 11.9 | 38.2 | 62.7 | 79.1 | 88.6 | 93.8 | 96.6 | 98.1 | 99.0 |
| 1.23-02 | 0.2 | 9.1 | 32.5 | 56.7 | 74.4 | 85.3 | 91.7 | 95.3 | 97.3 | 98.5 |
| 1.39-02 | 0.1 | 7.1 | 27.7 | 51.4 | 69.8 | 82.0 | 89.4 | 93.8 | 96.4 | 97.9 |
| 1.56-02 | 0.1 | 5.6 | 23.9 | 46.6 | 65.5 | 78.7 | 87.1 | 92.2 | 95.3 | 97.2 |
| 1.72-02 | 0.1 | 4.5 | 20.6 | 42.3 | 61.4 | 75.4 | 84.6 | 90.5 | 94.1 | 96.4 |
| 1.76-02 | 0.1 | 4.5 | 20.6 | 42.3 | 61.4 | 75.4 | 84.6 | 90.5 | 94.1 | 96.4 |
| 1.83-02 | 0.1 | 4.5 | 20.6 | 42.3 | 61.4 | 75.4 | 84.6 | 90.5 | 94.1 | 96.4 |
| 1.94-02 | 0.1 | 4.4 | 20.5 | 42.2 | 61.3 | 75.3 | 84.6 | 90.5 | 94.1 | 96.3 |
| 2.24-02 | 0.1 | 4.3 | 20.2 | 41.8 | 60.9 | 74.9 | 84.3 | 90.3 | 94.0 | 96.3 |
| 3.00-02 | 0.1 | 3.9 | 18.8 | 39.8 | 58.9 | 73.3 | 83.1 | 89.4 | 93.3 | 95.8 |
| 4.00-02 | 0.0 | 3.1 | 16.1 | 35.7 | 54.7 | 69.6 | 80.2 | 87.2 | 91.8 | 94.8 |
| 6.00-02 | 0.0 | 1.8 | 11.2 | 27.7 | 45.7 | 61.3 | 73.3 | 81.9 | 87.9 | 91.9 |
| 8.00-02 | 0.0 | 1.0 | 7.3 | 20.4 | 36.3 | 52.1 | 65.1 | 75.1 | 82.5 | 87.7 |
| 1.00-01 | 0.0 | 0.5 | 4.6 | 14.4 | 28.1 | 42.7 | 56.0 | 67.0 | 75.7 | 82.3 |
| 2.00-01 | 0.0 | 0.0 | 0.7 | 3.5 | 9.3 | 17.6 | 27.6 | 38.1 | 48.1 | 57.2 |
| 4.00-01 | 0.0 | 0.0 | 0.1 | 0.6 | 2.1 | 5.0 | 9.5 | 15.4 | 22.2 | 29.6 |
| 7.00-01 | 0.0 | 0.0 | 0.0 | 0.1 | 0.4 | 1.3 | 2.8 | 5.3 | 8.7 | 12.9 |
| 1.00+00 | 0.0 | 0.0 | 0.0 | 0.0 | 0.1 | 0.4 | 1.1 | 2.2 | 4.0 | 6.4 |

In addition, the clearing radius for the 10 - 100 μm contaminant particles is calculated. The clearing radius in this analysis is the root mean square radius of the removal distribution for each particle size. The product of the circular area corresponding to the clearing radius, and the areal number density of particles of the specific size range equals the number released. A summary of the clearing radius results for glass beads on 1/8 in. aluminum plate struck by cometary meteoroids of various mass is shown in Fig. 3-A.10.

Finally, a preliminary release velocity distribution is calculated by the particle release program. Since the distribution of particles released relative to distance from impact is determined and an array of velocity versus distance is input, by integration one may infer a velocity distribution. This calculation for each particle size is valid only if the release velocity is equal to the surface velocity at the time of peak acceleration. Of course, a given impact may cause surface accelerations that far exceed the required values for release of a certain particle size for some range of distances. In this case, some of these particles will be released sooner and at different velocities. Even if a particle is released at or near peak acceleration, when the surface velocity is known, it may have a lower velocity than the surface. This factor

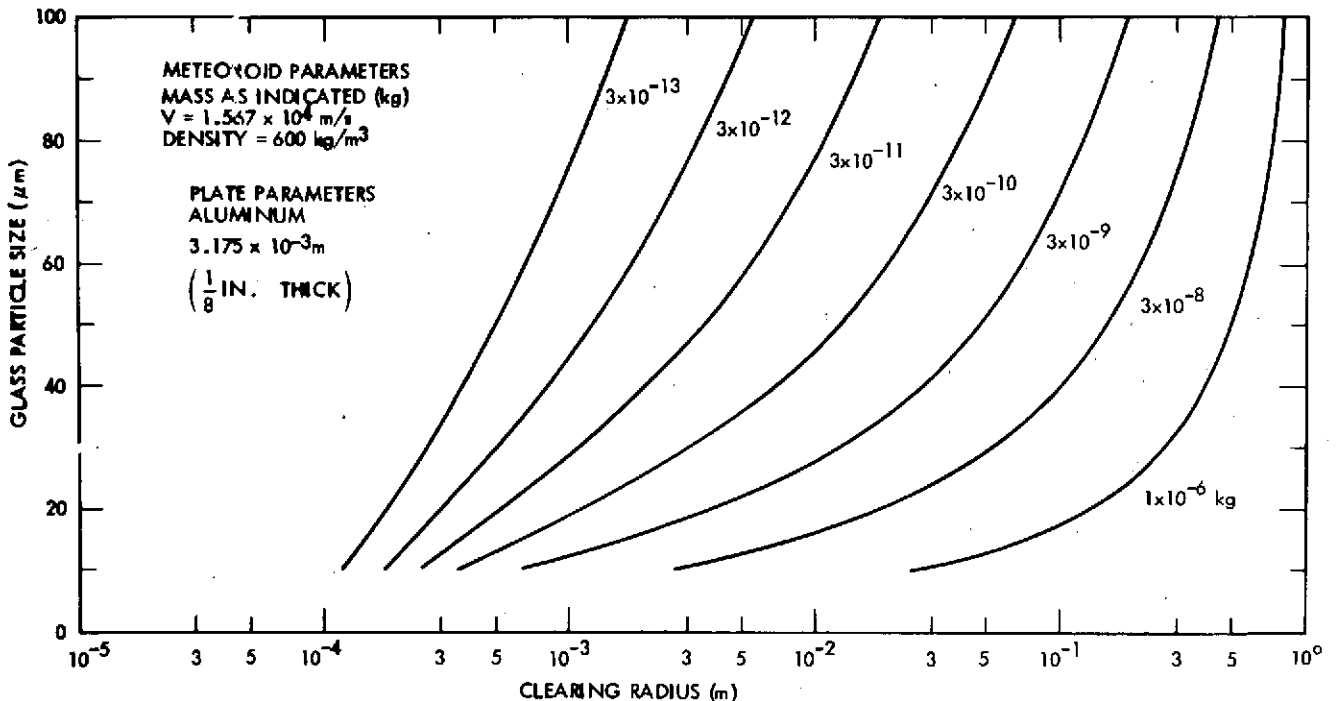


Fig. 3-A.10. Summary of calculated clearing radii

depends on the characteristics of the adhesion force. For short range forces, such as Van der Waals, the surface and particle release velocities are expected to be approximately equal, however. For the above reasons, the preliminary velocity distribution is probably skewed toward high velocities.

As examples of the applicability of the results of the meteoroid impact/particle release analysis, Figs. 3-A.11 and 3-A.12 are the post-impact glass bead profiles for our simulation of two experimental runs conducted by a LRC research group (Ref. 8). The surface acceleration data input to the particle release code for these two cases was shown in Figs. 3-A.6 and 3-A.8. In Fig. 3-A.11, a LRC data point, obtained by actually measuring the fraction of glass beads remaining on a test section at a certain distance from impact, is also indicated. Their qualitative results for the radius of the "cleared area" for these two impact cases with 37 μm beads are 3 cm for $E = 8 \text{ J}$ and 0.4 cm for $E = 0.8 \text{ J}$ (Ref. 8). Assuming these radii correspond to 50% removal and referring to Figs. 3-A.11 and 3-A.12, one finds very good agreement.

One more conclusion may be extracted from our analysis. Because of the sharp decrease of the peak acceleration with distance followed by a more gradual trend at larger distances and the probabilistic nature of the removal fraction as a function of acceleration, two extreme removal profiles are predicted. For large impacts (large mass) or particles so large that the acceleration exceeds the characteristic acceleration for removal (see para. 3.1.2.1) almost everywhere on the plate, the "cleared area" will be large, of course, but will have no distinct boundary. As either the size of the impact or the particles is reduced, eventually a point is reached where the "cleared area" has a quite distinct boundary. These predicted trends are evident in Figs. 3-A.11 and 3-A.12. This variation in the sharpness of the boundary of the "cleared area" was in fact observed (Ref. 8).

3.1.3 Future Activities

In the particle adhesion study, the acoustic emission detection tests have been reduced in scope due to resource allocations. Comprehensive release velocity tests are in progress and will be completed soon. No further experimental effort in this area is planned.

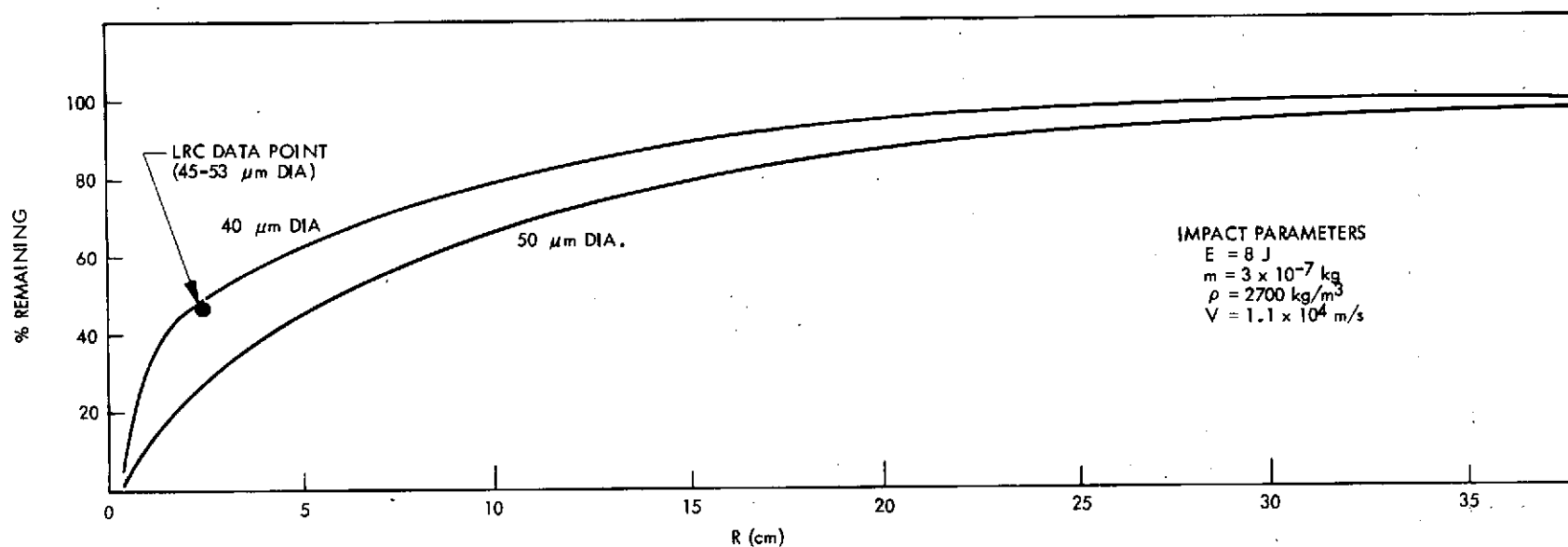


Fig. 3-A.11. Glass bead profile predicted post impact for simulation of LRC experiment, Case 1

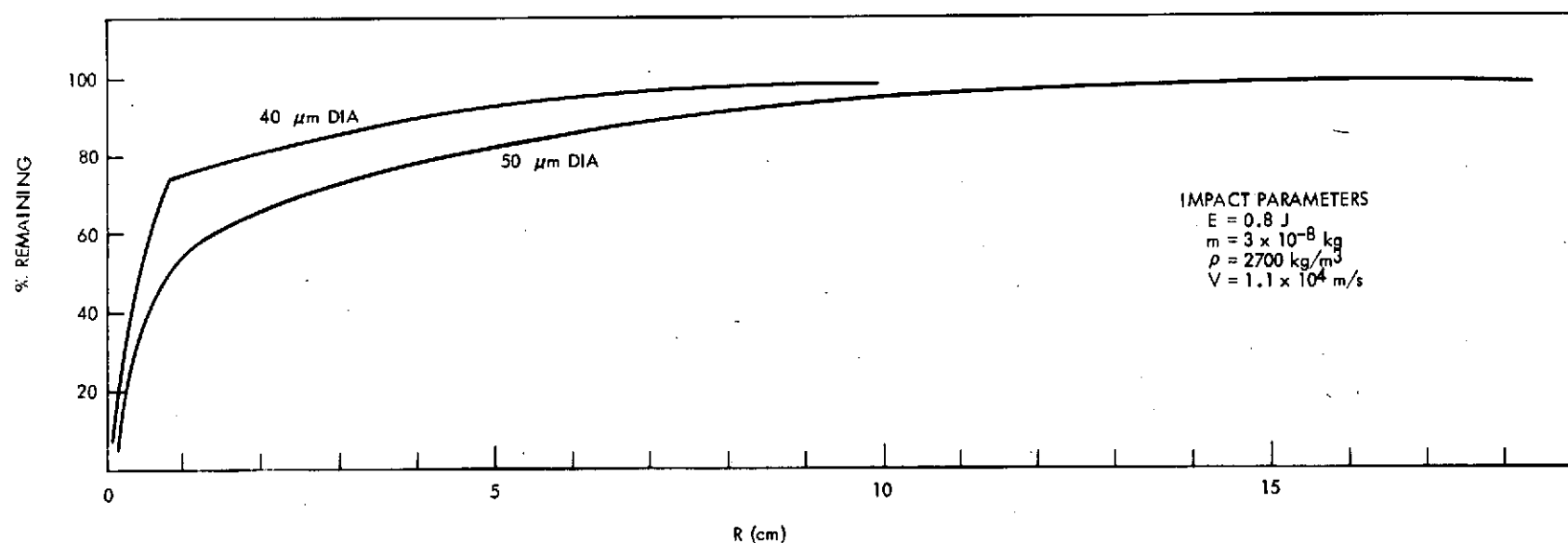


Fig. 3-A.12. Glass bead profile predicted post impact for simulation of LRC experiment, Case 2

Under meteoroid impact, the new analyses due to Yang are currently being programmed. The new mathematical function routines required have been developed, but the final codes are not complete. These codes will be run in an analogous manner to the present codes for comparison.

A major effort to model the three-dimensional electric field of the spacecraft will be continued. The necessary computer program will be developed.

The program integration activity will continue.

A new activity to assess the applicability of the present recontamination analysis to space shuttle and sample return missions will be started. New areas requiring analysis will be identified.

3.1.4 Presentations

Bauerle, C., "Spacecraft Recontamination," presented at American Society of Women Engineers meeting, San Francisco, California, June, 1973.

3.1.5 References

1. Planetary Quarantine Annual Review, Space Technology and Research, July 1971-July 1972, JPL Document 900-597, February, 1973.
2. Haudenschild, C., private communication.
3. Planetary Quarantine Semi-Annual Review, Space Research and Technology, 1 January - 30 June 1973, JPL Document 900-636, October 1973.
4. Zimon, A. D., "Adhesion of Dust and Powder," transl. M. Corn, Plenum Press, 1969.
5. Nelson, B., private communication.
6. Corn, M., J. Air Pollution Control Assoc., Vol. 11, 1961.
7. Robinson, E., private communication.
8. Humes, D. H., et al., private communication.
9. Ludloff, K. G., "A Hydrodynamic Model for Hypervelocity Impact," UCLA Ph.D. thesis, 1967.
10. Sneddon, I. N., "Fourier Transforms," McGraw-Hill Book Company, Inc., 1951.

11. Mitra, M., "Disturbance Produced in an Elastic Half-Space by Impulsive Normal Pressure," Proc. Camb. Phil. Soc. 60, 1964.
12. Knott, K., "The Equilibrium Potential of Magnetospheric Satellite in Eclipse Situation," Planetary and Space Science, 20, No. 8, 1972.
13. Divine, T. N., "Interplanetary Charged Particle Environments," JPL TM 33-637, 1973.
14. Whipple, E. C., Jr., "The Equilibrium Electric Potential of a Body in the Upper Atmosphere and in Interplanetary Space," NASA TMX 55368, 1965.

SECTION IV

SPACECRAFT CLEANING AND DECONTAMINATION TECHNIQUES
(NASA No. 193-58-63-02)

| <u>Contents</u> | <u>Title and Related Personnel</u> |
|------------------------|--|
| Subtask A para. 4.1 | PHYSICAL REMOVAL OF SPACECRAFT MICROBIAL BURDEN Cognizance: H. Schneider Associate Personnel: W. Jensen E. Roos (Bionetics) |
| Subtask B para. 4.2 | EVALUATION OF PLASMA CLEANING AND DECONTAMINATION TECHNIQUES Cognizance: S. Fraser (Boeing) D. Taylor Associate Personnel: R. Olson (Boeing) W. Leavens (Boeing) |

4.1 PHYSICAL REMOVAL OF SPACECRAFT MICROBIAL BURDEN

4.1.1 Subtask A Introduction

Present planetary quarantine constraints for flyby and orbiter vehicles require maintaining the microbial burden on the spacecraft below a certain critical level. State-of-the-art clean room facilities and contamination control techniques do not assure that this critical level can be maintained throughout necessary assembly and test operations.

Previous activities under this task concentrated on the study of vacuum technique with and without the use of a brush, and on blow cleaning by means of extra dry high purity nitrogen. A test device was developed that would allow for the simulation and evaluation of these techniques under controllable conditions with an observation of the behavior of the test particulates under a 100 X microscope. As described in detail in JPL documents 900-597 and 900-636, the following problems were identified.

- 1) Brushes efficiently detach particles of the smallest detectable size ($2-3\mu\text{m}$) but entrainment into the flow is extremely poor. The flow resistance across the bristle is very high, and flow velocities near the surface are too low to accomplish entrainment and transport of the detached particles into the vacuum system. Consequently, the bristles quickly become saturated with particles and the brush becomes a particle source rather than a cleaning tool. To avoid this, frequent cleaning, and/or perhaps, if use requires, biological decontamination of the brushes during or between uses would be necessary.
- 2) Vacuum flow alone (without the aid of a brush) efficiently detaches and removes particles larger than $10\mu\text{m}$ size if 1) the surface is dry, 2) flow velocities are near critical (choked flow) and 3) nozzle stand-off distance from the surface is approximately $150-200\mu\text{m}$. The removal efficiency drops off sharply at larger stand-off distances.
- 3) Blow cleaning efficiently removes particles greater than $5\mu\text{m}$ in size from normally dry (i. e. $\leq 50\%$ RH) surfaces at pressures

on the order of 30 psig across the blow nozzle. Pressures on the order of 50 to 80 psig are necessary to efficiently remove particulate matter smaller than 50 μm from oily (fingerprinted) surfaces.

- 4) The cleaning of moist surfaces was very inefficient under all of the conditions tested.

4.1.2 Approach

The objectives during this reporting period were to reduce the blow pressures required for efficient flow cleaning and to resolve some of the problems associated with brush cleaning. As mentioned in earlier reports, many areas exist on the spacecraft where we will depend on brush cleaning, because they are irregularly shaped and too vulnerable to potential damage resulting from vacuum or blow cleaning.

4.1.2.1 Flow Cleaning. The approach taken utilizes pulse effects to enhance particle detachment. Accessories to the existing apparatus were designed and manufactured that are capable of producing jet pulses up to 18,000 Hz and focused harmonic pressure fluctuations up to 30,000 Hz. A new device was designed and manufactured that allows for a more repeatable and controllable seeding of the test samples with glass beads or standard dust.

4.1.2.2 Brush Cleaning. The objective during the initial phase of the report period was to establish material selection criteria for the design of the test brushes. Tests to establish the mechanical properties of candidate brush fibres and their compatibility with sterilization and decontamination procedures have been conducted. The problems to be resolved next are those of accumulative contamination of the brush due to packing and poor reentrainment, and the restoration of brush cleanliness during use. A new test apparatus for brushes is being designed that will allow for a controlled simulation of a complete brush cleaning cycle consisting of consecutive linear passes over the sample surface to be cleaned, a neutralizing device (to remove static charges) and a vacuum grid to restore brush cleanliness.

4.1.3 Significant Accomplishments

4.1.3.1 Flow Cleaning. Pulse-blow-vacuum cleaning tests were conducted on glass slides seeded with glass beads. To generate pulse effects, the blow jet was interrupted by means of a variable speed rotary mask. An improvement in removal efficiency over steady-state blow is evident. Best results were obtained at low frequencies on the order of 20 to 30 Hz and at pressures between 10 and 15 psig. Tests with GM standard dust are in progress.

4.1.3.2 Brush Cleaning. Tests to establish the mechanical properties of candidate bristle material for cleaning brushes have been completed. The tests show that the material in use (natural sable hair) has a very low fatigue resistance and tends to break up and to shed during use. Dupont Felor fiber was found to have most acceptable properties as a substitute material, particularly in regard to utilization in rotary cleaning brushes. Details regarding these tests are outlined in Appendix A.

Tests with Felor fiber to establish its compatibility with sterilization and decontamination procedures are in progress and have not been concluded at the time of this report.

4.1.4 Future Activities

4.1.4.1 Flow Cleaning. Because of the encouraging results obtained to date, emphasis will be given to the evaluation of jet "blocking" techniques. The next evaluation will be the utilization of resonating (standing wave) tubes to transfer the pulse generated from the rotary mask to the surface which, if workable, would have practical advantages for the cleaning of areas that are difficult to reach. Means to generate pulse effects without jet blocking will also be tested. An apparatus has been prepared to produce jet oscillation by means of resonating rods and wedges. Trial and error tests with ultrasonic methods using the existing Hartmann generator will be conducted to establish whether further investigations in this direction are worthwhile.

4.1.4.2 Brush Cleaning. Aerodynamical and removal efficiency tests will be conducted with Felor test brushes using the linear sweep applicator described in para. 4.1.2.2. The test brushes consist of five to seven 3 mm diameter Felor bundles equally spaced abreast sweeping a 2.5 cm wide area over a 5 cm x 5 cm sample plate. The cantilevered length of the brush hair will be varied from 5 to 15 mm. The brushes will be tested in single row and staggered double row arrangement. The objective of these tests is to establish design criteria for a self cleaning rotary test brush.

4.1.4.3 Electrical Charges. Concern was expressed about the possibility of generating static charges on sensitive electronic equipment when working surfaces with high velocity flow and/or brush action. The brush test apparatus provides for a neutralization of the brush hair during use to establish charge effects on the removal efficiency. It is not within the scope of the present task to measure charges, neither for brush nor for flow application. Quantitative charge studies may be necessary for a final acceptance of the chosen cleaning methods.

4.2 EVALUATION OF PLASMA CLEANING AND DECONTAMINATION TECHNIQUES

4.2.1 Subtask B Introduction

Heat and chemicals have been traditionally used as spacecraft microbial decontaminants. However, certain materials and complex equipment often suffer degradation and a loss in reliability due to heat damage or chemical incompatibility. In addition, these traditional methods are not readily adaptable for use in space, i. e., on interplanetary sample return missions.

Plasma cleaning and sterilization involves exciting a gas and passing it over the material to be sterilized. The apparatus used includes a gas exciter (radio frequency), sterilization chamber and vacuum pump. In operation, specimens are placed in the sterilization chamber, pressure reduced, and excited gas is introduced. Sterilization is believed to occur, although the parameters are not well understood, particularly as they may be applied to typical spacecraft applications. The plasma process does not appear to degrade materials which have been tested to date and, in addition, does not significantly raise the temperature of the object being sterilized.

The program's objective is to develop and apply plasma gas sterilization technology to problems associated with planetary quarantine.

4.2.2 Approach

Phase I was concerned with parametric research to define optimum operating conditions for plasma sterilization. Previous preliminary Boeing data showed the feasibility of using an argon plasma, at low pressures, to inactivate Bacillus subtilis var. niger spores. Radio frequency (rf) power values were also shown to affect the rate of spore death. Phase I was designed to define, via specific test matrices, optimum rf power and the "best" single gas and chamber pressure required for plasma sterilization. In addition, both theoretical and experimental plasma physics functions were performed. A description of the two tasks that comprised Phase I follows.

4.2.2.1 Plasma of Single Gases. The objective of this task was to determine the relative effectiveness of different gas plasmas for sterilizing. Plasmas of argon, helium, nitrogen and oxygen were generated by radio frequency electrodeless excitation. Samples of microorganisms were exposed to the plasma flows and analyses for survivors were performed.

The test equipment used in this study is diagrammed in Fig. 4-B.1. Gas, monitored by a flowmeter, passed into the discharge region. External copper electrodes excited the gas and initiated ionization. The radio frequency power supply provided the energy coupling into the gas at 13.56 MHz (FCC requirements). After rf excitation, the gas passed out of the electrode region and the "active" species were carried through the glass sterilization chamber and eventually exhausted by a mechanical pump. The electronics package consisted of an a-c power supply No. 516F-2, transmitter No. 32S-3, rf linear amplifier No. 30S-1, antenna tuner No. 180S-1, and a directional wattmeter No. 302C-3 (Collins Radio Company, Cedar Rapids, Iowa).

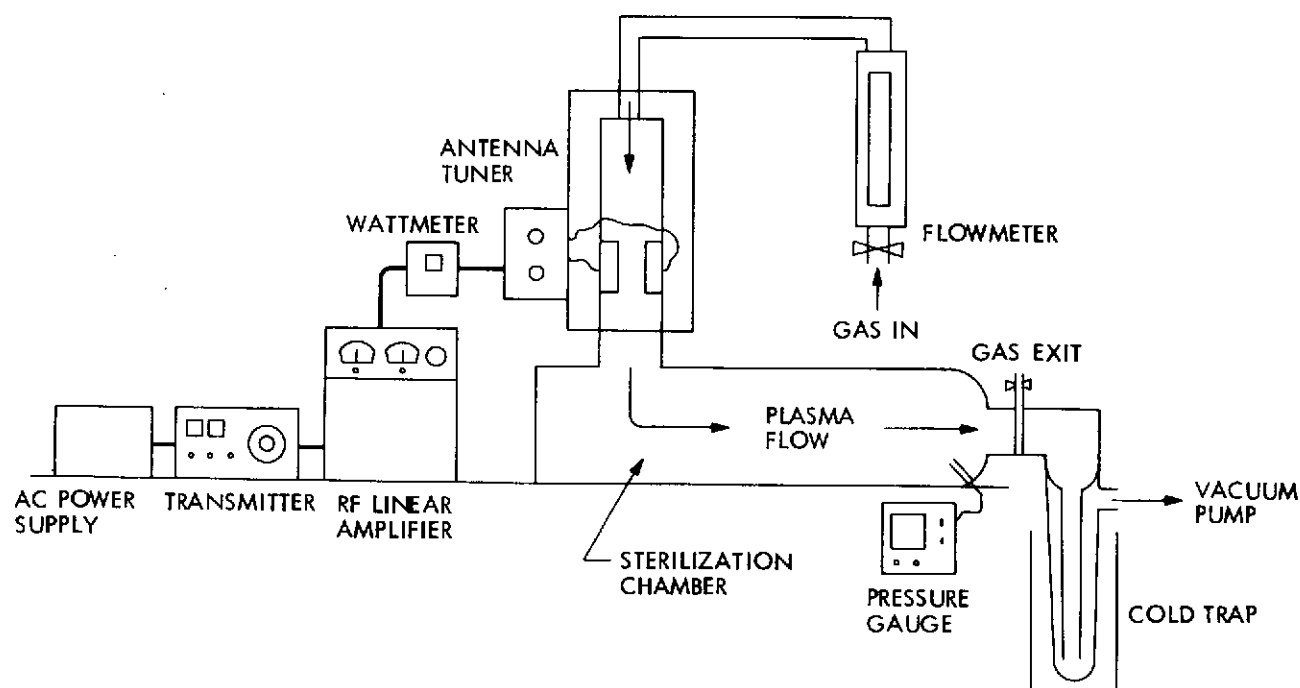


Fig. 4-B.1. Plasma sterilizer research unit

In operation, test samples were positioned in the sterilization chamber, the pressure reduced, test gas flow adjusted, and then power was applied to excite the gas via the external rf coupled electrodes. The configuration of the plasma sterilizer was such that ionized gas flowed over the samples through the chamber (Fig. 4-B.2).

Parametric values for rf power, chamber pressure, gas flow and exposure time were varied. The test matrix is shown in Table 4-B.1. The gases, argon and helium, were each tested under these variables. The gases, oxygen and nitrogen, were found to produce less effective sterilizing plasmas during equipment checkout. Therefore, only the longest test exposure, 15 minutes, was studied.

The effectiveness of plasma gas for sterilizing was determined by exposing a controlled number of the sporeformer Bacillus subtilis var. niger to the plasma and analyzing for survivors. The test samples consisted of stainless steel planchets inoculated with approximately 10^5 spores.

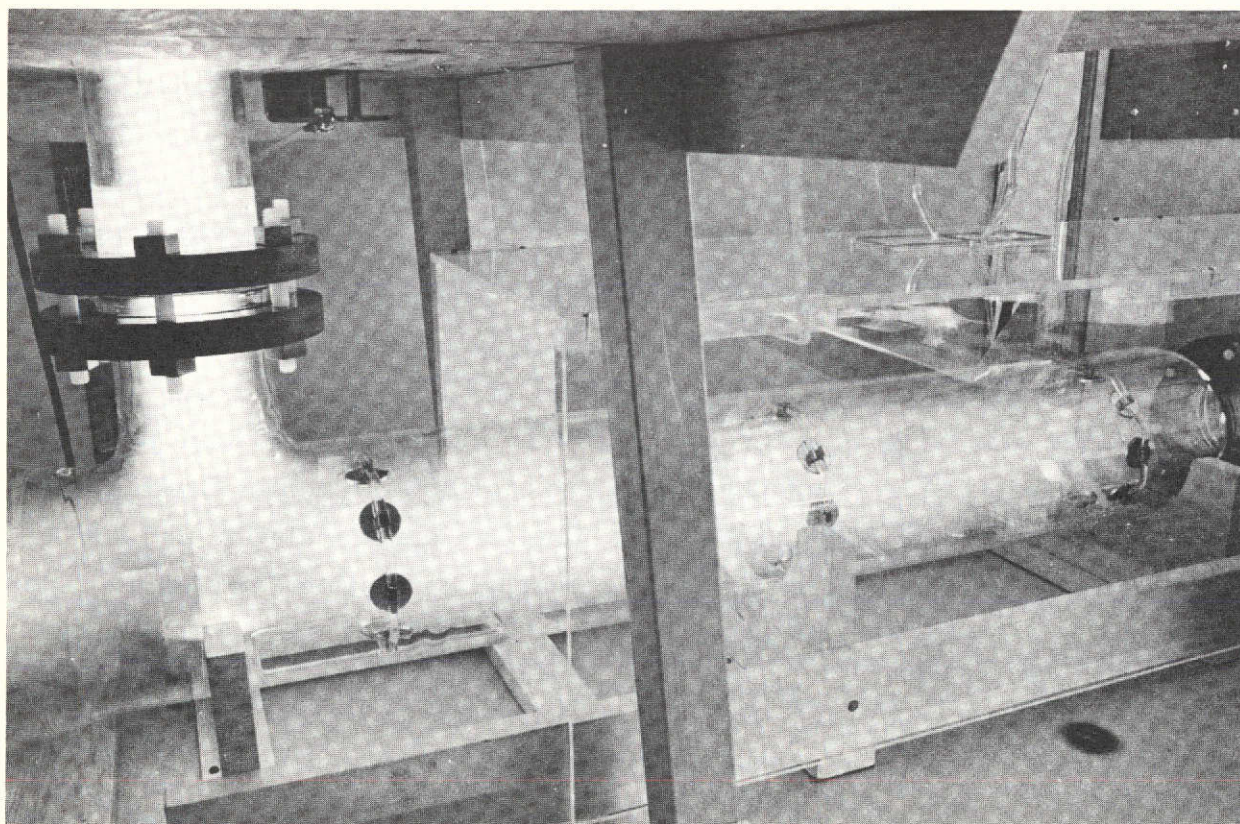


Fig. 4-B.2. Helium plasma flowing through sterilization chamber

Table 4-B. 1. Test Matrix

| RF POWER, watts | EXPOSURE TIME, min | CHAMBER PRESSURE, mm Hg | | | | | |
|-----------------------|--------------------------|-------------------------|-------------|------|-------------|------|-------------|
| | | 0.2 | | 0.5 | | 1.0 | |
| | | GAS FLOW, cc/min | | | | | |
| | | 10 | 20 | 10 | 20 | 10 | 20 |
| 50 | 5 | A-1 * | A-4 | B-7 | B-10 | C-13 | C-16 |
| | 10 | A-2 | A-5 | B-8 | B-11 | C-14 | C-17 |
| | 15 | A-3 | <u>A-6</u> | B-9 | <u>B-12</u> | C-15 | <u>C-18</u> |
| 150 | 5 | D-19 | D-22 | E-25 | E-28 | F-31 | F-34 |
| | 10 | D-20 | D-23 | E-26 | E-29 | F-32 | F-35 |
| | 15 | D-21 | <u>D-24</u> | E-27 | <u>E-30</u> | F-33 | <u>F-36</u> |
| 300 | 5 | G-37 | G-40 | H-43 | H-46 | J-49 | J-52 |
| | 10 | G-38 | G-41 | H-44 | H-47 | J-50 | J-53 |
| | 15 | G-39 | <u>G-42</u> | H-45 | <u>H-48</u> | J-51 | <u>J-54</u> |

*Test Number

The test configuration for each plasma test consisted of locating the inoculated samples at three positions in the sterilizing chamber (Fig. 4-B.3). At each position a glass ring held six test planchets and two sterile control planchets. Therefore, each complete test, or loaded chamber, was composed of 18 inoculated test planchets and six sterile controls.

Appropriate ambient die-off and procedural test controls were conducted for each test. Analyses of the exposed samples and controls were performed per standardized microbial recovery procedures. These procedures were adapted from NASA Standard Procedures for the Microbial Examination of Space Hardware NHB 5340.1A, and included sample inoculation and drying in a Class 100 clean bench, microbial removal by sonication, and enumeration with Trypticase Soy Agar pour plates.

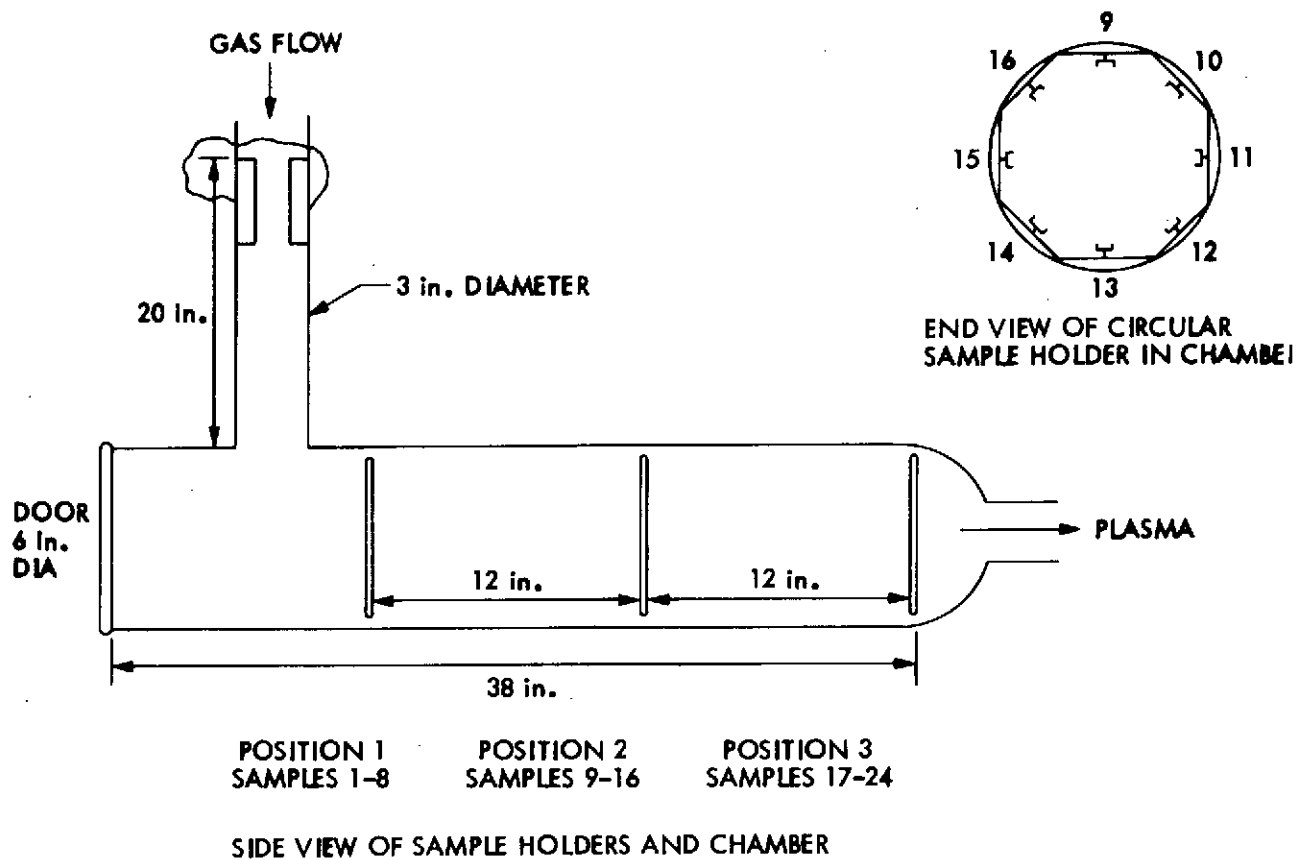


Fig. 4-B.3. Sample holders and chamber

An additional analysis was conducted during the single gas task. For all test variables of the test matrices, temperatures at the three chamber positions were measured and recorded immediately following a 15 minute plasma exposure. Temperature probes consisted of stainless steel planchets soldered to thermocouples.

4.2.2.2 Plasma Physics. The plasma used in these experiments is generated by an rf discharge in low pressure gas. It consists of free electrons, positive ions, and (in some cases) negative ions. In polyatomic gas species, the ions may be atomic or molecular. The plasma is much less dense than the gas; for every ion or electron there may be millions of neutral gas atoms or molecules

The neutral gas is flowing from an inlet on one side of the rf discharge, through the test chamber, to a vacuum pump. The plasma is carried along by the gas. Once outside the rf discharge region, the plasma decays as electrons and ions recombine, and at each recombination event, the ionization energy is released, usually as light, often in the ultraviolet (UV) region.

Plasma characteristics were determined by Langmuir probe measurements. An electrode or "probe" in the plasma was connected to an external power supply and the current collected by the probe was measured as a function of the applied voltage.

The two most likely microbial kill mechanisms in plasmas are UV irradiation from the recombining plasma, or sputtering of the cell wall by ion bombardment. Helium and argon are good UV sources. Most of the volume recombination in argon and helium at low pressures will be two-body radiative recombination. Much of the recombination energy will appear in UV lines with the resonance line at 58 nanometers. There will also be a lower energy UV continuum (60-110 nanometers) due to a three-body radiative recombination, a neutral atom being the third body. The UV spectrum from surface recombination is not known, but is probably similar to the three-body recombination spectrum. In helium, some of the continuum can pass through most UV windows (sapphire, quartz), but the line radiation cannot. Nitrogen should be a poor UV source, since recombination of negative and positive ions will tend to radiate the recombination energy in long wavelength molecular bands.

Sputtering is also suggested as a kill mechanism, especially for the argon plasma, because the ion bombardment energy is sufficient to cause sputtering. This would require opening the cell wall to allow outgassing of the cell. Sputtering rates are not known for organic materials. For inorganics there is some data on sputtering by argon ions, and similar sputtering rates could damage cell walls significantly. Sputtering has a mass-dependent threshold. At the available ion energies, argon might sputter effectively, whereas helium could not sputter most materials at all. The only significant exception being that helium ions might sputter the hydrogen atoms in organic materials.

Several experiments were conducted to distinguish between the kill mechanisms. These experiments were conducted in helium plasma. The

planchets were connected to power supplies, and kill was measured with the planchet voltage set at several points on the probe curves. Sample spore planchets were not normally connected to any outside voltage, so the spores were usually at floating potential. By putting the planchet at ground potential, the bombarding ion energy is increased, but not the flux. Similarly, at voltage near and above ground potential the same flux of ions strikes the surface of planchets with less energy. Sputtering kill should drop drastically; UV kill should stay approximately constant. Just above space potential, the ions can no longer reach the planchet surface, and both sputtering and the surface recombination contribution to UV kill should stop (see paragraph 4.2.3.2).

Another experimental approach was to protect B. subtilis spores from UV and the plasma constituents. This was accomplished by covering three sample planchets with green glass. In addition, spores were exposed to UV by covering three samples with sapphire windows. These samples also were protected from the plasma constituents. Uncovered spore samples were included and these were exposed to the complete plasma environment: ions, electrons, and recombination UV. This test was conducted with the parameters of entry G-42 of Table 4-B.1 and helium plasma.

4.2.3 Significant Accomplishments

4.2.3.1 Plasma of Single Gases. Plasmas of the gases argon, nitrogen, oxygen and helium were tested for their sterilizing effectiveness. Data obtained are presented.

1. Argon Plasma. The percentage of Bacillus subtilis spores surviving argon plasma exposure is presented in Table 4-B.2. From these data it is noted that:

- 1) The number of survivors decreased as chamber pressure decreased. A pressure of 0.2 torr resulted in more microbial kill.
- 2) An argon flow of 20 cc per minute did not result in more active plasma than 10 cc per minute.

Table 4-B.2. Percent Survival of Bacillus Subtilis Spores
Due to Argon Plasma Exposure^a

| RF POWER, watts | ARGON FLOW, cc/min | PLASMA EXPOSURE, min | CHAMBER PRESSURE, mm Hg | | | | | | | | |
|-----------------------|--------------------------|----------------------------|-------------------------|-------|--------|-------|--------|--------|--------|--------|--------|
| | | | 0.2 | | | 0.5 | | | 1.0 | | |
| | | | POS 1 | POS 2 | POS 3 | POS 1 | POS 2 | POS 3 | POS 1 | POS 2 | POS 3 |
| 50 | 10 | 5 | 0.15 ^b | 51.02 | 89.80 | 38.78 | 89.80 | 73.47 | 100.00 | 100.00 | 100.00 |
| | | 10 | 0.24 | 63.27 | 100.00 | 28.57 | 75.51 | 89.80 | 95.92 | 100.00 | 100.00 |
| | | 15 | 0.18 | 13.67 | 79.59 | 6.53 | 97.60 | 95.92 | 91.84 | 91.84 | 100.00 |
| | 20 | 5 | 0.09 | 26.53 | 95.92 | 30.61 | 100.00 | 100.00 | 100.00 | 100.00 | 100.00 |
| | | 10 | 0.39 | 24.49 | 79.59 | 1.65 | 95.92 | 97.96 | 81.63 | 100.00 | 100.00 |
| | | 15 | 0.33 | 3.88 | 79.59 | 0.27 | 75.51 | 87.76 | 85.71 | 100.00 | 100.00 |
| 150 | 10 | 5 | 0.18 | 0.45 | 20.41 | 0.29 | 67.35 | 91.84 | 51.02 | 89.80 | 100.00 |
| | | 10 | 0.07 | 0.19 | 3.67 | 0.22 | 59.19 | 65.31 | 7.55 | 93.88 | 100.00 |
| | | 15 | 0.05 | 0.29 | 4.69 | 0.03 | 13.67 | 73.47 | 0.22 | 83.67 | 89.80 |
| | 20 | 5 | 0.19 | 0.17 | 4.08 | 0.19 | 8.37 | 93.88 | 1.14 | 81.63 | 85.71 |
| | | 10 | 0.14 | 0.12 | 0.24 | 0.22 | 0.22 | 65.31 | 0.18 | 61.22 | 85.71 |
| | | 15 | 0.09 | 0.05 | 0.31 | 0.06 | 0.27 | 63.27 | 0.18 | 83.67 | 75.51 |
| 300 | 10 | 5 | 0.15 | 11.63 | 55.10 | 20.41 | 89.80 | 100.00 | 79.59 | 89.80 | 93.88 |
| | | 10 | 0.05 | 12.24 | 61.22 | 2.65 | 91.84 | 97.60 | 77.55 | 83.67 | 81.63 |
| | | 15 | 0.05 | 10.41 | 77.55 | 0.31 | 83.67 | 87.76 | 30.61 | 46.94 | 38.78 |
| | 20 | 5 | 0.07 | 1.27 | 71.43 | 3.27 | 81.63 | 93.88 | 75.51 | 85.71 | 87.76 |
| | | 10 | 0.12 | 0.35 | 79.59 | 0.24 | 75.51 | 81.63 | 55.10 | 53.06 | 79.59 |
| | | 15 | 0.08 | 0.01 | 65.31 | 0.11 | 67.35 | 87.76 | 48.98 | 97.96 | 85.71 |

^a 4.9×10^4 spores at 0 time

^b Mean of 6 replicates

- 3) A power input of 150 watts (rf) appeared to excite argon to a more effective sterilizing state than 300 watts (rf).
- 4) Using Position 3 as a conservative reference point, optimum kill throughout the chamber occurred at operating conditions of 150 watts and 0.2 torr pressure for argon plasma.

Sample temperatures, recorded after 15 minute argon plasma tests, ranged from 21° to 70° C. Chamber positions 2 and 3 experienced no temperatures in excess of 30° C at all test conditions.

2. Nitrogen Plasma. Generally, B. subtilis spores were not affected to any great degree by exposure to nitrogen plasma for 15 minutes (Table 4-B.3). Sample temperatures during plasma exposure ranged from 22° to 38° C.

Table 4-B.3. Percent Survival of Bacillus Subtilis Spores
due to 15 min Nitrogen Plasma Exposure^a

| RF POWER, watts | CHAMBER PRESSURE, mm Hg | | | | | | | | |
|--------------------|-------------------------|-------|-------|-------|-------|-------|-------|-------|-------|
| | 0.2 | | | 0.5 | | | 1.0 | | |
| | POS 1 | POS 2 | POS 3 | POS 1 | POS 2 | POS 3 | POS 1 | POS 2 | POS 3 |
| 50 | 88.9 ^b | 88.9 | 86.7 | 100.0 | 97.8 | 100.0 | 100.0 | 80.0 | 100.0 |
| 150 | 6.9 | 75.1 | 88.9 | 82.2 | 93.3 | 97.8 | 73.3 | 80.0 | 91.1 |
| 300 | 0.0 | 64.4 | 82.2 | 60.0 | 93.3 | 100.0 | 75.6 | 80.0 | 82.2 |

^a 4.5×10^4 at 0 time

^b Mean of 6 replicates

3. Oxygen Plasma. Oxygen plasma was found to be a relatively weak sterilizing agent. Although some lethality was noted at the two lower chamber pressures (0.2 and 0.5 torr), effective reductions in microbial percentages were not obtained (Table 4-B.4). Under the test conditions for plasma production, it appears that oxygen plasma was slightly more lethal than nitrogen, but nowhere near as efficient as argon plasma. Sample temperatures during oxygen plasma production were comparable to those recorded in nitrogen plasma.

4. Helium Plasma. Table 4-B.5 is the survival data obtained from exposing B. subtilis spores to helium plasma. From these data it is noted that:

- 1) The number of survivors decreased as the chamber pressure decreased. A greater total spore kill was observed at 0.2 torr than at 1.0 torr.
- 2) Differences in helium flow did not greatly change plasma sterilizing effectiveness.

Table 4-B.4. Percent Survival of Bacillus Subtilis Spores
due to 15 min Oxygen Plasma Exposure^a

| RF POWER, watts | CHAMBER PRESSURE, mm Hg | | | | | | | | |
|--------------------|-------------------------|-------|-------|-------|-------|-------|---------------------|-------|-------|
| | 0.2 | | | 0.5 | | | 1.0 | | |
| | POS 1 | POS 2 | POS 3 | POS 1 | POS 2 | POS 3 | POS 1 | POS 2 | POS 3 |
| 50 | 35.5 ^b | 74.2 | 71.0 | 64.5 | 80.6 | 83.9 | TEST NOT APPLICABLE | | |
| 150 | 0.0 | 74.2 | 25.8 | 35.5 | 77.6 | 73.9 | 100.0 | 100.0 | 100.0 |
| 300 | 0.0 | 9.7 | 64.5 | 0.1 | 71.0 | 67.3 | 77.6 | 96.8 | 93.5 |

^a 3.1×10^5 spores at 0 time

^b Mean of 6 replicates

- 3) A power input of 300 watts (rf) excites the helium to a very effective sterilizing level.
- 4) Using Position 3 as the most conservative reference point, a spore reduction of 3.21 logs occurred at operating conditions of 300 watts and 0.2 torr pressure for helium plasma.
- 5) Helium plasma was generally more efficient as a sterilizing agent than argon, oxygen or nitrogen. Microbial kill was noted at most of the operating conditions of the test matrix.

Sample temperatures during helium plasma production ranged from 19° to 50°C (Table 4-B.6).

4.2.3.2 Plasma Physics. Measurements of the plasma properties have been made, and experiments relating plasma phenomena and spore kill have been carried out. In this section, the plasma characteristics are described; some of the relevant plasma phenomena are explained; and the results of a kill mechanism experiment are described.

Table 4-B.5. Percent Survival of Bacillus Subtilis Spores due to Helium Plasma Exposure^a

| RF POWER, watts | HELIUM FLOW cc/min | PLASMA EXPOSURE min | CHAMBER PRESSURE, mm Hg | | | | | | | | |
|-----------------|--------------------|---------------------|-------------------------|-------|-------|-------|-------|-------|-------|-------|-------|
| | | | 0.2 | | | 0.5 | | | 1.0 | | |
| | | | POS 1 | POS 2 | POS 3 | POS 1 | POS 2 | POS 3 | POS 1 | POS 2 | POS 3 |
| 50 | 10 | 5 | 0.04 ^b | 28.57 | 38.10 | 11.43 | 66.67 | 80.95 | 35.71 | 47.62 | 54.76 |
| | | 10 | 0.02 | 13.33 | 22.14 | 4.52 | 42.86 | 35.71 | 23.33 | 35.71 | 47.62 |
| | | 15 | 0.03 | 19.29 | 23.57 | 0.24 | 26.19 | 26.19 | 11.67 | 26.19 | 33.33 |
| | 20 | 5 | 1.24 | 40.49 | 47.62 | 9.05 | 52.38 | 47.62 | 19.52 | 28.57 | 26.19 |
| | | 10 | 0.08 | 28.57 | 54.76 | 1.24 | 28.57 | 35.71 | 14.52 | 26.19 | 26.19 |
| | | 15 | 0.03 | 22.62 | 45.24 | 0.88 | 22.86 | 19.05 | 10.71 | 22.14 | 21.90 |
| 150 | 10 | 5 | 0.01 | 0.17 | 10.00 | 0.02 | 10.95 | 13.81 | 2.86 | 40.48 | 38.10 |
| | | 10 | 0.00 | 0.02 | 2.86 | 0.00 | 3.81 | 12.14 | 0.64 | 33.33 | 40.48 |
| | | 15 | 0.00 | 0.01 | 4.52 | 0.00 | 4.29 | 11.67 | 0.09 | 28.57 | 38.10 |
| | 20 | 5 | 0.04 | 0.31 | 33.33 | 0.48 | 73.81 | 97.62 | 1.00 | 35.71 | 33.33 |
| | | 10 | 0.02 | 0.06 | 15.71 | 0.04 | 61.90 | 95.24 | 0.07 | 28.57 | 33.33 |
| | | 15 | 0.01 | 0.03 | 9.05 | 0.04 | 30.95 | 71.43 | 0.04 | 23.81 | 35.71 |
| 300 | 10 | 5 | 0.04 | 0.05 | 11.43 | 0.01 | 6.90 | 15.00 | 0.03 | 8.81 | 16.43 |
| | | 10 | 0.01 | 0.01 | 0.07 | 0.00 | 5.00 | 11.43 | 0.01 | 13.81 | 13.81 |
| | | 15 | 0.00 | 0.01 | 0.08 | 0.00 | 2.21 | 10.71 | 0.01 | 8.81 | 16.90 |
| | 20 | 5 | 0.03 | 0.12 | 0.36 | 0.03 | 7.38 | 76.19 | 0.03 | 6.19 | 9.52 |
| | | 10 | 0.01 | 0.02 | 0.12 | 0.01 | 0.76 | 73.81 | 0.02 | 7.14 | 7.86 |
| | | 15 | 0.00 | 0.01 | 0.06 | 0.02 | 0.33 | 59.52 | 0.01 | 5.71 | 10.48 |

^a 4.2×10^5 spores at 0 time^b Mean of 6 replicates

The properties of the plasma have been studied by Langmuir probe techniques. The first probe results revealed that the plasma has several unusual features which demand care in interpreting measurements.

Most rf generated flowing plasmas are characterized by low electron and ion temperatures and rapid volume recombination downstream from the ionization region (between the rf plates). The visible light from these "flowing afterglows" is dominated by the recombination spectrum, and the UV light by a continuum at energies well below the resonance line. None of the ions and electrons in such discharges have sufficient energy for impact damage to any surface.

The rf generated flowing plasma used in these experiments, however, is quite different. While the ions are still cold (meaning perhaps 1000°K), the

Table 4-B.6. Temperature of Stainless Steel Planchets Immediately After 15 min Exposure to Helium Plasma, deg. C

| RF POWER, watts | HELIUM FLOW, cc/min | CHAMBER PRESSURE, mm Hg | | | | | | | | | | | |
|-----------------|---------------------|-------------------------|----|----|----------------|----------|----|----|----|----------|----|----|----|
| | | 0.2 | | | | 0.5 | | | | 1.0 | | | |
| | | POSITION | | | | POSITION | | | | POSITION | | | |
| | | 1 | 2 | 3 | 4 ^a | 1 | 2 | 3 | 4 | 1 | 2 | 3 | 4 |
| 50 | 10 | 27 | 23 | 22 | 20 | 29 | 23 | 22 | 21 | 27 | 23 | 23 | 22 |
| | 20 | 27 | 23 | 22 | 20 | 27 | 22 | 22 | 20 | 26 | 23 | 23 | 22 |
| 150 | 10 | 34 | 24 | 22 | 21 | 38 | 23 | 22 | 22 | 35 | 23 | 23 | 22 |
| | 20 | 32 | 23 | 21 | 20 | 33 | 19 | 19 | 19 | 34 | 23 | 23 | 22 |
| 300 | 10 | 44 | 30 | 26 | 22 | 43 | 27 | 23 | 20 | 50 | 24 | 22 | 22 |
| | 20 | 40 | 30 | 27 | 22 | 41 | 27 | 26 | 22 | 47 | 24 | 23 | 22 |

^a Probe outside chamber - ambient

electrons are fairly hot, having a temperature of approximately 80,000°K in the helium plasma, for example. The unusually high electron temperature is due to rf fields which leak from the excitation area. These fields are measured at 30-50v/cm, which is not sufficient to cause breakdown, but is enough to heat the plasma.

High electron temperatures have several important effects on the behavior of the plasma. First, the recombination rate is lower and, consequently, the plasma can flow further. Second, insulating walls and other objects drawing zero net current from the plasma are charged to a negative potential, called the floating potential, V_f

$$V_f \approx - \frac{KT_e}{e} \frac{1}{2} \ln (m_+/m_-) \quad (1)$$

where T_e is the electron temperature, K is Boltzmann's constant, m_+ is the ion mass, and e and m_- are the charge and mass of the electron. (The term "temperature" is used merely to denote the average electron energy, and does not necessarily imply a Boltzmann distribution, although Eq. (1) is most accurate for a Boltzmann distribution.)

All floating (insulators and any other surface collecting zero net current) surfaces are bombarded by ions attracted by the negative potential. In nitrogen, for example, the observations indicate that ions with energies up to 42 electron volts are bombarding the floating surfaces.

The floating potential given by Eq. (1) is not measured with respect to ground potential but instead with respect to the potential of the nearby plasma, called space potential or plasma potential. In most plasmas, space potential is close to ground potential, and floating potential, when measured with respect to ground, is given by Eq. (1). In this plasma, however, space potential is high, being about 75 volts above ground, and floating potential, although properly negative with respect to space potential Eq. (1), is positive with respect to ground. As a result, the ions would bombard a grounded surface at higher energies than a floating surface.

The potential drop between the plasma and a "floating" object (a spore, for example) occurs over a distance, called the Debye length, which is characteristic of electrostatic effects in plasmas. The number of ions which will bombard the surface with the full energy given by the floating potential depends on whether or not they can travel one Debye length without colliding with a neutral gas atom. For the helium plasma in these experiments at the lower pressures, the necessary conditions for full energy are met.

The flux of ions bombarding a floating surface is relatively independent of the pressure, and is proportional to the ion density in the nearby plasma. The total flux of accelerated heavy particles, however, increases with pressure because of charge transfer collisions - an ion being accelerated toward the surface may pick up an electron from a passing neutral, and continue (now neutral itself) with no further acceleration, while the passing neutral (now an ion) is accelerated the rest of the way to the surface.

The Debye length is relevant to another important physical process that must be considered for future investigations--penetration of holes and cracks. The one λ_D thick region where the potential drops from space potential to floating potential is called a Langmuir sheath, a space-charge sheath, or just a sheath. This sheath acts to conceal any surface feature smaller in characteristic dimension than λ_D .

The result of the experiment to find an effect in helium plasma of grounding the sample planchet in comparison to allowing the planchet to remain at floating potential was negative. That is, the survival fraction showed no apparent relationship to ion energy as might be expected if sputtering were the dominant kill mechanism.

Table 4-B.7 contains the data obtained from a screening test to detect the presence of UV in helium plasma. Spores that were protected from UV survived. Spores that were covered with a sapphire window, and saw wavelengths in the UV region (140 to 300 nanometers), did not survive. The data may be interpreted that UV, or rather something shorter than 350 nanometers, was present in the helium plasma, and that it was lethal to the spores. The

Table 4-B.7. Number of Bacillus Subtilis Spores Surviving
15 min Exposure to Helium Plasma^a

| SPORES ^a | Chamber Position | | |
|---|-------------------|-------------------|-------------------|
| | 1 | 2 | 3 |
| Glass Covered (no UV) | 2.7×10^5 | 2.0×10^5 | 2.3×10^5 |
| Uncovered | 3.0×10^0 | 1.0×10^1 | 5.3×10^1 |
| Sapphire Covered (UV) | 6.0×10^1 | 5.6×10^1 | 2.5×10^4 |
| Uncovered | 3.0×10^0 | 4.3×10^1 | 4.3×10^1 |
| ^a 4×10^5 Spores at 0 Time | | | |

data may also suggest that exposure to the lethal agent is not dependent on having the helium plasma constituents in direct contact with the spores. Thus, it appears that sputtering is not the dominant kill mechanism in helium plasma.

4.2.4 Summary and Conclusions

The data of the results of plasma experiments completed during Phase I indicate that the combination of a low chamber pressure (0.2 mm Hg), an ionization power input of 300 watts (rf), and the single gas helium are most efficient for killing B. subtilis spores. These parameters are expected to be the operating conditions in future plasma tests to determine the microbial range of plasmas against various microbial species.

In addition, the data indicate that sterilization, with helium plasma, is only weakly dependent on those factors which would strongly affect high sputtering rates. These results, although preliminary, suggest that UV irradiation is the dominant kill mechanism in plasma.

4.2.5 Future Activities

Phase II will concentrate on integrating the data obtained during Phase I with expanded biological testing, kill mechanisms of plasmas, and possible increases in plasma lethality due to mixed gases. A continuing plasma physics evaluation will be part of Phase II.

Phase III efforts will be primarily directed towards ascertaining spacecraft materials and plasma compatibility and determining the effectiveness of plasma gas for sterilizing surfaces of various configurations. The program approach will result in data applicable for use in development of preliminary design concepts for plasma sterilizers for space or terrestrial applications.

4.2.6 Presentations

Fraser, S. J., "Evaluation of Plasma Cleaning and Decontamination Techniques," presented at NASA Spacecraft Sterilization Technology Seminar, San Francisco, California, February, 1974.

SECTION V

PLANETARY QUARANTINE KSC OPERATIONS
(NASA No. 193-58-63-05)

Contents

Title and Related Personnel

Subtask A
para. 5.1

TEFLON RIBBON EXPERIMENTS

Cognizance: J. R. Puleo

Associate
Personnel: G. Oxborrow
N. Fields

Subtask B
para. 5.2

MICROBIOLOGICAL STUDIES ON
UNMANNED SPACECRAFT

Cognizance: J. R. Puleo

Associate
Personnel: G. Oxborrow
N. Fields

5.1 TEFLON RIBBON EXPERIMENTS

5.1.1 Subtask A Introduction

The objective of this study is to characterize the thermal resistance profiles of naturally occurring bacterial spores associated with assembly facilities at Kennedy Space Center.

The validity of the currently accepted sterilization cycle should be confirmed. The cycle, to be valid, should be effective on bacterial spores associated with spacecraft in residence at Kennedy Space Center, Florida.

5.1.2 Significant Accomplishments

5.1.2.1 Experimental Conditions

1. Microbiology. An experimental sterilization facility was established at the Planetary Quarantine Laboratory, ETR/Cape Kennedy, Florida. The system consists of a temperature controlled oven with a nitrogen gas supply containing a known concentration of water. Water vapor during sterilization cycle may be controlled. Moisture analyzers with an accuracy of $\pm 5\%$ of full scale are utilized to monitor the gas flowing over spore samples contained in the oven. A temperature controller was developed and installed which gives flexibility to temperature-time sterilization cycles. Experiments were conducted to fulfill the requirement for aseptic technique. Experiments were also performed to test the homogeneity of the model terminal sterilization oven. The results showed that the thermal oven was homogeneous.

Aluminum trays (7" wide \times 74" long \times 40" high) containing two 3" \times 72" ribbons of teflon (5 mil FEP Dupont) were located in the Low Bay area of the Manned Spacecraft Operations Building (MSOB), a class 100,000 clean room, and in the Vehicle Assembly Building (VAB), an assembly area.

The teflon ribbons were cleaned in the same manner as stainless steel strips described in "NASA Standard Methods for the Microbiological Examination of Space Hardware," NHB 5340.1A, October 1968. New ribbons were preconditioned by two exposures to dry heat for three (3) hours at 175C prior to a third heating interval for sterilization. Ribbons were sterilized

before exposure in 250 ml beakers covered with aluminum foil. Ribbons were exposed to the clean room environment for seven (7) days, following which each ribbon was rolled up and aseptically inserted into a sterile stainless steel holder, and placed into sterile 600 ml beakers covered with aluminum foil. Aluminum trays were wiped with membrane filtered 70% isopropyl alcohol after exposed ribbons were collected. While handling the teflon ribbons, personnel used clean room garments and sterile gloves.

Control and test ribbons were selected randomly and 8 of 32 ribbons were used for N_0 determinations. The relative humidity and temperature of the assembly areas were monitored constantly. The recovery medium was TSA broth (same formula as TSA except without agar), plus 0.2% yeast extract and 0.1% soluble starch; TSA plus yeast extract and starch was used for determining total and spore counts on control ribbons. Each control ribbon was rolled up and placed in a sterile jar, 400 ml of sterile rinse solution (0.002% Tween 80) was added and the jars insonated for six (6) minutes, removed, manually shaken twenty-five (25) times and then insonated again for six (6) minutes. Five ml portions were plated in duplicate for total counts, and duplicate 50 ml portions were heat shocked (80C, twenty-five (25) minutes) and plated for spore counts from ribbons exposed in the MSOB. In the VAB, where a higher concentration of airborne bacterial spores were collected on the ribbons, the appropriate dilutions were made, and plated in duplicate for both total and spore counts. Plates were incubated at 32 C and colonies counted after 2, 3, and 7 days. Test ribbons were placed in the thermal oven from front to rear in the order of retrieval from the clean room. Each oven shelf contained eight test ribbons plus three sterile control ribbons. A total of 24 test ribbons and 9 sterile control ribbons were used per run. Test ribbons and sterile control ribbons were placed in the oven and exposed to dry nitrogen, as specified in para. 2.2.2 of NHB 8020.12, 6 to 8 hours prior to start of heat cycle. Sterile forceps were used in handling the ribbons into and out of the oven. After the thermal treatment, each ribbon with stainless steel holder was placed into a sterile jar and 400 ml of sterile broth was added aseptically. The jars were incubated at 32 C and observed for the presence of growth at 7 days and weekly up to 28 days. The sterile control ribbons were treated in the same manner as the test ribbons. During assay of ribbons, personnel wore clean room gown, hat, sterile gloves and mask.

The thermal oven was located in a vertical laminar flow clean bench which was attached to a horizontal laminar flow clean bench. The two benches were enclosed by a plexiglas canopy and plastic curtains. In essence, the thermal experiments and assays were done in a small clean room under class 100 hoods.

The thermal experiments were conducted in a dry heat oven under the following conditions:

- 1) Volume of oven - 1.5 cubic feet.
- 2) Nitrogen flow rate to oven during thermal experimental runs - 6 CF/hr or approximately 3 L/min. Between runs, the oven is purged with dry nitrogen.
- 3) Moisture content of dry nitrogen used - approximately 0.004 mg/L (5 ppm) (MIL-P-27401B).
- 4) Moisture content of nitrogen during thermal runs 1.2 mg/L (1500 ppm).
- 5) Thermal Profile used - High Thermal Inertia (Fig. 5-A.1.)

5.1.2.2 Results. All thermal experiments were conducted using the proposed sterilization cycle for unmanned landers (Fig. 5-A.1.) The thermal resistance of naturally occurring airborne bacterial spores collected on exposed teflon ribbons in the MSOB clean room are shown in Table 5-A.1. With the exception of two experiments, survivors were recovered from all thermal experiments.

Table 5-A.2 shows that extending the heating time from 5 to 15 additional hours at temperature, or pretreatment of teflon ribbons at 85C for two hours, prior to subjecting them to the heat cycle, failed to achieve sterilization.

Tables 5-A.3 and 5-A.4 show the results when the overall water concentration in the oven was reduced from 1.2 mg/L (R.H. 0.133%) to 0.01 mg/L (R.H. 0.001%) at the 113 C high thermal inertia cycle. Survivors were recovered from six experiments out of eighteen.

Table 5-A.5 shows the results when aluminum ribbons were compared to teflon ribbons and the water concentration was increased to 2.4 mg/L (R.H. 0.3%). In five experimental runs, survivors were recovered from three runs.

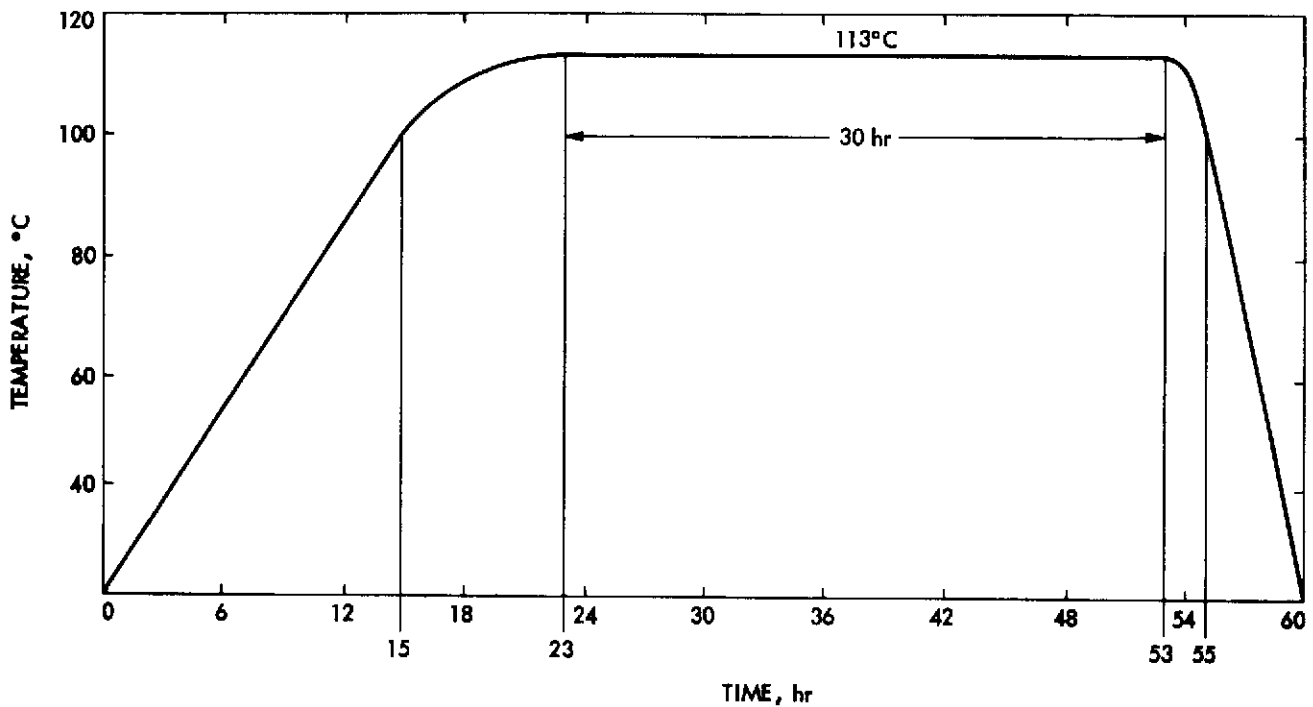


Fig. 5-A.1. Viking sterilization cycle

Table 5-A.1. Thermal Resistance of Spores Collected on Teflon Ribbons - MSOB, KSC (1.2 mg/L water)

| EXPERIMENT NUMBER | N_0 SPORES | POSITIVE/TOTAL | MPN FOR RIBBON | CONTROLS POSITIVE/TOTAL |
|-------------------|-------------------|--|----------------|-------------------------|
| 2 | 1.4×10^2 | 1/24 | 0.042 | 0/9 |
| 5 | 4.2×10^2 | 1/22 | 0.047 | 0/9 |
| 6 | 4.2×10^2 | 6/24 | 0.287 | 0/9 |
| 7 | 5.3×10^2 | 1/12 (TEFLON ONLY) 1/12 (TEFLON/FIBERGLASS) | 0.087 0.087 | 0/9 |
| 8 | 5.8×10^2 | 1/12 (TEFLON ONLY) 2/12 (TEFLON/FIBERGLASS) | 0.087 0.182 | 0/9 |
| 9 | 3.5×10^2 | 3/12 (TEFLON ONLY) 1/12 (TEFLON/FIBERGLASS) | 0.287 0.087 | 0/9 |
| 10 | 2.2×10^2 | 6/24 | 0.287 | 0/9 |
| 11 | 1.8×10^2 | 0/24 | 0.0 | 0/9 |
| 12 | 2.0×10^2 | 0/24 | 0.0 | 0/9 |
| 14 | 1.4×10^2 | 1/24 | 0.042 | 0/9 |
| 16 | 2.4×10^2 | 3/24 | 0.134 | 0/9 |

Table 5-A. 2. Thermal Resistance of Spores Collected on
Teflon Ribbons – MSOB, KSC (1.2 mg/L water)

| EXPERIMENT NUMBER | N ₀ SPORES | POSITIVE/TOTAL | MPN FOR RIBBON | CONTROLS POSITIVE/TOTAL |
|----------------------|--------------------------|----------------|----------------|----------------------------|
| 13 | 1.6×10^2 | 1/24 | 0.042 | 0/9 |
| 15 | 7.9×10^2 | 1/24 | 0.042 | 0/9 |
| 17 | 1.5×10^2 | 1/24 | 0.042 | 0/9 |
| 18 | 2.1×10^2 | 4/24 | 0.182 | 0/9 |

13 Thermal profile 113 C - Extended 5 hr at temperature (total time at temperature 35 hr)

15 Thermal profile 113 C - Extended 10 hr at temperature (total time at temperature 40 hr)

17 Thermal profile 113 C - Extended 15 hr at temperature (total time at temperature 45 hr)

18 Thermal profile 113 C - Teflon ribbons pretreated at 85°C for 2 hr prior to start of High Thermal Inertia Cycle

Table 5-A. 3. Thermal Resistance of Spores Collected on
Teflon Ribbons – MSOB, KSC (0.01 mg/L water)

| EXPERIMENT NUMBER | N ₀ SPORES | POSITIVE/TOTAL | MPN FOR RIBBON | CONTROLS POSITIVE/TOTAL |
|----------------------|--------------------------|----------------|----------------|----------------------------|
| 19 | 3.7×10^2 | 0/24 | 0.0 | 0/9 |
| 20 | 2.1×10^2 | 2/24 | 0.087 | 0/9 |
| 21 | 2.8×10^2 | 0/23 | 0.0 | 0/9 |
| 22 | 2.3×10^2 | 0/24 | 0.0 | 0/9 |
| 23 | 1.0×10^2 | 0/24 | 0.0 | 0/9 |
| 24 | 1.3×10^2 | 0/24 | 0.0 | 0/9 |
| 25 | 8.9×10^1 | 0/24 | 0.0 | 0/9 |
| 26 | 4.9×10^1 | 0/24 | 0.0 | 0/9 |
| 27 | 5.6×10^1 | 0/24 | 0.0 | 0/9 |

Table 5-A.4. Thermal Resistance of Spores Collected on
Teflon Ribbons – MSOB, KSC (0.01 mg/L water)

| EXPERIMENT NUMBER | No SPORES | POSITIVE/TOTAL | MPN FOR RIBBON | CONTROLS POSITIVE/TOTAL |
|----------------------|-------------------|----------------|----------------|----------------------------|
| 28 | 3.5×10^1 | 0/24 | 0.0 | 0/9 |
| 29 | 4.3×10^1 | 0/24 | 0.0 | 0/9 |
| 30 | 1.8×10^2 | 1/24 | 0.042 | 0/9 |
| 31 | 1.6×10^2 | 0/24 | 0.0 | 0/9 |
| 32 | 1.1×10^2 | 1/24 | 0.042 | 0/9 |
| 33 | 1.7×10^2 | 1/24 | 0.042 | 0/9 |
| 34 | 7.6×10^1 | 1/24 | 0.042 | 0/9 |
| 35 | 1.6×10^2 | 0/24 | 0.0 | 0/9 |
| 36 | 1.2×10^2 | 1/24 | 0.042 | 0/9 |

Table 5-A.5. Thermal Resistance of Spores Collected on
Teflon Ribbons – MSOB, KSC (2.4 mg/L water)

| EXPERIMENT NUMBER | No SPORES | POSITIVE/TOTAL | MPN FOR RIBBON | CONTROLS POSITIVE/TOTAL |
|----------------------|-------------------|------------------------------|----------------|----------------------------|
| 37 | 6.0×10^1 | 1/12 TEFLON 0/12 ALUMINUM | 0.087 0.0 | 0/9 |
| 38 | 8.1×10^1 | 5/12 TEFLON 2/12 ALUMINUM | 0.613 0.182 | 0/9 |
| 39 | 5.3×10^1 | 0/12 TEFLON 1/12 ALUMINUM | 0.0 0.087 | 0/9 |
| 40 | 7.6×10^1 | 0/12 TEFLON 0/12 ALUMINUM | 0.0 0.0 | 0/9 |
| 41 | 5.9×10^1 | 0/12 TEFLON 0/12 ALUMINUM | 0.0 0.0 | 0/9 |

Due to the low spore N_0 obtained and the reduced activity in the MSOB, the fallout experiment was moved to the Vehicle Assembly Building (VAB) in an attempt to increase the number of airborne bacterial spores. The results obtained are shown in Table 5-A.6. In the VAB environment, spore levels of $10^3 - 10^4$ per ribbon were obtained, and an increase in the number of positive ribbons was observed after the sterilization cycle. In the three experiments conducted at a water concentration of 2.4 mg/L, there were 40 positive ribbons out of 72. No differences were observed between the collecting ability of teflon or aluminum ribbons, although teflon surfaces tended to collect a slightly greater number of microorganisms. Aluminum ribbons were eliminated as a collecting surface because it was discovered that after exposure to the thermal sterilization cycle, and the ribbons were placed into TSA broth, the aluminum foil would deteriorate and form a precipitate in the broth. It was observed that if bacterial growth occurred before the deterioration, little or no precipitate developed. No changes in the pH of the TSA broth were observed.

Six thermal experiments were completed in the VAB environment during this period. Survivors were recovered from four experiments when the water concentration was maintained at 0.01 mg/L and the bacterial spore concentration per teflon ribbon was 10^3 (Table 5-A.7).

Table 5-A.6. Thermal Resistance of Spores Collected on Teflon Ribbons - VAB, KSC (2.4 mg/L water)

| EXPERIMENT NUMBER | N_0 SPORES | POSITIVE/TOTAL | MPN FOR RIBBON | CONTROLS POSITIVE/TOTAL |
|----------------------|-------------------|-------------------------------|----------------|----------------------------|
| 1 | 2.2×10^3 | 8/12 TEFLON 4/12 ALUMINUM | 1.099 0.406 | 0/9 |
| 2 | 8.4×10^3 | 9/12 TEFLON 0/12 ALUMINUM | 1.387 0.0 | 0/9 |
| 3 | 1.3×10^4 | 11/12 TEFLON 8/12 ALUMINUM | 2.485 1.099 | 0/9 |

Table 5-A-7. Thermal Resistance of Spores Collected on
Teflon Ribbons - VAB, KSC (0.01 mg/L water)

| EXPERIMENT NUMBER | N ₀ SPORES | POSITIVE/TOTAL | MPN FOR RIBBON | CONTROLS POSITIVE/TOTAL |
|----------------------|--------------------------|----------------|----------------|----------------------------|
| 4 | 6.4×10^3 | 4/24 | 0.182 | 0/9 |
| 5 | 4.5×10^3 | 5/24 | 0.234 | 0/9 |
| 6 | 6.1×10^3 | 5/24 | 0.234 | 0/9 |
| 7 | 7.3×10^3 | 3/24 | 0.134 | 0/9 |
| 8 | 3.0×10^3 | 0/24 | 0.00 | 0/9 |
| 9 | 4.7×10^3 | 0/24 | 0.00 | 0/9 |

Heat survivors were isolated and identified. In all experiments, the survivor from each positive ribbon was found to be a pure culture. Of the 112 bacillus isolates which survived the thermal exposure and have been identified, only six (6) were found to be able to grow anaerobically. Generally, heat survivors were found to have the following characteristics:

- 1) Produce smaller colonies and grow much slower on laboratory media than non-heat stressed environmental isolates of the genus Bacillus.
- 2) Sporulate poorly on sporulation media.
- 3) Biochemically less active than non-heat stressed environmental isolates.

Studies are presently being conducted to determine if the above characteristics are inherent properties of the organisms or are the result of thermal exposure.

There are at least two unknown factors involved in the thermal inactivation kinetics of naturally occurring bacterial spore populations. These factors are, 1) influence of spore N₀, and 2) influence of water concentration. Figure 5-A.2 shows the effect of spore N₀ on the number of heat survivors using two different water concentrations. The results showed that when the

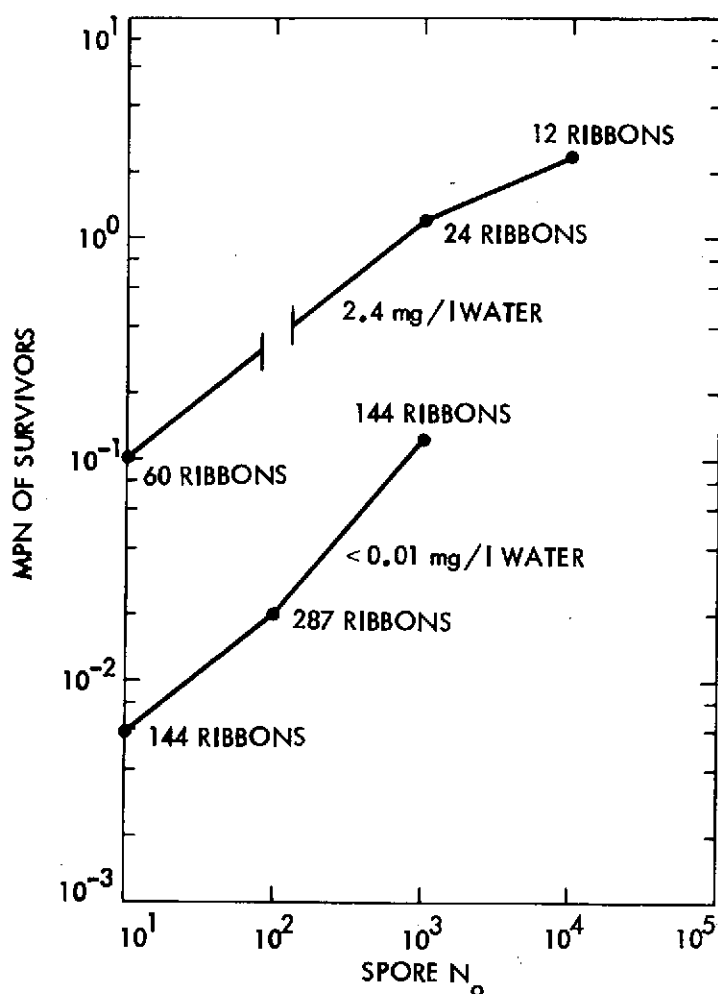


Fig. 5-A. 2. Influence of spore N_0 on heat survivors

water concentration was kept constant at 0.01 mg/L, the number of survivors recovered increased as the spore N_0 increased. Similar results were obtained when the water concentration was maintained at 2.4 mg/L throughout the sterilization cycle.

Influence of water concentration on the heat survivors is shown in Fig. 5-A. 3. If the spore N_0 is kept constant, and the water concentration is varied, the number of heat survivors increases. At a water concentration of 0.01 mg/L an approximate one log difference in the survivors were observed between the ribbons containing spore concentrations of 10^2 and 10^3 .

In summary, forty-seven (47) ribbon experiments were completed in two environmental areas. The results revealed that both spore N_0 and water concentration appear to influence the number of heat survivors recovered. Heat

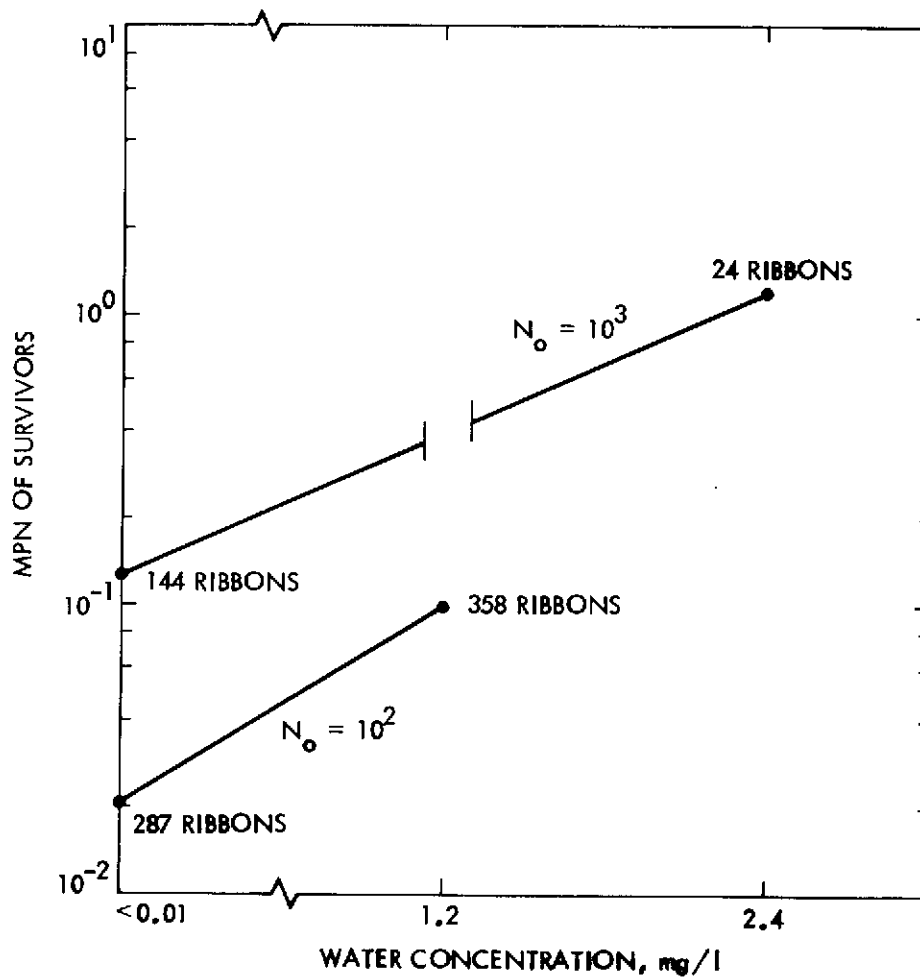


Figure 5-A.3. Influence of water concentration on heat survivors

survivors have different characteristics than non-heat stressed environmental isolates. No apparent differences were observed in the ability of teflon and aluminum surfaces to collect microbial contaminants, although aluminum was found to deteriorate after being exposed to the heat sterilization and placed into TSA broth.

5.1.3 Future Activities

Future activities in these studies are to continue to evaluate the influence of water concentration and the bacterial spore N_o on the thermal inactivation kinetics of naturally occurring spore populations; investigate the use of other collecting surface materials, i. e., stainless steel; and finally to

do environmental airborne fallout studies in other geographic areas where the Viking spacecraft will be assembled, to determine if spore populations, concentration and thermal resistances are similar to those found at Cape Kennedy, Florida.

5.1.4 Presentations

Puleo, J. R., "Results of Teflon Ribbon Experiments," presented to AIBS Planetary Quarantine Advisory Panel, Cocoa Beach, Florida, November, 1973.

Puleo, J. R., "Teflon Ribbon Experiments," presented at NASA Spacecraft Sterilization Technology Seminar, San Francisco, California, February, 1974.

5.2 MICROBIOLOGICAL STUDIES ON UNMANNED SPACECRAFT

5.2.1 Subtask B Introduction

The objective of this subtask is to determine the microbiological profile of pertinent unmanned spacecraft.

This study documents the number and types of microorganisms on all automated spacecraft which may carry earth organisms to the planets.

This type of work is required by NASA policy and lays a foundation upon which future policy can be formulated.

5.2.2 Significant Accomplishments

Studies were continued to assess the levels and types of microorganisms present on automated outbound spacecraft. Prior to launch, microbiological profiles were performed on the Mariner Venus/Mercury (MVM) 1973 spacecraft and on the Viking Proof Test Shroud at Cape Kennedy, Florida. The quantitative and qualitative results were submitted to the Planetary Quarantine Officer.

5.2.3 Future Activities

Perform microbial assays on Viking and other outbound automated unmanned spacecraft.

5.2.4 Presentations

Puleo, J. R., "Microbiological Studies on Unmanned Spacecraft," presented at NASA Spacecraft Sterilization Technology Seminar, San Francisco, California, February, 1974.

900-655

APPENDIX A
CLEANING AND DECONTAMINATION MATERIAL

APPENDIX A

CLEANING AND DECONTAMINATION MATERIAL

A.1 INTRODUCTION

The physical removal of particulates from spacecraft surfaces is primarily accomplished by means of vacuum brushes. The sable tail hair was chosen as the bristle material in the past because it tapers to a fine tip, and is compatible with all spacecraft surfaces. These properties, however, also have a number of disadvantages. Because of the sable hair taper, it is soft, tending to pack, restricting the air flow. The brushes become saturated with particles and can be a source of foreign matter if not cleaned frequently. Also, the bristles wear off at the tips, particularly around the brush outer edges.

The tapered shape of the sable bristle requires that it be bonded into the brush body. These adhesives, as well as the bristle, are not compatible with sterilization and biological decontamination procedures required for spacecraft cleaning in recent and future programs. In addition, sable tail hair has become difficult to obtain on the free world market.

Because of the above circumstances, the replacement of sable bristle is desired. This replacement material must be suitable in fulfilling the requirements of spacecraft cleaning, and be readily available. The objective of the discussed study was to find such a material.

Several synthetic monofilament fibres have been developed for the brush industry. Some of these fibres are used for the cleaning of delicate surfaces, such as magnetic tapes and coated optical lenses. These synthetic fibres include various polymers (i. e. , polyamides (nylons), polyethylene, polypropylene, polystyrene, polyester, etc.). Several natural bristles (e. g. , pony, squirrel) were also considered as possible replacement materials.

The replacement material must be: (1) compatible with the standard decontamination and sterilization procedures, (2) show resistance to packing and entanglement, and (3) have the ability to maintain cleanliness during usage.

A. 2 APPROACH

An industrial search of fibre* suppliers and specialty brush manufacturers was made. This search obtained information on fibres that could be used to replace the sable bristle. Several of these firms suggested fibres that should be considered as possible replacement candidates. Some of these suggested candidates were:

- 1) Pony Hair. This bristle is used in dusting brushes. High quality pony hair is mechanically tapered in Europe, and is called "Italian Sable." This treated bristle is used in fine tip brushes.
- 2) Squirrel (or badger) hair. This bristle is used for polishing candy and confectionary. This bristle flags easily, and is sometimes mixed with nylon filament to improve fatigue life.
- 3) Nylons. These filaments have excellent fatigue life. Nylons are used for cleaning delicate surfaces such as that previously mentioned. Nylons are also now being used for cosmetic brushes, an industry previously dominated by the natural bristles. These nylons used for this type of application must have small diameters.

Technical data revealed that only the nylons and polyester filaments had capabilities to be compatible with the planned decontamination and sterilization procedures. Therefore, this described effort concentrated mainly on the significant mechanical and physical properties of selected fibres, with the standard fibre being the sable bristle. The evaluation of the selected fibre compatibility with sterilization temperatures and isopropyl alcohol is in progress at the time of this report.

A. 2. 1 Experimental Techniques

The most important mechanical properties were stiffness (modulus of elasticity), bend recovery (matting resistance), and fatigue resistance. These properties were determined by using the procedures established by DuPont's

*Fibre is used collectively in this report for both the natural bristle and synthetic monofilament. When the terms "bristle" or "filament" are used, they refer to the type of fiber being discussed.

Plastics Department. These test procedures are described as follows with the importance of each stated:

- 1) Modulus of Elasticity. This property is required to determine the brush trim length and stiffness. The test is based on ASTM standard test method D-638. The ultimate tensile strength can be determined by ultimate failure load.
- 2) Bend recovery. This test was run to show the ability of the fibre to return to its original configuration. Each fibre was wrapped around a 2.38 mm (0.094 in.) diameter rod a minimum of ten times under a weight determined by the diameter. This weight, in grams, was set equal to half of the square of fibre diameter in mils. This fibre was held for four minutes before it was removed and then placed in 296K (73°F) water for one hour. Bend recovery was determined by the number of remaining loops and/or part of a loop.
- 3) Fatigue resistance. This test was made to show the ability of fibre to resist flexing. Fatigue shows up as breaking, splitting or complete failure and is the typical failure for rotating brushes. A tuft of bristles was placed in a rotating head at 500 rpm with the bristles striking an impact bar twice in each revolution. The individual fibres were tested at 4% maximum strain. Therefore, the distance of rotating head to the impact bar was $k = d_f + d_f/0.04$, where d_f = fibre diameter. The time of test was held proportional to the diameter, $(1/d_f)$. Four tufts of fibres were tested in each test.

Qualitative tests were conducted to determine the fibre abrasion resistance, its abrasiveness, and static electrical charge build up. These tests are described as follows:

- 1) Abrasion resistance. No direct measurement taken on the wear of the fibres. The wear on the fibres from the impact bar in fatigue resistance testing was observed through scanning electron microcroscope (SEM) examination.

2) Fibre abrasiveness and static electrical charge build-up.

Abrasiveness of the fibres was observed on simulated spacecraft surfaces (e.g., polished aluminum, thermal control blankets, etc.) by the fibre scratching. Fibre abrasiveness is a function of the fibre diameter and stiffness. Tufts of fibres were run against simulated spacecraft parts for 1-, 2- and 5-minute periods. Static electricity was determined to be present by the attraction of dust and small pieces of paper after these time periods. These tests were run concurrently.

A. 2. 2 Test Apparatus

The test apparatus used to determine the fibre tensile strength and modulus was an INSTRON Universal Testing machine. Hard rubber grips were used with the synthetic filaments while the natural bristles required special mounting with reinforced tape tabs. The constant diameter of each natural bristle determined the test gage length used.

Part of the test apparatus used to determine the bend recovery is illustrated in Fig. I. Because natural bristles are almost entirely tapered, the bend recovery test was not made on the natural bristle.

The test apparatus used to determine the fatigue resistance of the fibres is shown in Fig. II. The tufts were rotated 90° in the holding fixture after each period equivalent to 25% of the total test time required. Each tuft was made by placing a bundle of bristles in shrink tubing, as illustrated in Fig. III.

Both fibre abrasiveness and static electrical charge build up were determined with the same test apparatus, as shown in Fig IV. The distance from the test plate to the base of the fibre tuft was determined in order to obtain 30° angle at the fibre tip. To check the effectiveness of an antistatic ionizing device, a polonium element was held within 2.54 cm (1.0 in.) of the rotating tufts.

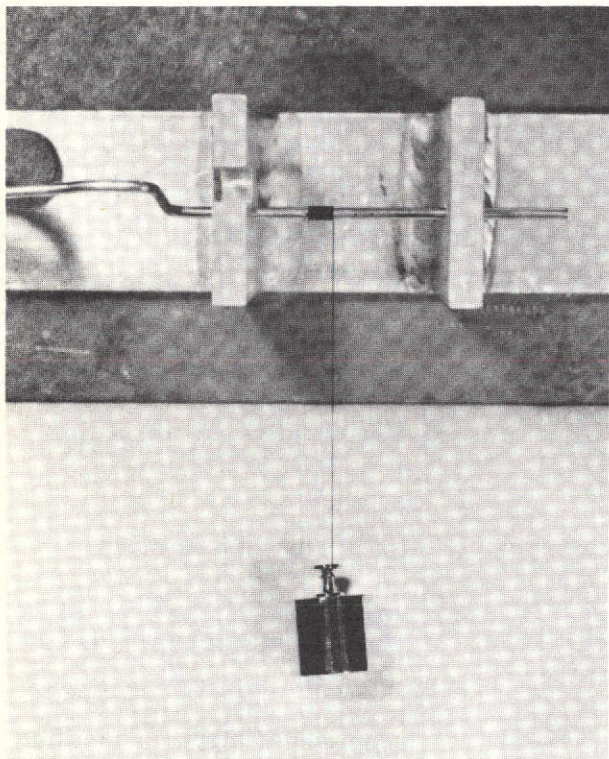


Fig. I. Bend Recovery Mandrel with Filament

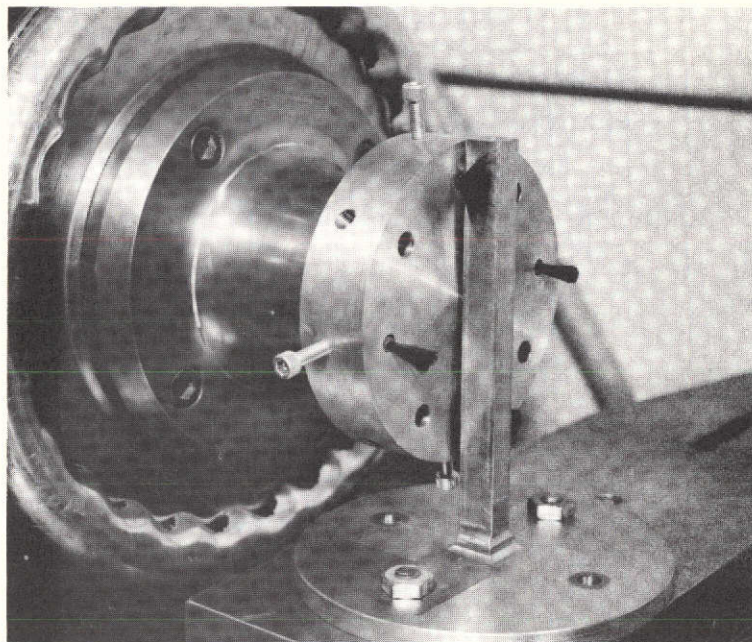


Fig. II. Fatigue Testing

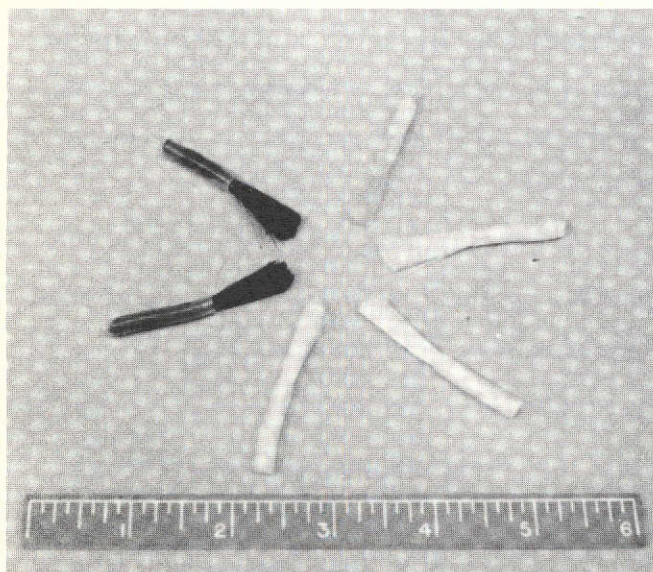


Fig. III. Tufts of Fibres

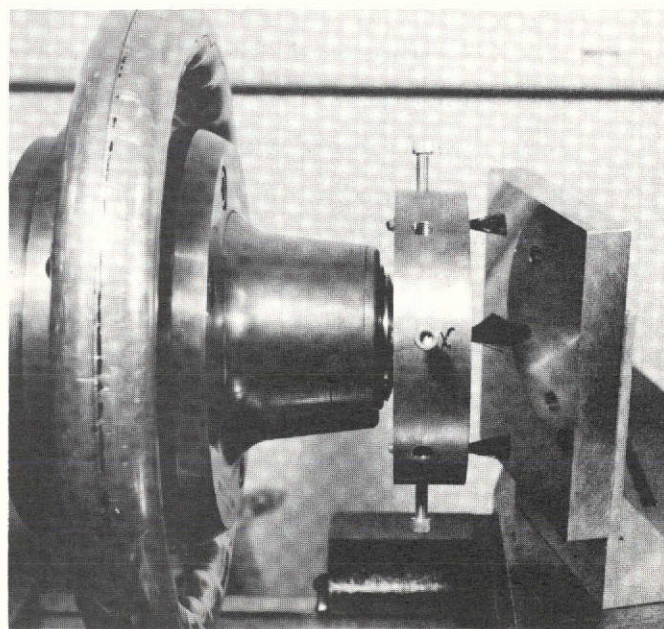


Fig. IV. Static Electricity and Abrasive Test Apparatus

A.3 SIGNIFICANT ACCOMPLISHMENTS

A.3.1 Bristle Material Differences

Sable hair was used as the standard because of its long usage in the brushes for the physical removal of particulates from the spacecraft. SEM examination showed that the unused sable hair has a very fine tip (Fig. V), but has an increasing amount of flaking particulates as the base is approached (Fig. VI). Hairs that had been used in a vacuum cleaning brush were relatively clean (Fig. VII), but showed the effect of wear at the tip end (Fig. VIII). This tip had been broken off from the usage and showed the results of abrasion where the scales were rubbed smooth.

Other natural unused bristles appeared to be similar to the unused sable in regard to scaling and/or particle burden. Pony hair, shown in Fig. IX, did not taper to a fine tip as the sable hair. Mechanical tapering is done to pony hair to bring it to a fine point. While some squirrel hair tapers to a fine tip, the majority of the hairs were blunt and had a larger center core that appeared to be soft and weak. Hollow squirrel hair was also found where the core had fallen out. Ox ear hair has a very clean appearance and looked like a possible candidate (Fig. X), but was noted to be brittle.

Likewise, the synthetic filaments, which technical data showed exhibited the best resistance to heat and chemical sterilization and decontamination, were viewed with the SEM. These filaments were either very smooth, as shown for one nylon, Felor in Fig. XI, or were die marked as shown by one of the other nylon filaments (Fig. XII).

Since the ends of these synthetic fibres are blunt cut, shown by Fig. XII, a mechanical treatment was developed by the brush industry to taper the ends to a fine tip. Fig. XIII shows one example of Felor nylon used in cosmetic brushes.

A.3.2 Mechanical and Physical Properties

The average mechanical properties are presented in Table I with the physical properties. The physical properties were not determined for those bristles that exhibited poor mechanical properties in fatigue. An example

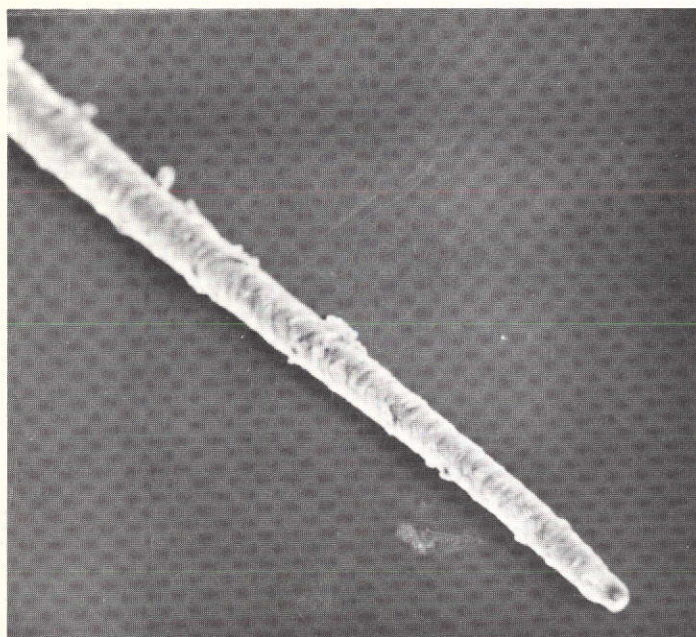


Fig. V. Tip of Unused Sable Hair (710X)



Fig. VI. Middle of Unused Sable Hair (950X)



Fig. VII. Middle of Used Sable Hair (1200X)

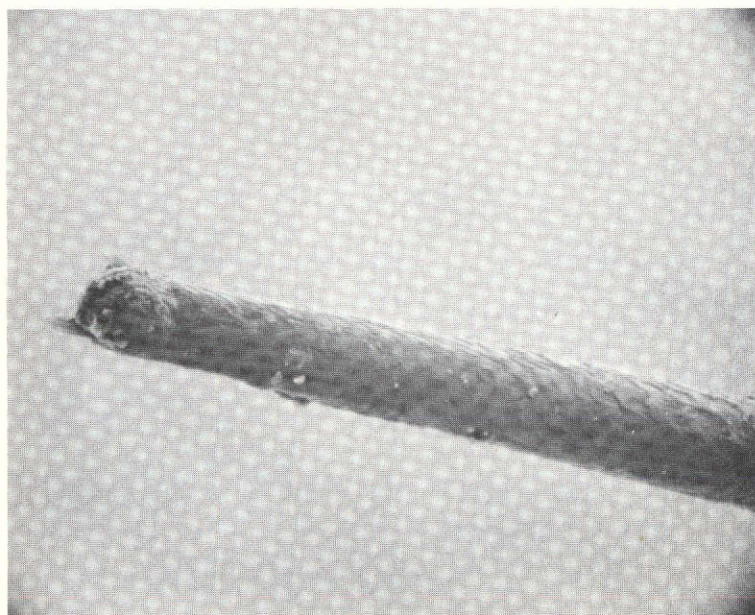


Fig. VIII. Tip of Used Sable Hair (1100X)

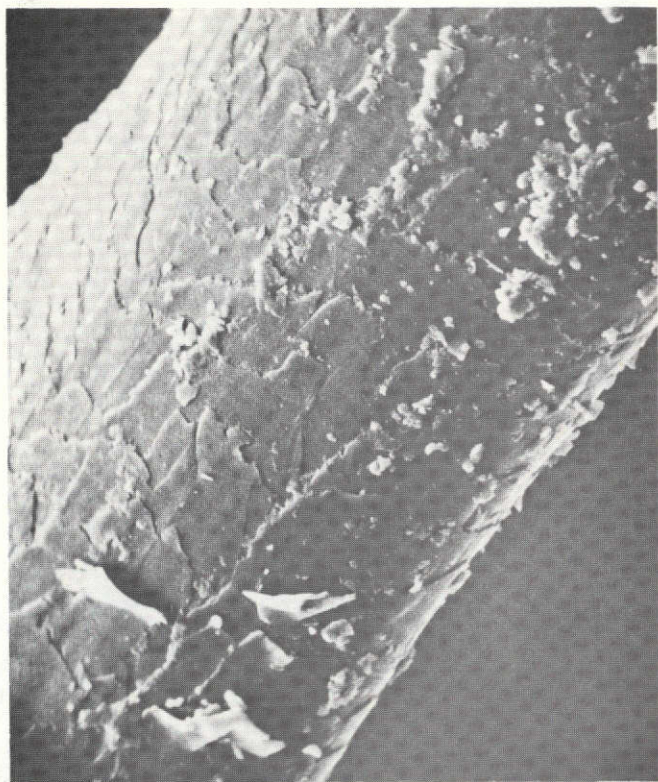


Fig. IX. Pony Hair (900X)

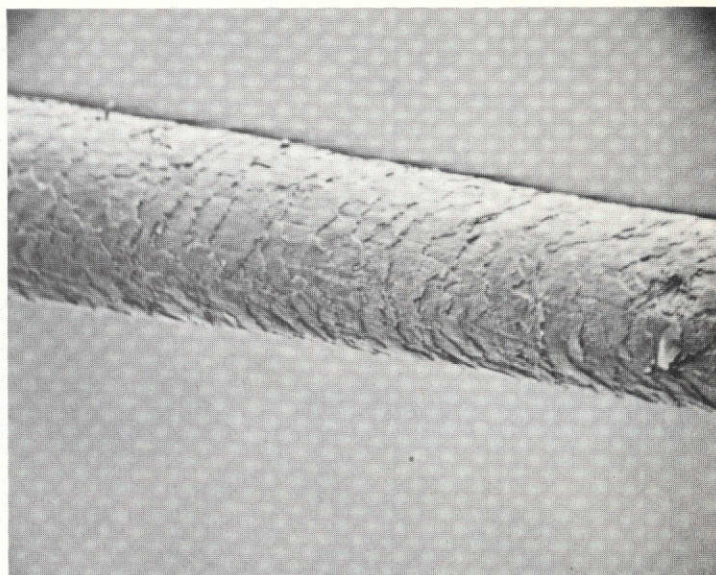


Fig. X. Ox Ear Hair (480X)

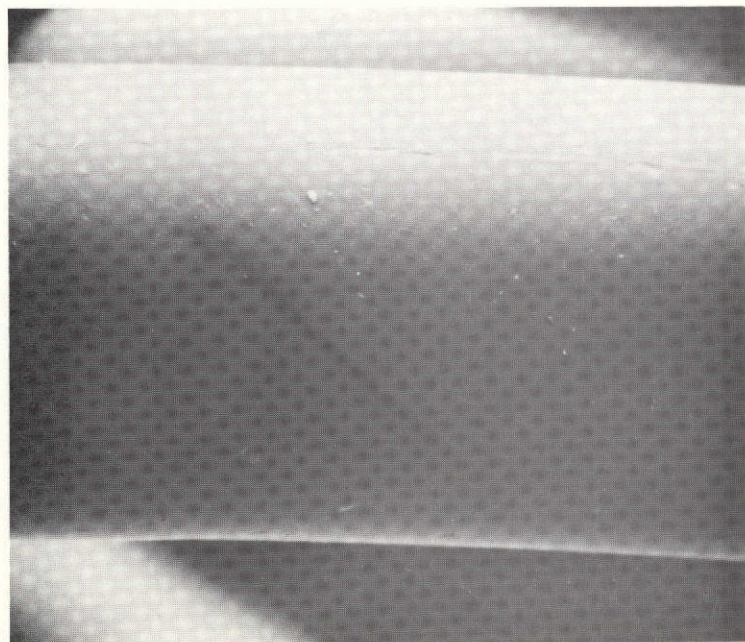


Fig. XI. Felor, Nylon Filament (650X)

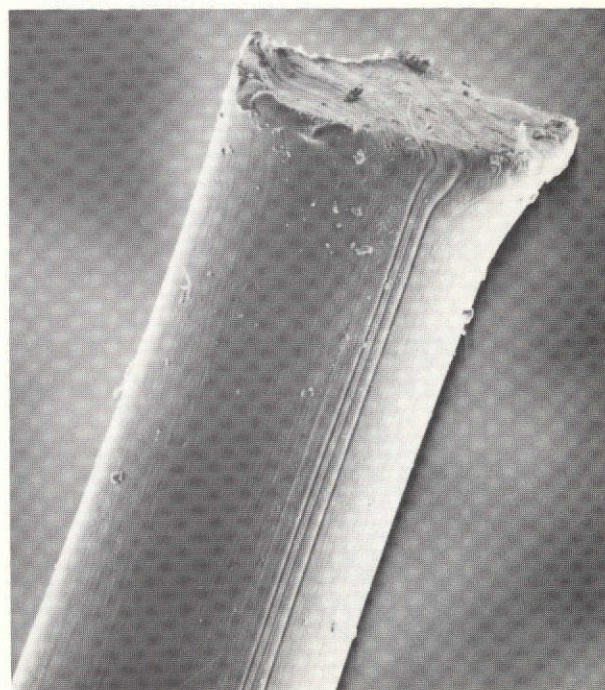


Fig. XII. Blunt Cut Tip Nylon 6/6 (200X)

would be the Nylex and Quill fibres. These fibres were made from 6/10 polymer, but had poor fatigue properties compared to the solid round cross section fibre of the same polymer because of their configuration.

Physical tests on Tynex were not completed. The sample received was too small, and the 3.96 GN/m^2 modulus with 0.3 m (0.012 in.) diameter indicated that the fibre would be abrasive. This indication was based on the data collected with the 0.15 mm (0.006 in.) diameter nylon 6/6 and 6/10 fibres, which were both abrasive and had a lower modulus around 2.6 GN/m^2 . While this material is available in smaller diameters, a sample of the smaller diameter fibres was not obtained. Mechanical tipping would be required to make it acceptable as a brush fibre for the intended JPL usage.

All the fibre materials, except polyester, exhibited a static electrical charge build up when they brushed against the various simulated spacecraft surfaces. The polonium cartridge (antistatic charge device) prevented this static charge build up when placed adjacent to these rotating bundles of fibres.

The effect of fatigue testing on the fibre was dramatic. The number of fibre failures went from almost none to almost entirely all of the tuft. When the fatigued fibres were examined with the SEM, the type of failures could be cataloged as to the amount of abrasion, or as to the type failure, splitting or breaking.

Sable hair had the poorest fatigue resistance. SEM examination showed that those bristles which remained were severely abraded to about half the original diameter as shown in Fig. XIV. Many of the broken bristles were found to be split on the end (Fig. XV) or broken (Figs. XVI and XVII) by the impact bar.

Felcor had the best fatigue resistance. SEM examination showed only a small amount of abrasion had occurred (Fig. XVIII) after viewing the entire filament. This marking was noted on several tested filaments, but never on an untested filament (Fig. XI).

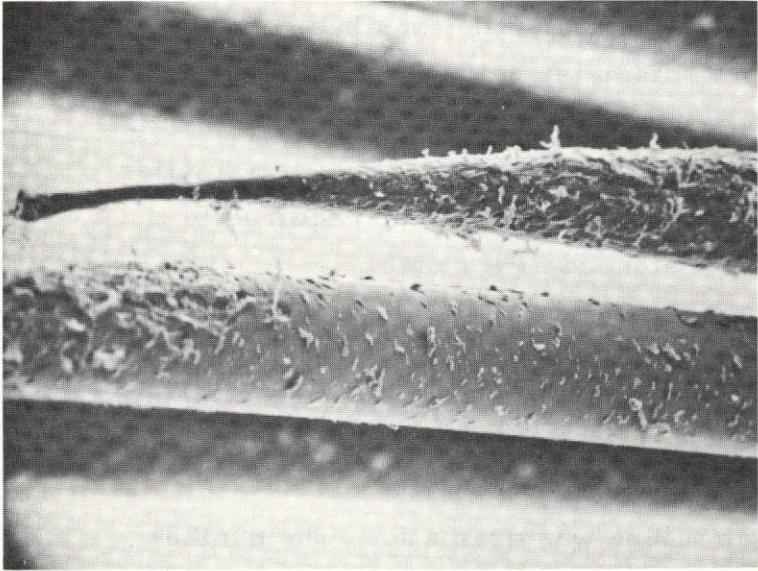


Fig. XIII. Mechanically Treated Felor Filament (200X)

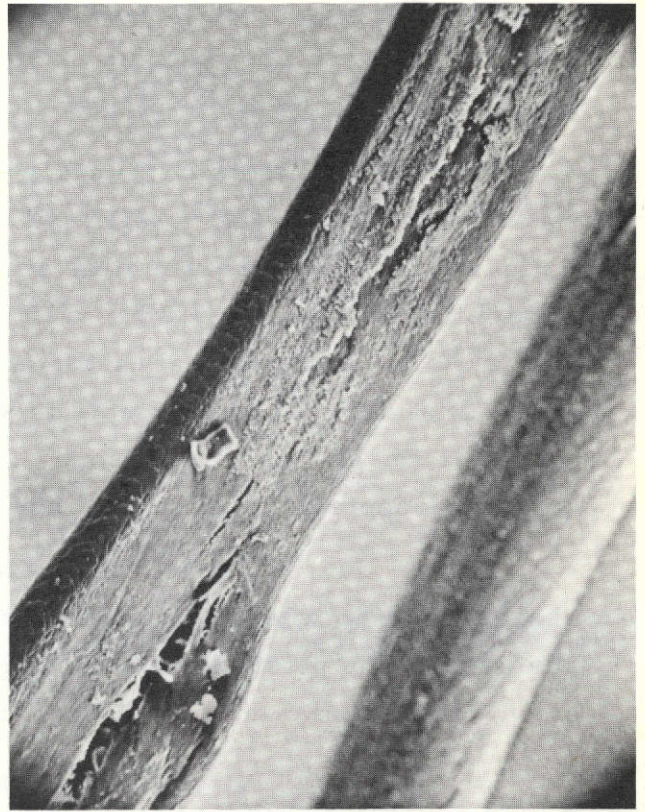


Fig. XIV. Abraded Sable Hair After Fatigue Testing (350X)



Fig. XV. Split Sable Hair After Fatigue Testing (225X)

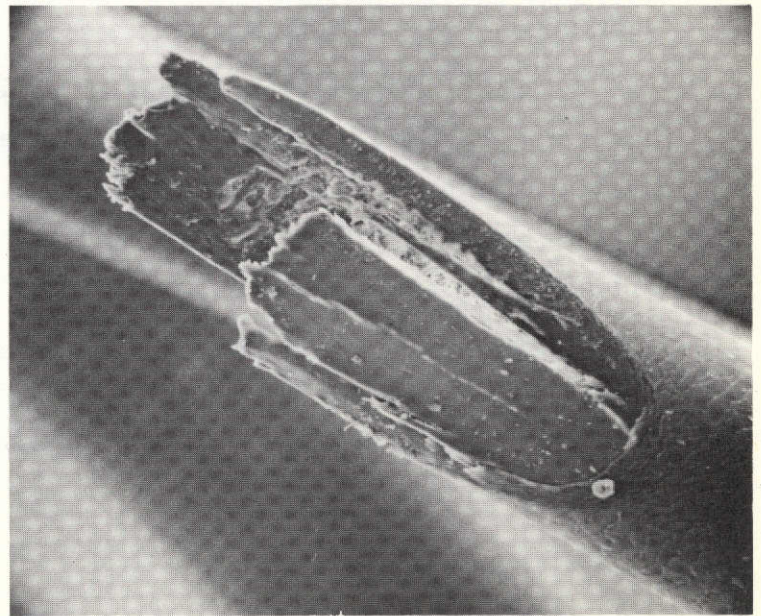


Fig. XVI. Broken Sable Hair After Fatigue Testing (380X)

Table I. Brush Fibre Properties

| Company and Fibre | Fibre Type | Fatigue Resis % | Recovery % | Strength MN/m ² | Modulus GN/m ² | Abrasiveness On (1) | | | Static Charge Buildup (2) | | |
|---|--------------------------|-----------------|------------|----------------------------|---------------------------|---------------------|----|------|---------------------------|-----|------|
| | | | | | | Al | TB | Gr/E | Al | TB | Gr/E |
| <u>Dupont</u> | | | | | | | | | | | |
| Felcor [®] | Nylon, copolymer | 98+ | 98 | 504.3 | 2.39 | No | No | No | No | Yes | Yes |
| Tynex [®] | Nylon 6/12 | 94 | 94 | 425.0 | 3.96 | ND (3) | ND | ND | ND | ND | ND |
| <u>Polymers, Inc.</u> | | | | | | | | | | | |
| 610 | Nylon 6/10 Round Shape | 75 | 98 | 340.0 | 2.53 | Yes | ND | ND | Yes | ND | ND |
| Nylex [®] | Nylon 6/10 X Shape | 30 | 99 | 340.0 | 2.53 | ND | ND | ND | ND | ND | ND |
| Quill [®] | Nylon 6/10 Hollow, round | 48 | 95 | 340.0 | 2.53 | ND | ND | ND | ND | ND | ND |
| <u>Whiting</u> | | | | | | | | | | | |
| 66 | Nylon 6/6 Round Shape | 90 | 91 | 380.7 | 2.62 | Yes | ND | ND | Yes | ND | ND |
| Plyer [®] | Polyester Round Shape | 90 | 80 | 357.6 | 2.74 | Yes | No | No | No | No | No |
| Sable | Natural (4) | 25 | -- | 91.9 | 0.82 | No | No | No | Yes | Yes | Yes |
| (1) Scratches placed on Al (polish aluminum plate), TB (thermal control blanket), GR/E (graphite/epoxy skin, hi-gain ant.) (2) Static electrical charge sufficient to attract small items such as dust, small pieces of filter paper, etc. Code same as for (1). (3) ND - Not determined. (4) Unused | | | | | | | | | | | |

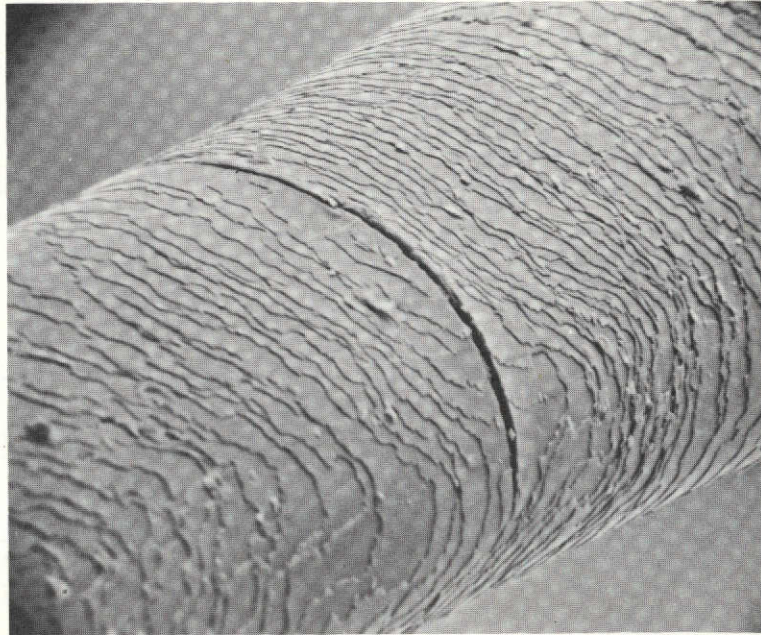


Fig. XVII. Cracked Sable Hair (1000X)

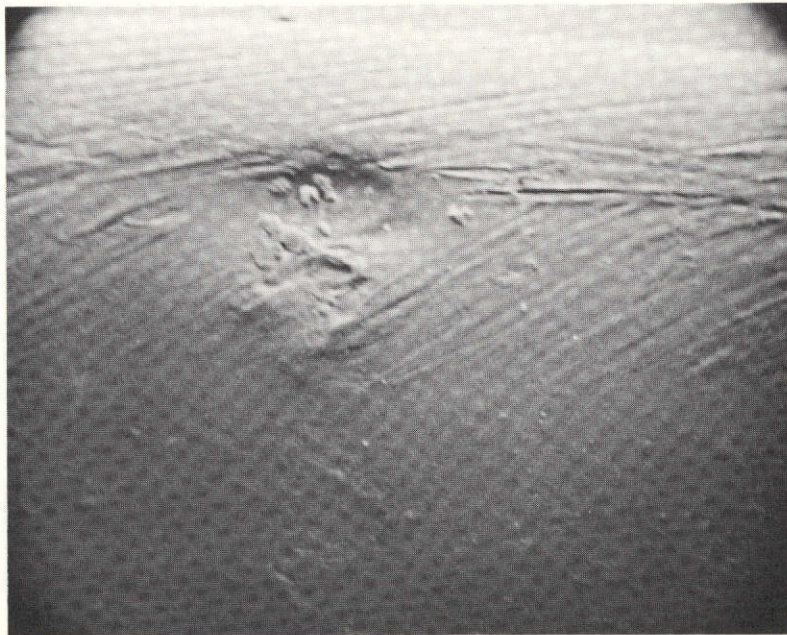


Fig. XVIII. Fatigued Felor (1500X)

A.4 SUMMARY AND CONCLUSIONS

Based on the published information on nylon's chemical resistance, and the preceeding data, Felor (a nylon copolymer) is recommended as the sable hair replacement.

Present work on the Felor being done will check its resistance to heat sterilization. Likewise, it will be tested for its resistance to autoclave sterilization procedures and isopropyl alcohol.